

**Characterization of CO₂-mediated Microvascular Blood Flow Responses in Skeletal Muscle
Tissue and Investigation of Underlying Mechanisms Using Direct CO₂ Microenvironment
Perturbations**

by © Meaghan A. McCarthy, BSc

A Thesis submitted to the School of Graduate Studies in partial fulfillment of the requirements
for the degree of

Master of Science in Medicine, Cardiovascular and Renal Sciences

Division of BioMedical Sciences, Faculty of Medicine

Memorial University of Newfoundland

October 2022

St. John's Newfoundland and Labrador

Abstract

Several vasoactive molecules are involved in coordinating microvascular blood flow with metabolic demand in skeletal muscle tissue; however, the involvement of some metabolites, such as carbon dioxide (CO_2), are not well-characterized. The objective of this thesis was to characterize CO_2 -mediated microvascular blood flow responses in skeletal muscle tissue and investigate potential underlying mechanisms, including ATP-sensitive potassium ion (K_{ATP}) channels and oxygen saturation (SO_2)-dependent release of ATP from red blood cells (RBC). A microfluidic gas exchange chamber was used to impose rapid and direct changes in the tissue CO_2 concentration of the extensor digitorum longus muscle of Sprague-Dawley rats. IVVM video sequences of capillary blood flow were recorded and analyzed offline for hemodynamic (RBC velocity, supply rate (SR), hematocrit (Hct)) and RBC SO_2 measurements using a custom MATLAB software. Rapid and significant changes in capillary RBC velocity and SR were observed following incremental increases and dynamic step-changes in tissue CO_2 . The involvement of K_{ATP} channels was investigated following systemic administration of glibenclamide (GLI, 5 mg / kg) (K_{ATP} channel antagonist). The magnitude of capillary RBC velocity and SR responses to CO_2 perturbations decreased following GLI administration. SO_2 remained constant throughout various CO_2 perturbations during baseline and after treatment with GLI. These findings support a significant involvement of CO_2 in local microvascular blood flow regulation in skeletal muscle tissue, the presence of an SO_2 -independent mechanism, and a partial dependence on K_{ATP} channel activation.

All animal protocols were approved by Memorial University's Institutional Animal Care Committee.

Keywords: Carbon dioxide, capillary, blood flow regulation, K_{ATP} channel, skeletal muscle, microfluidic device

General Summary

The cardiovascular system consists of a complex network of blood vessels responsible for delivering blood flow to body tissues and ensuring they receive enough oxygen and nutrients to function properly, while simultaneously removing metabolic waste products, such as carbon dioxide (CO_2). There are several ways that active muscle fibers communicate their metabolic needs to the vascular system, including the production of substances capable of interacting with blood vessels to adjust blood flow to tissue. The identity of several substances associated with increased tissue activity and their roles in regulating blood flow have been established; however, the involvement of other important substances, such as CO_2 , have not been well defined in skeletal muscle tissue. Using a novel experimental technique to cause rapid and direct changes in tissue CO_2 environment, we provide evidence supporting a significant role for tissue CO_2 in coordinating blood flow responses in the smallest vessels of the body, as well as a partial dependence of this response on the activity of a specific ion channel and no dependence on oxygen saturation (SO_2)-dependent ATP release from red blood cells.

Acknowledgements

I would like to take a moment to acknowledge the people who have helped make the completion of this degree possible and to extend my sincerest thank yous.

To my advisory committee, Dr. Reza Tabrizchi and Dr. Bruno Stuyvers, for taking the time to provide their valuable insight and constructive feedback, and for their assistance in the development of this thesis.

To the Natural Sciences and Engineering Research Council, Canadian Institutes of Health Research, and Memorial University of Newfoundland for the funding and scholarships that have supported my project and made it possible. This includes NSERC Discovery and CIHR grants, an NSERC CGS-M scholarship, and the MUN Faculty of Medicine Dean's Fellowship Award.

To my fellow lab members, Gaylene Russell McEvoy, Brenda Wells, and Meghan Kiley, for welcoming me into the lab, for creating a positive and collaborative environment, and for always being willing to help and answering my many questions along the way.

To my family, for their unwavering support and belief in me and in my goals.

And to my supervisor, Dr. Graham Fraser, for the guidance and support he has provided throughout every step of my program. The kindness, patience, and expertise he offers to his students help make a challenging experience into a positive one and for it, I am truly grateful.

Co-Authorship Statement

This thesis is organized into 3 chapters. The first chapter contains a literature review to provide readers with necessary background information. The second chapter is a manuscript containing original research. The third chapter summarizes key findings and discusses limitations and future directions.

This thesis contains the following manuscript that is in preparation:

MA McCarthy, GM Russell McEvoy, ME Kiley, BN Wells, GM Fraser
Characterization and Investigation of Potential Mechanisms Underlying CO₂-mediated
Microvascular Blood Flow Regulation in Skeletal Muscle Tissue. (In preparation for submission
to *The Journal of Physiology*)

Experimental design was completed by MA McCarthy and GM Fraser.

Surgical protocols were completed by GM Fraser.

The microfluidic gas exchange chamber was three-dimensionally (3D) printed by GM Russell McEvoy.

ME Kiley assisted in the collection of pilot data included in Figure 2.1.

GM Russell McEvoy and BN Wells assisted in collecting blood gas samples presented in Table 2.1.

The collection, analysis, and organization of data as well as the preparation of figures, interpretations of results, and preparation of the manuscript presented in the current thesis were completed by MA McCarthy with critical review by GM Fraser.

Table of Contents

| | |
|--|-------------|
| Abstract..... | ii |
| General Summary | iv |
| Acknowledgements | v |
| Co-Authorship Statement | vi |
| List of Figures..... | x |
| Chapter 1: | x |
| Chapter 2: | x |
| List of Tables | xii |
| List of Appendices..... | xiii |
| List of Abbreviations and Symbols | xiv |
| Chapter 1 – Literature Review | 1 |
| 1.1 Introduction and Objectives: | 1 |
| 1.2 An Overview of Microvascular Blood Flow Regulation in Skeletal Muscle Tissue..... | 2 |
| 1.3 Carbon Dioxide Transport and Influence on the Oxygen-Dissociation Curve | 9 |
| 1.4 The Role of Erythrocyte-derived Adenosine Triphosphate (ATP) Release in Blood Flow Regulation | 15 |
| 1.5 CO₂-mediated Microvascular Blood Flow Response and Suggested Underlying Mechanisms | 21 |

| | |
|--|-----------|
| 1.6 Involvement of Vascular K_{ATP} Channels in Microvascular Blood Flow Regulation.. | 30 |
| 1.7 Intravital Video Microscopy (IVVM) and Striated Muscle Tissue Preparations | 36 |
| 1.8 Experimental Techniques Used to Alter Arterial and Tissue Gas Concentrations and the Use of a Microfluidic Gas Exchange Chamber | 44 |
| Chapter 2 – | 51 |
| Characterization and Investigation of Potential Mechanisms Underlying CO₂-mediated Microvascular Blood Flow Regulation in Skeletal Muscle Tissue..... | 51 |
| 2.1 Introduction..... | 51 |
| 2.2 Methods..... | 57 |
| 2.2.1 Surgical Procedure: | 57 |
| 2.2.2 Dual Spectrophotometric Intravital Microscopy | 58 |
| 2.2.3 Microfluidic Gas Exchange Chamber | 59 |
| 2.2.4 Experimental Protocols 1A, 1B, 1C, and 1D: Characterization of CO₂-mediated microvascular blood flow response. | 60 |
| 2.2.5 Experimental Protocol 2: Investigation of the role of ATP-sensitive K⁺ ion (K_{ATP}) channels in CO₂-mediated blood flow regulation. | 62 |
| 2.2.6 Data Analysis and Statistical Tests: | 63 |
| 2.3 Results | 64 |
| 2.3.1 Experimental Protocols 1A, 1B, 1C, and 1D: Characterization of CO₂-mediated microvascular blood flow response. | 65 |
| 2.3.2 Experimental Protocol 2: Investigation of the role of ATP-sensitive K⁺ ion (K_{ATP}) channels in CO₂-mediated blood flow regulation. | 81 |

| | |
|---------------------------|-----|
| 2.4 Discussion..... | 89 |
| Chapter 3 – Summary | 108 |
| Conclusion: | 108 |
| Limitations: | 110 |
| Perspectives: | 112 |
| List of References | 114 |
| Appendix A | 132 |
| Appendix B | 133 |

List of Figures

Chapter 1:

| | |
|--|----|
| Figure 1. 1. Hemoglobin (Hb) oxygen-dissociation curves generated based on human Hb P ₅₀ (36 mmHg). | 13 |
| Figure 1. 2. An overview of the analysis process for intravital video microscopy (IVVM) sequences using a custom MATLAB software. | 42 |
| Figure 1. 3. Wavelength dependence of the deoxy- and oxyhemoglobin molar attenuation coefficient. | 43 |
| Figure 1. 4. Schematic depicting the multiple components of a three-dimensionally (3D) printed microfluidic gas exchange chamber. | 47 |
| Figure 1. 5. Microfluidic gas exchange chamber. | 48 |

Chapter 2:

| | |
|--|----|
| Figure 2. 1. Capillary hemodynamics in rat skeletal muscle at a range of tissue CO ₂ concentrations. | 66 |
| Figure 2. 2. Mean time series plots demonstrating the change in RBC velocity in response to low (A) and high (B) tissue CO ₂ perturbations over a 2-minute period. | 68 |
| Figure 2. 3. Time series plots demonstrating the change in RBC supply rate in response to low (A) and high (B) tissue CO ₂ perturbations over a 2-minute period. | 69 |
| Figure 2. 4. Time series plots demonstrating the change in capillary hematocrit in response to low (A) and high (B) tissue CO ₂ perturbations over a 2-minute period. | 70 |
| Figure 2. 5. Time series plots demonstrating the change in RBC oxygen saturation in response to low (A) and high (B) tissue CO ₂ perturbations over a 2-minute period. | 71 |
| Figure 2. 6. Capillary hemodynamics and RBC oxygen saturation in rat skeletal muscle in response to oscillating tissue CO ₂ concentrations using a gas exchange chamber. | 74 |
| Figure 2. 7. Time series plots demonstrating the change in mean RBC velocity (A), RBC supply rate (B), hematocrit (C), and RBC oxygen saturation (D) in response oscillating tissue CO ₂ perturbations over a 4-minute period. | 76 |
| Figure 2. 8. Capillary hemodynamics in rat skeletal muscle in response to oscillating tissue O ₂ concentrations using a gas exchange chamber. | 78 |
| Figure 2. 9. Time series plots demonstrating the change in mean RBC velocity (A), RBC supply rate (B), hematocrit (C), and RBC oxygen saturation (D) in response oscillating tissue O ₂ perturbations over a 4-minute period. | 80 |
| Figure 2. 10. Capillary hemodynamics in rat skeletal muscle at a range of tissue CO ₂ concentrations following intravenous administration of glibenclamide (GLI, 5 mg/kg). | 82 |

| | |
|---|----|
| Figure 2. 11. Capillary hemodynamics in rat skeletal muscle in response to oscillating tissue CO ₂ concentrations following intravenous administration of glibenclamide (5 mg/kg). | 84 |
| Figure 2. 12. Time series plots demonstrating the change in mean RBC velocity (A), RBC supply rate (B), hematocrit (C), and RBC oxygen saturation (D) in response oscillating tissue CO ₂ perturbations following intravenous administration of glibenclamide (5 mg/kg). | 85 |
| Figure 2. 13. Capillary hemodynamics in rat skeletal muscle in response to oscillating tissue O ₂ concentrations following intravenous administration of glibenclamide (5 mg/kg). | 87 |
| Figure 2. 14. Time series plots demonstrating the change in mean RBC velocity (A), RBC supply rate (B), hematocrit (C), and RBC oxygen saturation (D) in response oscillating tissue O ₂ perturbations following intravenous administration of glibenclamide (5 mg/kg). | 88 |

List of Tables

| | |
|--|----|
| Table 2. 1. Mean measurements of systemic circulatory, respiratory, and blood gas conditions (n = 21 animals)..... | 64 |
|--|----|

List of Appendices

| | |
|------------------|-----|
| Appendix A..... | 132 |
| Appendix B | 133 |

List of Abbreviations and Symbols

| | |
|--------------------------------------|---|
| Ach: | Acetylcholine |
| ADP: | Adenosine diphosphate |
| AE1: | Anion exchanger |
| ASIC: | Acid-sensing ion channel |
| ATP: | Adenosine triphosphate |
| BaCl ₂ : | Barium chloride |
| cAMP: | Cyclic adenosine monophosphate |
| CA: | Carbonic anhydrase |
| Ca ²⁺ : | Calcium ion |
| CFTR: | Cystic fibrosis transmembrane conductance regulator |
| cGMP: | Cyclic guanosine monophosphate |
| CO ₂ : | Carbon dioxide |
| DMSO: | Dimethyl sulfoxide |
| dH ₂ O: | Distilled water |
| EDL: | Extensor digitorum longus |
| FOV: | Field of view |
| GEC: | Gas exchange chamber |
| GLI: | glibenclamide |
| H ⁺ : | Hydrogen ion, Proton |
| Hb: | Hemoglobin |
| HCO ₃ ⁻ : | Bicarbonate |
| H ₂ CO ₃ : | Carbonic acid |
| Hct: | Hematocrit |
| H ₂ O: | Water |
| H ₂ S: | Hydrogen sulfide |
| IVVM: | Intravital video microscopy |
| K ⁺ : | Potassium ion |
| K _{ATP} channel: | ATP-sensitive potassium ion channel |
| <i>k</i> _{CO₂} : | Solubility coefficient |
| Mg ²⁺ : | Magnesium ion |

NaOH: Sodium hydroxide
NE: Norepinephrine
NO: Nitric oxide
NOS: Nitric oxide synthase
nNOS: Neuronal nitric oxide synthase (NOS)
O₂: Oxygen
PCO₂: Partial pressure of carbon dioxide
PDMS: Polydimethylsiloxane
pK₁: Dissociation constant
PO₂: Partial pressure of oxygen
RBC: Red blood cell
SNS: Sympathetic nervous system
SO₂: Oxygen saturation
SR: Supply rate
V_{RBC}: Red blood cell velocity
VSMC: Vascular smooth muscle cell

Chapter 1 – Literature Review

1.1 Introduction and Objectives:

A positive correlation between blood supply and tissue metabolic demand has been well-established, and it involves the integration of a variety of vasoactive mediators and signals throughout several levels of the vascular tree to induce coordinated and spatially specific blood flow responses. Blood is transported through an expansive and highly branched network of blood vessels, known as the systemic circulation, and is distributed throughout the body based on broad systemic factors as well as on the varying metabolic demands located within and among different tissues. The microvascular system accounts for a significant proportion of the overall systemic circulation and is composed of the smallest blood vessels in the body in closest proximity to the tissues. Due to their proximity to the tissue environment, microvessels have an important role in sensing and communicating the metabolic needs of tissues into larger upstream vessels capable of initiating significant changes in both the magnitude and distribution of blood flow to adequately match dynamic and variable metabolic demands. A variety of vasoactive molecules associated with increased muscle metabolism have been shown to significantly contribute to local blood flow regulation, such as oxygen (O_2), adenosine, potassium (K^+), and adenosine triphosphate (ATP). However, the involvement of other physiologically relevant molecules, such as carbon dioxide (CO_2), in coordinating local blood flow responses throughout the skeletal muscle tissue microcirculation is not well understood. Understanding the factors that influence the delivery of blood to the microvascular system is crucial as the capillary networks are the primary location for gas and nutrient exchange as well as the removal of metabolic waste products, which ensures an optimal environment for proper cellular functioning. This thesis aims

to advance our current understanding of microvascular blood flow regulation in skeletal muscle tissue, specifically of CO₂-mediated blood flow responses at the microvascular and capillary levels. A novel experimental technique was used to impose rapid and direct changes in the tissue microenvironment and was combined with intravital video microscopy sequences of resulting blood flow responses to achieve the objectives of this project, which are as follows:

1. Characterize both the magnitude and time course of capillary hemodynamic and oxygen saturation responses to a physiological range of tissue CO₂ conditions in skeletal muscle tissue.
2. Evaluate the involvement of vascular ATP-sensitive potassium (K_{ATP}) channels in CO₂- and O₂-mediated microvascular blood flow regulation.
3. Investigate the relationship between CO₂- and O₂-mediated blood flow responses as well as the potential presence of overlapping regulatory mechanisms, such as red blood cell (RBC)-derived ATP release and the involvement of vascular K_{ATP} channels.

1.2 An Overview of Microvascular Blood Flow Regulation in Skeletal Muscle Tissue

The systemic circulation of the cardiovascular system is composed of an extensive and highly branched network of blood vessels that are responsible for ensuring that adequate amounts of O₂ and essential nutrients are being delivered to the tissues while simultaneously removing metabolic waste products. Oxygenated blood is delivered to the heart by the pulmonary veins from the lungs and is pumped into the rest of the body through large vessels called arteries. Arteries exiting the heart branch into increasingly smaller vessels to form the systemic circulation, which is responsible for supplying blood to every organ and tissue to sustain proper

cellular functioning. Once small arteries reach the organ or tissue they are supplying, they are referred to as feed arteries which continue to branch into a vascular network composed of the smallest vessels in the body, collectively known as the microvascular system, or simply the microcirculation. The microvascular system also includes a network of increasingly smaller vessels called arterioles, with the smallest terminal arterioles branching into groups of capillaries composed of between 2 and 20 vessels per group in striated muscle tissue (Myrhage & Hudlická, 1976; Skalak & Schmid-Schönbein, 1986; Delashaw & Duling, 1988; Murrant et al., 2017). The capillaries account for a significant proportion of the systemic circulation and are physiologically important since capillary walls act as the final interface between the bloodstream and the cellular environment and are the primary site of gas and nutrient exchange. The deoxygenated and metabolic waste carrying blood exiting capillary networks is collected by small venules, which are the last vessel type in the microvascular system, and transported through a venous system of increasingly larger veins back to the heart and pulmonary circulation. The distribution of blood flow throughout the vast network of vessels located among and within tissues is a dynamic process that depends on broad systemic hormonal and cardiovascular factors (such as heart rate, blood pressure, cardiac output, blood volume, and sympathetic tone) as well as the local metabolic demand of tissues, with higher volumes of blood being directed towards highly vascularized and metabolically active areas, such as skeletal muscle tissue (Laughlin & Armstrong, 1982; Hargreaves et al., 1990; Berg & Sarelius, 1995; Joyner & Casey, 2015). The close proximity of the microvascular system to metabolically active tissue allows microvessels to rapidly sense changes in the tissue microenvironment and therefore, have an important role in coordinating local blood supply with tissue metabolic demand, especially at the arteriolar level.

Due to their small radii, arterioles are often referred to as resistance vessels and they have a key role in facilitating blood flow through the systemic circulation by influencing the total peripheral resistance and contributing to the large blood pressure gradient between the arteries and capillaries (Davis et al., 1986). In addition to their inherently smaller radii, arteriolar vessel walls have a vascular smooth muscle cell (VSMC) layer that is highly innervated by the sympathetic nervous system (SNS) and they experience a partial constriction under normal conditions, known as vascular tone (Marshall, 1982; Davis, 1993; Korthuis, 2011). Vascular tone is regulated by a combination of factors, including VSMC myogenic activity, SNS-derived norepinephrine (NE) release, and endothelium-derived vasoactive molecules such as nitric oxide (NO) (Marshall, 1982; Davis, 1993; Sandoo et al., 2010; Korthuis, 2011). The presence of vascular tone enables arterioles to either increase or decrease in diameter from their baseline state by altering VSMC contractility, which causes an inversely proportional change in the magnitude of vascular resistance present at the location of the corresponding diameter change, according to Poiseuille's Law (Sutera & Skalak, 1993). Coordinated changes in diameter and vascular resistance along a vessel segment influences the ease of blood flow through the vessel, with flow increasing in areas of low resistance and decreasing in areas of high resistance. Therefore, vascular tone is an important feature that allows arterioles to have a significant role in regulating both the magnitude and distribution of blood flow throughout and among tissues by creating paths of relative high and low resistance. Arteriolar vascular tone is influenced by a variety of extrinsic factors, such as SNS activity and circulating hormones, as well as local factors, such as changes in the concentration of molecules associated with metabolism (O_2 , CO_2 , hydrogen ion (H^+), K^+ , adenosine, ATP, etc.) and physical changes in the vessel's environment (temperature, shear stress, and stretching) (Hogan et al., 1982; Koller & Kaley, 1991; Davis, 1993; Ward, 1996;

Welsh & Segal, 1996; VanTeeffelen & Segal, 2003; Ngo et al., 2010; Korthuis, 2011; Riemann et al., 2011; Lamb & Murrant, 2015; Dora, 2017; Charter et al., 2018).

Due to their ability to alter their diameter and their sensitivity to the metabolic state of the surrounding tissue, it is well established that arterioles have a primary role in regulating blood flow distribution (Segal, 2005). This role is described by the metabolic hypothesis, which aims to explain the observed increase in muscle blood supply during conditions of increased metabolic demand and suggests that vasoactive metabolites produced locally in the tissue have a significant role in this coordination (Laughlin & Armstrong, 1982; Van Beekvelt et al., 2001; Murrant et al., 2017). Several vasoactive signals are generated during conditions of increased muscle metabolism, such as increased oxygen consumption, ATP breakdown, and K^+ efflux as well as the production of adenosine, CO_2 , and H^+ (Clifford & Hellsten, 2004). The metabolic hypothesis postulates that the vasoactive signals produced in the tissue interact with the microvasculature to induce appropriate alterations in arteriolar tone and capillary red blood cell (RBC) flow rates that are proportional to the tissue's metabolic rate (Murrant et al., 2017). To support this hypothesis, it has been shown that muscle contraction elicits an increase in arteriolar diameter and that the increase is proportional to the number of muscle fibers stimulated (Gorczynski et al., 1978; Berg et al., 1997; Milkau et al., 2010). In addition, arteriolar vasodilation is accompanied by a simultaneous increase in arteriolar blood flow and capillary RBC velocity (Kurjiaka & Segal, 1995; Mitchell et al., 1997). Since a wide variety of metabolites are produced during muscle metabolism, a significant amount of research has been conducted to inform this hypothesis and demonstrate the involvement of several metabolites in coordinating microvascular blood flow responses (Sarelius & Pohl, 2010). It has also been demonstrated that vasoactive agents produced

during muscle contraction (such as adenosine, K^+ , and NO) not only influence arteriolar diameter individually, but also interact and influence combined responses to these stimuli (Lamb & Murrant, 2015). Therefore, during conditions of elevated muscle metabolism, there are multiple overlapping, redundant, and competing vasoactive signals that arterioles must integrate to initiate an appropriate vascular response (Segal et al., 1989; Cohen & Sarelius, 2002; Murrant & Sarelius, 2002; Sarelius & Pohl, 2010; Lamb & Murrant, 2015).

To induce significant changes in the magnitude and/or distribution of microvascular blood flow, it is necessary to initiate a coordinated change in vessel diameter and vascular resistance along the length of vessel segments throughout several levels of the vascular tree (Kurjiaka & Segal, 1995; Segal & Jacobs, 2001; Segal, 2005). To accomplish this, local arteriolar responses to increased muscle metabolism and physiologically relevant stimuli (such as acetylcholine (ACh), NE, O_2 , K^+ , adenosine, and ATP) can be communicated to larger upstream arteriolar branches and small arteries (Duling & Berne, 1970; Segal & Duling, 1986a, 1986b; Segal et al., 1989; Song & Tyml, 1993; Ellsworth et al., 1995; Kurjiaka & Segal, 1995; McCullough et al., 1997; Dietrich et al., 2000; Hungerford et al., 2000; Segal & Jacobs, 2001; Looft-Wilson et al., 2004; Figueroa & Duling, 2008; de Wit, 2010; Ngo et al., 2010; Riemann et al., 2011; Dora, 2017; Lamb et al., 2018). The rapid transmission of vasomotor responses along vessel walls is known as a conducted vasomotor response (Bagher & Segal, 2011b). Previous research has been done to investigate this phenomenon and demonstrates that conducted vasomotor responses involve the spread of electrical signals along both the endothelial and/or VSMC layers of blood vessels via gap junctions composed of connexin proteins (primarily connexins 37 and 40) (Segal et al., 1989; Xia & Duling, 1995; Xia et al., 1995; Welsh & Segal, 1998; de Wit et al., 2000; Segal &

Jacobs, 2001; Figueroa et al., 2003; Looft-Wilson et al., 2004; Segal, 2005; Figueroa & Duling, 2008; de Wit, 2010; Milkau et al., 2010). The type of vascular cells involved (endothelial and/or smooth muscle cells), as well as the mechanism underlying the spread of conducted responses, both appear to depend on the identity of the vasoactive stimuli, which further supports the presence of multiple pathways in coordinating microvascular blood flow responses (Welsh & Segal, 1998; Figueroa & Duling, 2008; de Wit, 2010; Milkau et al., 2010).

Coordinated vascular responses along the arteriolar network influence the amount of oxygen and nutrients being delivered to the tissue by altering downstream capillary blood flow (Gorzynski et al., 1978; Delashaw & Duling, 1988; Mitchell et al., 1997; Fry et al., 2013). Since capillary vessel walls lack a VSMC layer and are unable to significantly alter their own diameters, terminal arterioles are logically viewed as the primary mediators of capillary blood flow. At rest, capillaries support spatially heterogeneous blood flow distribution that is controlled by a combination of active changes in arteriolar diameter, downstream pressure gradients, as well as passive rheological factors such as uneven distribution of RBCs at vessel bifurcations (Gorzynski et al., 1978; Honig et al., 1982; Pries et al., 1989; Hargreaves et al., 1990; Pries et al., 1990; Fry et al., 2013). In addition, variations in both the mean oxygen and cell flows through terminal arterioles have also been suggested to contribute to heterogeneous O₂ delivery and blood flow in downstream capillary networks (Sarelius, 1993). In response to increased O₂ demand, such as during striated muscle contractions, the number of both arterioles and capillaries supporting RBC flow increase to match the novel metabolic requirements of the tissue (Gorzynski et al., 1978; Fry et al., 2013). However, this statement has also been challenged since previous research has shown that most capillaries support RBC flow at rest, which suggests

that alterations in O₂ delivery may be accomplished by influencing RBC hemodynamic variables, such as velocity, instead of capillary recruitment (Poole et al., 2013). In striated muscle tissue, contraction-induced arteriolar vasodilation initiates a coordinated increase in flow through entire capillary networks, which further supports their role in regulating downstream capillary blood flow (Gorczynski et al., 1978; Honig et al., 1982; Delashaw & Duling, 1988).

In addition to the significant involvement of arterioles in regulating capillary perfusion and coordinating blood flow distribution, capillaries themselves are also actively involved in local blood flow regulation (Murrant et al., 2017). Capillaries are sensitive to variations in the metabolic state of their surrounding tissue and direct stimulation of specific capillary beds, either by muscle fiber stimulation or application of both physiological events and pharmacological agents, can initiate significant increases in arteriolar diameter and capillary RBC velocity that are similar in magnitude to responses originating at the arteriolar level (Dietrich & Tyml, 1992a, 1992b; Song & Tyml, 1993; Berg et al., 1997; Mitchell et al., 1997; Cohen & Sarelius, 2002; Murrant & Sarelius, 2002). Capillary endothelial cells are electrically coupled to upstream arterioles and generate electrical signals in response to changes in their tissue environment (Beach et al., 1998; McGahren et al., 1998). These electrical signals are transmitted upstream through several orders of the arteriolar network to initiate a coordinated change in microvascular tone and a spatially specific increase in capillary blood flow directed toward the stimulated muscle fibers (Dietrich & Tyml, 1992a, 1992b; Song & Tyml, 1993; Berg et al., 1997; Twynstra et al., 2012). Several physiologically relevant vasoactive molecules, including ACh, K⁺, adenosine, and NE, have been shown to initiate conducted vascular responses at the capillary level (Dietrich & Tyml, 1992a, 1992b; Song & Tyml, 1993; Mitchell et al., 1997; Lamb et al.,

2018). In addition, vasoactive agents produced during muscle contraction, such as adenosine, NO, and K^+ , have also been shown to interact and influence each other's responses initiated at the capillaries (Lamb et al., 2018). Therefore, like arterioles, there is compelling evidence that capillaries can also sense and integrate a variety of vasoactive signals generated during increased muscle metabolism to direct appropriate changes in upstream arteriolar diameter and hence downstream capillary perfusion (Song & Tyml, 1993; Lamb et al., 2018). While several vasoactive agents related to increased muscle metabolism have been shown to be involved in local blood flow regulation, the contribution of other molecules in regulating capillary blood flow responses in skeletal muscle tissue have not been well defined, such as CO_2 . The objectives of the current thesis, as outlined in section 1.1, aim to address this gap in the literature and advance our current understanding of CO_2 -mediated blood flow regulation at the capillary level in skeletal muscle tissue.

1.3 Carbon Dioxide Transport and Influence on the Oxygen-Dissociation Curve

Carbon dioxide is a small, neutrally charged gas molecule that is a well-known by-product of aerobic cellular metabolism and whose production increases significantly during conditions of elevated metabolic demand, such as during exercise (venous pCO_2 (rest) = 47 mmHg, venous pCO_2 (exercise) = 78 mmHg (Sun et al., 2001)). The amount of CO_2 present in the tissues following energy production is tightly and rapidly regulated by two main biological systems, the respiratory and the cardiovascular systems, as well as by biochemical reactions and the slower contribution of other biological systems such as the renal system. Due to its small, uncharged nature, it is generally accepted that CO_2 produced within cells diffuses readily across cellular membranes, through the interstitial environment, and toward the capillaries of the microvascular

system (Wright, 1934; Missner et al., 2008). Once CO₂ reaches the capillaries, it is transported along its concentration gradient into the bloodstream where it is moved convectively into the pulmonary circulation in the lungs, crosses both the capillary and alveolar membranes, and is expelled into the external environment. When CO₂ is in the bloodstream, it is transported by three main forms: dissolved, converted into bicarbonate (HCO₃⁻), or bound to hemoglobin (Hb). The simplest form of CO₂ transport is the dissolution of CO₂ in blood plasma since it is readily soluble (solubility coefficient (k_{CO_2}) = 0.0308 mmol/L mm Hg⁻¹ for plasma at 37 °C), accounting for between 5 and 10% of the total mass of CO₂ in the blood (Wieth et al., 1982; Arthurs & Sudhakar, 2005; Levitzky, 2017).

The majority of CO₂ is transported as bicarbonate (HCO₃⁻), accounting for between 80 and 90% of the total mass of CO₂ in the blood (Wieth et al., 1982; Levitzky, 2017). A rapid and reversible reaction between CO₂ and water (H₂O) is catalyzed by the carbonic anhydrase (CA) enzyme to produce carbonic acid (H₂CO₃), which rapidly dissociates into equal amounts of bicarbonate (HCO₃⁻) and hydrogen ions (H⁺), as seen in (1) (dissociation constant (pK₁) = 6.10) (Hastings et al., 1928; Enns, 1967; Tanishita et al., 1985). This is referred to as the bicarbonate buffer system. Some CO₂ hydration occurs in extracellular environments and is catalyzed by membrane-bound CA (isozyme CA IV) localized on endothelial cell membranes, the sarcolemma, and the sarcoplasmic reticulum of muscle fibres (Waheed et al., 1992; Sender et al., 1994; Decker et al., 1996; Geers & Gros, 2000). However, a large concentration of carbonic anhydrase enzymes is present in RBCs and as such, a large amount of CO₂ hydration and HCO₃⁻/H⁺ production in the bloodstream occurs within these cells (Ali Akbar & Brown, 1996; Geers & Gros, 2000; Moini et al., 2002). The RBC membrane is highly permeable to CO₂ (permeability coefficient: 0.35-3.2

cm/s) and therefore it crosses into the cell with ease (Gutknecht et al., 1977; Gros et al., 1981; Missner et al., 2008). The HCO_3^- produced in RBCs is rapidly transported across the membrane through a $\text{HCO}_3^-/\text{Cl}^-$ anion exchanger (AE1) into the more alkaline plasma (plasma pH 7.4 vs. RBC pH 7.25) (Greco & Solomon, 1997; Swietach et al., 2010). To prevent acidification within the RBC, H^+ is also buffered and often serves to stabilize deoxyhemoglobin, which will be discussed later in this section (Matthew et al., 1979a, 1979b; Chu & Ackers, 1981; Friend et al., 1981; Jensen, 2004). The movement of HCO_3^- into the plasma and the buffering of H^+ in RBCs facilitates further CO_2 hydration within these cells by shifting the reaction forward, according to Le Chatelier's Principle, and increases the CO_2 carrying capacity of the blood (Jensen, 2004).



The remaining CO_2 is bound to either plasma proteins or hemoglobin in RBCs (carbamino-hemoglobin) and accounts for between 5 and 10% of total CO_2 carried by the blood (Wieth et al., 1982; Levitzky, 2017). Carbon dioxide reacts rapidly with terminal amine groups on proteins to form carbamino compounds and an equal concentration of H^+ (Forster et al., 1968; Gros & Rollema, 1980). The affinity of CO_2 for Hb is influenced by several factors including RBC oxygen saturation (SO_2), 2,3-DPG concentration (a by-product of glycolysis), pH, and temperature (Christiansen et al., 1914; Dash & Bassingthwaite, 2010). The binding of H^+ and CO_2 to Hb proteins is significant because of the impact it has on the oxygen-dissociation curve. The oxygen-dissociation curve describes the amount of oxygen bound to tetrameric hemoglobin proteins (SO_2) at different partial pressures of O_2 (PO_2) and is sigmoidal in shape. The sigmoid shape of the curve was first described by Bohr et al. (1904) and is physiologically important as it

facilitates optimal binding and dissociation of O₂ to and from Hb (Jensen, 2004; Levitzky, 2017). The steepness of the curve demonstrates that as tissue PO₂ decreases along the vascular tree, more O₂ bound to hemoglobin in RBCs dissociates and diffuses into the tissue. This is due to interactions between the four subunits of the Hb protein which each contain a heme group and an O₂ binding site. Under high oxygen conditions, such as that found in the lungs, the binding of O₂ to one subunit induces a series of conformational changes that make successive O₂ binding to other subunits easier, which allows for the transition between deoxy- and oxyhemoglobin conformations (Perutz, 1970, 1972; Baldwin & Chothia, 1979; Perutz et al., 1998). The reverse occurs when O₂-saturated RBCs pass through low O₂ environments, such as in the capillaries, which facilitates the dissociation of O₂ from Hb to match the metabolic demand of the tissue (Levitzky, 2017). The flatness of the curve during high PO₂ conditions (above 70 mmHg), such as in the lungs, is also important because it prevents a significant drop in RBC SO₂ in response to moderate decreases in PO₂ between 70 and 100 mmHg (when T = 37 °C, PCO₂ = 5%, and pH = 7.4) (Figure 1.1) (Levitzky, 2017). Therefore, during conditions of decreased PO₂, the amount of O₂ carried in the systemic circulation as oxyhemoglobin remains constant which enables the oxygen demands of the tissues to still be met. It is important to note that this range of PO₂ values is dependent on the P₅₀ value of O₂ binding to Hb, which will vary if the oxygen-dissociation curve is shifted and can vary considerably between Hb proteins of different species (Cartheuser, 1993). In addition to being influenced by PO₂, the oxygen-dissociation curve is sensitive to other factors including temperature, 2,3-DPG, pH, and CO₂ that cause the curves to be shifted to the left or right in response to alterations in these parameters (Figure 1.1) (Bohr et al., 1904; Nelson et al., 1981; Zwart et al., 1982; Dash & Bassingthwaite, 2010).

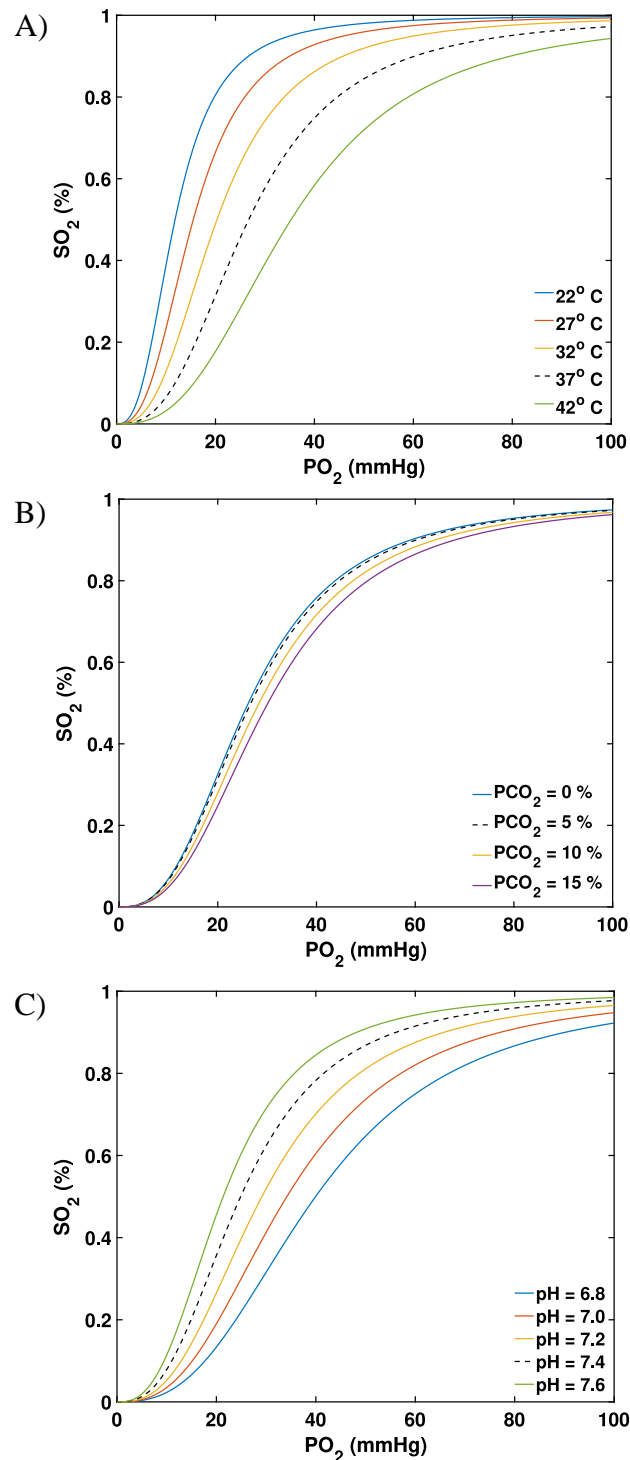


Figure 1. 1. Hemoglobin (Hb) oxygen-dissociation curves generated based on human Hb P_{50} (36 mmHg). The sigmoid-shaped curves plot the change in Hb oxygen saturation (SO_2) as a function of the partial pressure of O_2 (PO_2). The oxygen-dissociation curves experience right- and left-handed shifts in response to various stimuli, including temperature (A), the partial pressure of CO_2 (PCO_2) (B), and pH (C). Generated based on the model developed by Dash and Bassingthwaite (2010).

The influence of CO₂ and pH on the oxygen-dissociation curve is known as the Bohr effect (Bohr et al., 1904). During conditions of low pH and/or high CO₂, the oxygen-dissociation curve is shifted to the right (Figure 1.1). This shift decreases Hb's affinity for O₂ binding by requiring a higher PO₂ to reach a certain RBC SO₂. The mechanism underlying the Bohr effect involves the differing pKa values of the two hemoglobin protein conformations: oxyhemoglobin and deoxyhemoglobin (Kilmartin et al., 1973; Jensen, 2004). The pKa value describes the strength of acidic molecules and their ability to donate/accept protons (H⁺), with lower pKa values representing stronger acids. When hemoglobin undergoes a conformational change, the amino acids within the protein, and their associated hydrogen atoms, experience a different chemical environment and therefore have a different pKa value associated with them (Kilmartin et al., 1973; Jensen, 2004). Deoxyhemoglobin has a higher pKa value than oxyhemoglobin and therefore is a weaker acid that accepts H⁺ more readily (Kilmartin et al., 1973). Therefore, the H⁺ produced during both CO₂ hydration and carbaminohemoglobin formation stabilizes deoxyhemoglobin proteins, decreases Hb binding affinity for O₂, and promotes O₂ release into the surrounding tissue (Matthew et al., 1979a, 1979b; Chu & Ackers, 1981; Friend et al., 1981; Jensen, 2004).

In addition to the impact of CO₂ and pH on oxygen saturation, oxygen saturation also influences the binding of CO₂ and H⁺ to Hb, which is known as the Haldane effect (Christiansen et al., 1914). When O₂ binds to Hb, it induces a conformational change that alters the CO₂ binding site and its affinity for Hb. Therefore, increased O₂ binding in high PO₂ environments, such as in the lungs, decreases hemoglobin's affinity for CO₂ which facilitates its dissociation into the blood and removal by the lungs. The reverse occurs in low PO₂ environments which facilitates O₂

delivery and CO₂ removal from the tissues. In addition, the influence of HbO₂ on H⁺ binding can also be explained by the differing acidities of oxy- and deoxyhemoglobin since H⁺ binds more readily to weaker acids (deoxyhemoglobin) than stronger acids (oxyhemoglobin) (Christiansen et al., 1914; Kilmartin et al., 1973; Jensen, 2004). The physiological relevance of the sigmoid oxygen-dissociation curve and its sensitivity to the tissue environment supports a crucial role for RBC SO₂ in regulating proper gas transport to and from tissue environments. It has been hypothesized that changes in saturation may have an active role in coordinating local blood supply to match metabolic demand, which will be discussed in the next section.

1.4 The Role of Erythrocyte-derived Adenosine Triphosphate (ATP) Release in Blood Flow Regulation

Adenosine triphosphate (ATP) is an essential energy source produced during cellular respiration and is required for the optimal functioning of many cellular processes. To meet the energetic demand of highly metabolically active tissues, such as skeletal muscle and brain tissue, an adequate amount of oxygen must be delivered to ensure that sufficient ATP can be produced to sustain proper cellular functioning. This requires blood flow distribution to be a highly regulated process with signals being coordinated among different levels of the vascular tree as well as having mechanisms in place to communicate metabolic demand to the vascular system, as described in section 1.2 (Segal, 2005; Sarelius & Pohl, 2010; Bagher & Segal, 2011b; Murrant & Sarelius, 2015). While coordination between muscle metabolism and blood supply is widely accepted, and extensive research has been conducted to investigate the role of several vasoactive agents in this response, including ATP, the underlying mechanisms used to sense changing oxygen levels within the tissues and initiate appropriate vascular responses is still under investigation. Several potential oxygen sensor locations and mechanisms of action underlying

O₂-mediated blood flow regulation have been proposed and reviewed; however, this thesis will focus on mechanisms that may also be sensitive to variations in tissue CO₂ and pH and therefore, serve as a potential link between CO₂- and O₂-mediated blood flow responses (Ellis et al., 2012; Pittman, 2013; Jackson, 2016).

One potential location for the oxygen sensor is the red blood cell (RBC) itself. RBCs have an important role in convective oxygen transport by carrying large amounts of oxygen bound to hemoglobin (Hb) molecules as oxyhemoglobin (carries 20.1 mL of O₂ per 100 mL of blood) (Levitzky, 2017). In addition to oxyhemoglobin content, RBCs also contain a large amount of intracellular ATP molecules (Miseta et al., 1993). ATP is a vasoactive molecule that can influence the amount of blood flow, and therefore oxygen supply, being directed towards the tissues by initiating vascular responses via purinergic receptors (P_{2Y} and P_{2X}) located on vascular endothelial and smooth muscle cells (Ballard, 2014). Previous research has provided evidence supporting both a significant increase and decrease in arteriolar diameter in response to intra- and extraluminal administration of ATP, respectively (Ellsworth et al., 1995; McCullough et al., 1997; Dietrich et al., 2000; Nyberg et al., 2013). In addition, ATP-mediated changes in arteriolar diameter are transmitted from the site of stimulation into upstream vessels and capillary RBC supply rates have been shown to increase in striated muscle tissue following the application of ATP near capillary beds (Ellsworth et al., 1995; McCullough et al., 1997; Dietrich et al., 2000; Dora, 2017). These findings suggest that ATP-mediated vascular responses can be communicated into larger upstream vessels to initiate significant changes in both the magnitude and distribution of blood flow (Nyberg et al., 2013). Therefore, the ability for RBCs to act as an oxygen sensor and efficiently release ATP molecules suggests that they would be able to both

sense changes in tissue metabolism as well as initiate appropriate blood flow responses to match oxygen supply with demand (Ellis et al., 2012).

Initiation of RBC-derived ATP release has been proposed to occur in response to physiological stimuli such as simultaneous hypoxia and hypercapnia (Bergfeld & Forrester, 1992), hypoxia independently (Ellsworth et al., 1995; Dietrich et al., 2000; Sridharan, Adderley, et al., 2010; Sridharan, Sprague, et al., 2010; Racine & Dinunno, 2019), and independent pH changes (Ellsworth et al., 1995) as well as in response to mechanical deformation of RBCs (Sprague et al., 1998; Wan et al., 2008; Racine & Dinunno, 2019). The influence of hypoxia on RBC-derived ATP release is one of the most commonly studied initiation processes and low O₂ conditions have been associated with an increase in the extracellular concentration of ATP (Ellsworth et al., 1995; Dietrich et al., 2000; Sridharan, Adderley, et al., 2010; Sridharan, Sprague, et al., 2010; Racine & Dinunno, 2019). In addition, hypoxia-induced increases in extracellular ATP only occurs when RBCs are flowing through the vessels, providing strong evidence for the direct role of RBCs in this response (Dietrich et al., 2000). The shift in RBC oxygen saturation (SO₂), from oxyhemoglobin to deoxyhemoglobin, has a significant role in linking changes in the oxygen environment to RBC-derived ATP release (Jagger et al., 2001). The hypoxia-induced increase in extracellular ATP has been shown to be strongly correlated to changes in RBC SO₂ and ATP release is attenuated when deoxyhemoglobin concentrations remain constant under hypoxic conditions (Jagger et al., 2001). In addition to stimulating RBC-derived ATP release, changes in the deoxyhemoglobin concentration can influence ATP synthesis in RBCs by increasing the number of glycolytic enzymes available for glycolysis by competitively binding to a common membrane protein (Jagger et al., 2001). The involvement of glycolysis and increased ATP

synthesis have been studied in relation to hypoxia-induced ATP release and it has been shown that blocking key glycolytic enzymes attenuates the response (Jagger et al., 2001). These pieces of evidence provide support for SO_2 -dependent ATP synthesis and release from RBCs under conditions consistent with increased tissue metabolism and provide a potential link between O_2 and CO_2 mediated responses (Jagger et al., 2001).

Another important mechanism involved in RBC-derived ATP release is mechanical deformation of RBCs, which occurs when cells pass through smaller vessels and/or experience an increased flow rate (Sprague et al., 1998; Olearczyk et al., 2004; Wan et al., 2008). Mechanical deformation of RBCs via passage through small pores has been shown to significantly increase extracellular ATP (Sprague et al., 1998; Olearczyk et al., 2004; Wan et al., 2008) and reduced membrane deformability impairs hypoxia-induced release of ATP from RBCs (Sridharan, Sprague, et al., 2010; Racine & Dinunno, 2019). These bodies of evidence supports the importance of membrane deformation in RBC-derived ATP release and provide a link between mechanical (deformation) and physiological (O_2) stimuli in coordinating oxygen demand with supply (Sprague et al., 1998; Olearczyk et al., 2004; Wan et al., 2008; Sridharan, Sprague, et al., 2010; Racine & Dinunno, 2019). The presence of shear stress-dependent vasoactive mechanisms in the blood is especially relevant in vessels that experience a high degree of shear stress due to their small radii and relatively slower flow rates, i.e., in arterioles and capillaries (Lipowsky et al., 1978; Lipowsky et al., 1980; Papaioannou & Stefanadis, 2005)

Due to their size and anionic charge, ATP molecules cannot cross RBC membranes by diffusion, and it has been suggested that a signal transduction pathway is involved in releasing ATP from

the cells (Sprague et al., 2002; Olearczyk et al., 2004; Ellsworth et al., 2016; Richardson et al., 2020). Currently, it is thought that the activation of two subclasses of heterotrimeric G proteins (G_i and G_s) present in RBC membranes, possibly in response to mechanical deformation, are responsible for initiating the signal transduction pathway (Sprague et al., 2002; Olearczyk et al., 2004; Sridharan, Sprague, et al., 2010; Racine & Dinunno, 2019). Activated G proteins stimulate adenylyl cyclase enzymes within the RBC membrane which then increases production of cyclic adenosine monophosphate (cAMP), a second messenger involved in a wide variety of cellular processes (Sprague et al., 2001; Olearczyk et al., 2004; Sridharan, Sprague, et al., 2010; Racine & Dinunno, 2019). It is thought that cAMP then activates protein kinase A (PKA), which can phosphorylate a wide variety of targets including cystic fibrosis transmembrane conductance regulator (CFTR) (Sprague et al., 2001; Ellsworth et al., 2016; Richardson et al., 2020). Previous research has provided evidence supporting a crucial role of CFTR in deformation-induced RBC ATP release, however, it is unclear if CFTRs act as an ATP channel or if they influence other proteins (Sprague et al., 1998). Other channels have also been shown to be involved in hypoxia-induced ATP release, including integral membrane proteins band 3 and 4.5 as well as pannexin channels; however, controversial evidence regarding the role of pannexin channels has been reported (Bergfeld & Forrester, 1992; Sridharan, Adderley, et al., 2010; Qiu et al., 2011; Keller et al., 2017; Kirby et al., 2021). Finally, released ATP initiates vascular responses by stimulating the synthesis of vasoactive stimuli, such as nitric oxide (McCullough et al., 1997; Collins et al., 1998; Liang et al., 2005). The ATP-mediated vascular responses are thought to be controlled by a negative feedback loop due to the action of adenosine diphosphate (ADP), a by-product of ATP consumption, on $P2Y_{13}$ receptors located on RBC membranes (Wang et al., 2005).

Extensive evidence has been provided to support a mechanistic and regulated release of ATP from RBCs in response to both mechanical and physiological stimulation. However, it is also important to acknowledge the possible contribution of RBC hemolysis in increasing extracellular ATP concentrations. Previous evidence points to both shear stress and hypoxia-induced increases in extracellular ATP, which strongly is correlated to an increase in free hemoglobin concentration in the plasma, indicating that RBC hemolysis may have a significant contribution of ATP release (Sikora et al., 2014; Luneva et al., 2016). However, most studies supporting a mechanistic release of ATP from RBCs did control for the possible contribution of hemolysis in increasing extracellular ATP concentrations by excluding samples containing free hemoglobin in the supernatant following centrifugation. Therefore, it has also been suggested that RBC hemolysis and regulated RBC-derived ATP release both contribute to increased extracellular ATP, with the magnitude of RBC hemolysis contribution varying between normal and hypoxic conditions (20 - 50% vs. <10% of ATP from hemolysis, respectively) (Mairbaurl et al., 2013).

While the relationship between O₂-mediated blood flow regulation and RBC-derived ATP release has been investigated, the involvement of CO₂ in this release has not been an active area of investigation. Previous research has shown that simultaneous exposure to both hypoxia and hypercapnia, as well as independent changes in pH, were able to increase extracellular ATP (Bergfeld & Forrester, 1992; Ellsworth et al., 1995). However, these studies have yet to be completed *in vivo* and the independent role of CO₂ in RBC-derived ATP release has not been determined. Due to simultaneous changes in oxygen and carbon dioxide during conditions of elevated metabolism, such as during exercise, it is possible that an overlapping vasoactive pathway exists between the two molecules. However, the relationship and potential mechanistic

interaction between the two vasoactive stimuli is yet to be defined. The ability for both O₂ and CO₂ to influence the oxygen-dissociation curve and the SO₂-dependence of RBC-derived ATP release presents the possibility that the mechanism outlined above could also serve as a potential mechanism of CO₂-mediated blood flow regulation and a link between CO₂- and O₂-induced vascular responses. The relationship and potential mechanistic overlap between CO₂- and O₂-mediated microvascular blood flow regulation will be investigated in the current thesis through the simultaneous recording of capillary hemodynamic and RBC SO₂ measurements during both localized CO₂ and O₂ perturbations in skeletal muscle tissue, which addresses objective 3 outlined in section 1.1.

1.5 CO₂-mediated Microvascular Blood Flow Response and Suggested Underlying Mechanisms

Carbon dioxide produced within cells and tissues is not passively transported by the circulatory system but has an active involvement in its regulation by influencing vascular tone and blood flow. The vasoactive property of CO₂ has been established in a variety of vascular beds, including the microcirculatory systems within striated muscle and cerebral tissue. Elevation and depression of CO₂ concentrations, either in the blood or in the tissue, causes arteriolar vasodilation and vasoconstriction, respectively (Raper et al., 1971; Duling, 1973a; Kontos, Raper, et al., 1977; Kontos, Wei, et al., 1977; Wei et al., 1980; Ward, 1996). The degree of CO₂ reactivity of microvessels appears to differ between vascular beds (Kontos, Wei, et al., 1977; Ward, 1996). For example, pial arterioles in the cerebral microcirculation display strong vascular responses to changes in CO₂ between 0 and ~60 mmHg, while the diaphragmatic microcirculation does not experience a significant response until CO₂ concentrations above 80 mmHg are achieved (Kontos, Wei, et al., 1977; Ward, 1996). In addition to variable CO₂

reactivity between vascular beds, there is variability within vascular beds as well (Raper et al., 1971; Wei et al., 1980; Ward, 1996). The magnitude of CO₂-induced vascular responses is dependent on vessel size, with greater percent increases in arteriolar diameter being observed as vessel size decreases (Raper et al., 1971; Wei et al., 1980; Ward, 1996). The vessel-size dependency of CO₂-mediated responses may be due to the greater ability to influence CO₂ and/or pH in smaller, thin-walled vessels that support smaller blood volumes and lower relative blood flow rates. This hypothesis can be rationalized with Fick's 1st law of diffusion (2), which states that the movement of a substance across a surface or membrane is proportional to its concentration gradient.

$$Flux = -DkA \frac{dP}{dx} \quad (2)$$

Where D is diffusivity, k is solubility, A is area for diffusion, P is partial pressure, or concentration in the case of a solute, and x is the distance. Therefore, it is likely easier to influence the CO₂ concentration gradient between the tissue and the bloodstream and to facilitate diffusion of CO₂ into smaller vessels that are not rapidly supplied with large volumes of blood at arterial PCO₂. Differences in the magnitude of CO₂-induced responses based on location and vessel size demonstrate that conclusions drawn from one vascular bed cannot necessarily be translated to another and highlights the need to characterize responses in different tissues with varying metabolic demands, and at different levels of vasculature, to gain a complete understanding of blood flow regulation.

To date, the microvascular response to variations in CO₂ concentrations has been most well defined in cerebral microvessels. Graded increases in arteriolar diameter have been observed in

response to a stepwise increase in tissue CO₂ (Kontos, Wei, et al., 1977). The reactivity of arterioles to variations in tissue CO₂ concentrations (0 – 275 mmHg) depends on the magnitude of the CO₂ perturbation, with arterioles experiencing the greatest percent increase in diameter per 1 mmHg change in CO₂ between 0 and 60 mmHg (25% decrease between 0 and 43 mmHg and 12% increase between 43 and 60 mmHg) (Kontos, Wei, et al., 1977). The CO₂ reactivity of arterioles was shown to decrease above 60 mmHg of CO₂, with greater increases in CO₂ concentrations yielding a smaller percent change in arteriolar diameter per 1 mmHg change in CO₂ (7% increase in arteriolar diameter between 60 and 150 mmHg) (Kontos, Wei, et al., 1977). While the magnitude of cerebral arteriolar diameter changes to variations in tissue CO₂ concentrations have been described, the microvascular response in skeletal muscle tissue is yet to be fully characterized. The current thesis aims to address this gap in our understanding of CO₂-mediated blood flow regulation by providing direct measurements of both the magnitude and time transient of capillary hemodynamic responses to local CO₂ perturbations in skeletal muscle tissue (objective 1). It is necessary to develop a clear understanding of CO₂-mediated microvascular responses under normal conditions before investigating other questions, such as potential underlying mechanisms.

While the vasoactive property of CO₂ is well-established, the underlying mechanism responsible for CO₂-induced microvascular blood flow regulation, especially in skeletal muscle tissue, is not well defined. It has been suggested that local changes in tissue CO₂ initiate strong microvascular responses and that tissue CO₂'s influence on the microvascular system is a significant contributor to the vasoactive response observed due to variations in systemic CO₂ (Kontos, Wei, et al., 1977). The local action of CO₂ on smaller microvessels (under 100 μ m) is further supported by

the lack of involvement of neural activity (Wei et al., 1980; Wang et al., 1994; Pelligrino et al., 1995). Previous research has demonstrated that blocking neural activity was able to enhance hypercapnia-induced increases in arteriolar dilation in larger arterioles; however, they were unable to alter the CO₂-response in smaller arterioles (Wei et al., 1980; Wang et al., 1994; Pelligrino et al., 1995). These results suggest that the involvement of neural activity in regulating CO₂-mediated blood flow responses may decrease with vessel size. In addition, investigation of CO₂-induced responses in the cremaster microcirculation has indicated that while CO₂ is able to induce local arteriolar dilation, it is not able to initiate a significant conducted vascular response (Charter et al., 2018). Therefore, it has been suggested that CO₂ may exert its effects by influencing other vasodilators and/or regulatory mechanisms (Charter et al., 2018). While little is known regarding the mechanisms involved in CO₂-mediated microvascular responses in skeletal muscle, there have been some mechanisms investigated in the cerebral microcirculation, including the involvement of pH-dependent responses, adenosine, and NO that may also apply in other tissues and will be discussed in this section.

Due to the close relationship between CO₂ and H⁺ concentrations through the bicarbonate buffer system, one of the most common mechanisms associated with CO₂-induced vascular responses involves the corresponding change in pH. Decreasing and increasing pH surrounding arterioles results in significant arteriolar dilation and constriction, respectively (Kontos, Raper, et al., 1977; Charter et al., 2018). In addition, the magnitude of vascular responses to local changes in pH remained constant during simultaneous changes in CO₂ concentration and altering CO₂ independently of pH was unable to initiate changes in arteriolar diameter (Kontos, Raper, et al., 1977). Changes in extracellular pH have been suggested to be the primary mediator of acidosis-

induced vascular responses through action on vascular smooth muscle cell membranes (Kontos, Raper, et al., 1977; Toda et al., 1989; Tian et al., 1995). Vascular smooth muscle cell relaxation in response to elevated CO₂ was reversed following neutralization of pH (Toda et al., 1989; Tian et al., 1995). It has also been shown that decreasing pH while maintaining a physiological CO₂ concentration initiated a similar increase in cerebral artery relaxation as observed during hypercapnic conditions (You et al., 1994). These results suggest that CO₂-induced changes in pH have a significant role in CO₂-mediated blood flow regulation. One mechanism for pH-induced changes in vascular tone involves H⁺ outcompeting calcium ions (Ca²⁺) for shared binding sites on the sarcolemma, the sarcoplasmic reticulum, and contractile proteins in vascular smooth muscle cells, which results in smooth muscle relaxation (Wei et al., 1974). It has also been recently suggested that changes in extracellular pH activate acid-sensing ion channels (ASIC) expressed in neurons to initiate changes in CO₂-induced vasodilation; however, the expression and involvement of these channels in regulating microvascular tone in skeletal muscle tissue has not been defined (Faraci et al., 2019). While there is strong evidence supporting pH-dependent CO₂-mediated blood flow responses, most studies have not investigated the independent effects of CO₂ and as a result, the direct involvement of CO₂ in initiating vascular responses is not well defined. One study conducted by Charter et al. (2018) has provided evidence in the cremaster microcirculation that CO₂ initiates local arteriolar vasodilation during constant pH conditions. Therefore, it is possible that both pH-dependent and independent mechanisms are responsible for CO₂-mediated blood flow regulation. However, the mechanism that CO₂ and/or H⁺ uses to influence vascular tone is still under investigation.

One vasodilator suggested to be involved in CO₂-induced blood flow responses is NO. NO has been shown to be involved in coordinating cerebral blood flow responses with tissue metabolic demand as well as increase in concentration during hypercapnic conditions (Goadsby et al., 1992; Harada et al., 1997; Fathi et al., 2011). Previous research has supported the involvement of NO in CO₂-mediated blood flow responses by demonstrating that nitric oxide synthase (NOS) inhibition significantly attenuates, but does not eliminate, hypercapnia-induced increases in cerebral blood flow and arteriolar diameter as well as decreases vascular CO₂ reactivity (Iadecola, 1992; Wang et al., 1992; Pelligrino et al., 1993; Faraci et al., 1994; Iadecola & Zhang, 1994; Iadecola et al., 1994; Irikura et al., 1994; Wang et al., 1994; Reid et al., 1995; Ma et al., 1996; Estevez & Phillis, 1997; Schmetterer et al., 1997; Wang et al., 1998; Phillis et al., 2004). In addition, the degree of NO involvement appears to be dependent on the magnitude of the CO₂ concentration (Wang et al., 1992; Iadecola & Zhang, 1994). Previous studies have shown that NOS inhibition depresses CO₂-induced blood flow responses during moderate hypercapnia (40-80 mmHg CO₂) but does not impact responses during severe hypercapnia (100-200 mmHg CO₂) or during hypocapnia (Wang et al., 1992; Iadecola & Zhang, 1994). Based on these findings, it has been suggested that the mechanism(s) underlying CO₂-mediated blood flow regulation may differ based on the severity of hypercapnia (Iadecola & Zhang, 1994).

The source of NO production during hypercapnia and the specific mechanism(s) underlying its involvement has also been investigated. Currently, it is thought that neuronal NOS (nNOS) is the primary source of NO during hypercapnia and that NO has a permissive role in regulating CO₂-induced cerebral blood flow responses through a cyclic guanosine monophosphate (cGMP)-dependent pathway (Iadecola et al., 1994; Irikura et al., 1994; You et al., 1994; Ma et al., 1996;

Harada et al., 1997; Okamoto et al., 1997; Wang et al., 1998). Previous work has demonstrated that CO₂-induced increases in cerebral blood flow and arteriolar diameter are significantly reduced in the absence of functional nNOS, either by selective pharmacological inhibition or by using a type III NOS knockout animal model (Ma et al., 1996; Harada et al., 1997; Okamoto et al., 1997; Wang et al., 1998). In addition, variations in CO₂ have been shown to elicit vascular responses in the presence of endothelial cell damage and perivascular nerve inhibition, which suggests that these structures are not the source of NO during hypercapnia (Wang et al., 1994; You et al., 1994). Whether NO has a direct or permissive role in CO₂-mediated blood flow regulation has also been questioned. A permissive role suggests that a basal concentration of a substance is required for a process to occur while not being directly involved in the process itself. Previous studies have shown that hypercapnia-induced vascular responses that were inhibited after blocking NOS enzymes could be restored when the NO concentration was restored, which suggests that the presence of functional NOS enzymes is not necessary to observe a hypercapnic vascular response, that NOS activity is not directly responsible for the response, and that NO is likely involved by regulating the concentration of cGMP (Iadecola et al., 1994; Irikura et al., 1994; You et al., 1994; Okamoto et al., 1997; Wang et al., 1998). The involvement of cGMP is supported by a variety of findings; including, inhibition of CO₂-induced vascular relaxation following cGMP inhibition, an increase in the cGMP concentration during hypercapnia that is inhibited following NOS inhibition, and restoration of CO₂-induced responses following NOS inhibition through the replenishment of the cGMP concentration (Iadecola et al., 1994; Irikura et al., 1994; You et al., 1994; Wang et al., 1998). Together, these findings provide support for cGMP-dependent NO pathway underlying CO₂-mediated blood flow regulation; however, there are also studies that were unable to replicate these findings and

have suggested that both NO and cGMP are not essential for the observed CO₂-mediated vascular response (You et al., 1994; White et al., 1998; Rosenblum et al., 2002; Nakahata et al., 2003).

Adenosine is another endogenous vasodilator that is produced during conditions of increased metabolism and has an important role in coordinating blood flow with metabolic demand in both skeletal muscle and cerebral tissues (O'Regan, 2005; Ballard, 2014). Evidence supporting a role for adenosine in CO₂-mediated blood flow regulation has been provided in the cerebral circulation (Phillis & DeLong, 1987; Ibayashi et al., 1988; Simpson & Phillis, 1991; Estevez & Phillis, 1997; Phillis et al., 2004). An increase in adenosine concentration has been measured during hypercapnic conditions, and it has been suggested that adenosine influences CO₂-mediated blood flow responses by stimulating A_{2A} adenosine receptors (Phillis & DeLong, 1987; Estevez & Phillis, 1997; Phillis & O'Regan, 2003; Phillis et al., 2004). To support this hypothesis, previous studies have shown that inhibition of adenosine receptors and decreased adenosine availability both depress hypercapnia-induced increases in cerebral blood flow and arteriolar vasodilation as well as increases the magnitude of vasoconstriction observed during hypocapnic conditions (Phillis & DeLong, 1987; Ibayashi et al., 1988; Simpson & Phillis, 1991; Estevez & Phillis, 1997; Phillis et al., 2004). The reverse occurs when adenosine availability is increased, which amplifies the hypercapnia-induced increase in blood flow and reduces the magnitude of hypocapnia-induced vasoconstriction (Phillis & DeLong, 1987; Ibayashi et al., 1988). Together, these results support the involvement of adenosine in CO₂-mediated blood flow regulation in the cerebral circulation, including at the microvascular level.

However, some studies were unable to replicate these results and provided evidence against adenosine involvement in CO₂-induced blood flow responses. Some previous research has shown that hypercapnia-induced increases in cerebral blood flow and decreases in vascular resistance were not impacted following adenosine receptor inhibition (Emerson & Raymond, 1981; Hoffman et al., 1984; Morii et al., 1987). In the microcirculation, hypercapnia-induced arteriolar vasodilation was also maintained following administration of adenosine receptor antagonists as well as in A_{2A} receptor knock-out mice (Pelligrino et al., 1995; Miekisiak et al., 2009). In addition, unlike the size-dependency of vessel responsiveness to CO₂, adenosine-induced arteriolar vasodilation was not dependent on vessel size (Morii et al., 1986). One explanation for these findings may be that since it is more difficult to alter partial pressure of CO₂ (PCO₂) in larger, high flow vessels due to the continuous supply of CO₂, it may be more difficult to stimulate hypercapnia-induced adenosine-mediated blood flow responses. Another explanation that has been provided for these conflicting pieces of evidence is that there may be significant redundancy among CO₂-induced vasodilatory pathways (Phillis & O'Regan, 2003). To support this hypothesis, it has been shown that hypercapnia-induced increases in blood flow were only significantly attenuated by adenosine receptor antagonism in the presence of NOS inhibition; however, even during this combined inhibition, a pronounced hypercapnic response remained intact (Phillis & O'Regan, 2003). Together, these results suggest that adenosine may not be the only vasodilatory mechanism present during CO₂-mediated blood flow regulation and that both adenosine- and NO-independent pathways are also likely involved.

1.6 Involvement of Vascular K_{ATP} Channels in Microvascular Blood Flow Regulation

K_{ATP} channels are one of the many types of ion channels expressed in vascular cell membranes that have an important role in regulating vascular tone through their influence on membrane potential (Jackson, 1993, 2000b, 2005; Tykocki et al., 2017). K_{ATP} channels open and close in response to changes in intracellular concentrations of ATP and adenosine diphosphate (ADP). During conditions of decreased ATP and increased ADP, K_{ATP} channels open and cause membrane hyperpolarization through an efflux of K⁺. In vascular smooth muscle cells (VSMC), membrane hyperpolarization closes voltage-gated calcium channels which decreases Ca²⁺ influx and the amount cytosolic Ca²⁺ available for muscle contraction, resulting in vasodilation (Jackson, 2005; Tykocki et al., 2017). The reverse response occurs when K_{ATP} channels close during conditions of increased ATP and decreased ADP, which results in vasoconstriction (Jackson, 2005; Tykocki et al., 2017). Evidence supporting the expression of K_{ATP} channel subunits and their ability to initiate membrane hyperpolarization in endothelial cells, including those located within the microvascular system, has also been provided (Janigro et al., 1993; Langheinrich & Daut, 1997; Schnitzler et al., 2000; White & Hiley, 2000; Aziz et al., 2017). In endothelial cells, changes in membrane potential are believed to influence Ca²⁺ influx, likely through receptor-mediated mechanisms, and stimulate the release of endothelium-derived vasodilators such as NO (Jackson, 2005; Figueroa et al., 2007; Aziz et al., 2018). In addition, due to the electrical coupling present both along and between the endothelial and VSMC layers, K_{ATP} channel-mediated K⁺ efflux and the resulting endothelial cell membrane hyperpolarization initiated at the capillary level have been shown to be communicated into upstream arterioles to induce VSMC relaxation and vasodilation as well as influence downstream capillary blood flow (Beach et al., 1998; McGahren et al., 1998; Cohen & Sarelius, 2002; Murrant & Sarelius, 2002;

Hirai et al., 2021). Therefore, due to their ability to respond to changes in cellular metabolism, influence vascular tone along the vascular network and regulate downstream capillary blood flow, the role of K_{ATP} channels in blood flow regulation has been an active area of investigation and they have often been studied in relation to factors associated with CO_2 ; including functional hyperemia/muscle contraction, decreased pH, decreased O_2 , and release of adenosine and NO.

Functional (or active) hyperemia is a term used to describe increased blood flow during conditions of increased metabolic demand, such as during exercise. A mechanism of interaction between the tissue environment and the vascular system must be in place to ensure adequate amounts of oxygen and nutrients are being delivered to the tissue along with simultaneous removal of metabolic waste products, such as CO_2 . Vascular K_{ATP} channels have been suggested to be involved in the coordination of this response (Saito et al., 1996; Hammer et al., 2001; Cohen & Sarelius, 2002; Murrant & Sarelius, 2002; Holdsworth et al., 2016a; Colburn, Weber, et al., 2020; Hirai et al., 2021).

Previous research has demonstrated that exercise and muscle contraction-induced increases in hindlimb muscle blood flow and vascular conductance are significantly attenuated following administration of a selective K_{ATP} channel blocker, glibenclamide (GLI) (Holdsworth et al., 2016b; Colburn, Weber, et al., 2020). Vascular K_{ATP} channels are also involved in regulating hyperemic responses in the microcirculation with muscle contraction-induced arteriolar vasodilation being significantly attenuated following K_{ATP} channel blockade (Saito et al., 1996; Hammer et al., 2001; Cohen & Sarelius, 2002; Murrant & Sarelius, 2002). The degree of attenuation of the vasodilatory response with GLI varied with vessel size. Vasodilation in smaller

4th order arterioles was nearly abolished while vasodilation in larger arterioles (1st to 3rd order) was only attenuated (Saito et al., 1996; Hammer et al., 2001). In addition, local and conducted vasodilatory responses to muscle stimulation under capillary beds have been shown to be inhibited following capillary K_{ATP} channel blocking (Cohen & Sarelius, 2002; Murrant & Sarelius, 2002). The involvement of K_{ATP} channels in initiating conducted vascular responses shows that their activation can communicate changes in tissue environment to larger upstream vessels, which have the capacity to initiate significant changes in both the magnitude and distribution of blood flow directed towards the tissue. These results suggest that K_{ATP} channels are at least partially involved in mediating functional hyperemic responses and that they appear to have a greater contribution in smaller vessels that are in closer contact with the surrounding tissue environment (Saito et al., 1996; Hammer et al., 2001; Cohen & Sarelius, 2002; Murrant & Sarelius, 2002).

There is also evidence against the involvement of K_{ATP} channels in regulating functional hyperemic responses. There are a few studies that noted no attenuation of exercise-induced blood flow responses in the human forearm following selective K_{ATP} channel inhibition (Farouque & Meredith, 2003; Schrage et al., 2006). It has also been shown in the microcirculation that K_{ATP} channel inhibition was not able to significantly alter arteriolar diameter on its own and only had a significant impact when combined with NOS inhibition (Schemke & de Wit, 2021). To explain the variability of results, it has been suggested that K_{ATP} channels may have a different degree of involvement in different species, vascular beds, vessel sizes, and during different levels of exercise intensity (Saito et al., 1996; Farouque & Meredith, 2003; Schrage et al., 2006; Holdsworth et al., 2015).

Several changes in the tissue environment occur during conditions of increased cellular metabolism, including increased production of CO₂ and the corresponding change in pH. The activity of K_{ATP} channels expressed in cell membranes has been shown to be sensitive to variations in pH, which further supports a possible relationship between CO₂ and vascular K_{ATP} channels (Davies, 1990; Xu et al., 2001; Horiuchi et al., 2002; Wang et al., 2003). Hypercapnia-induced increases in whole-cell currents and membrane potential are significantly reduced following selective K_{ATP} channel inhibition; however, this hypercapnia-induced change in current and membrane potential is not observed when pH is maintained at a physiological level (Xu et al., 2001; Wang et al., 2003). These results indicate that the CO₂-induced change in pH is the primary mediator of the enhanced K_{ATP} channel activity and membrane current observed during hypercapnic conditions (Xu et al., 2001; Wang et al., 2003). Previous research has demonstrated that intracellular acidification (pH 7.2-6.0) of isolated cells has been shown to decrease the inhibitory action of intracellular ATP and magnesium (Mg²⁺) on K_{ATP} channels, which increases the probability of them being open and able to hyperpolarize cell membranes (Davies, 1990). In addition, acidosis-induced arteriolar vasodilation was reduced following selective K_{ATP} channel inhibition with GLI (Horiuchi et al., 2002). These pieces of evidence indicate that K_{ATP} channel activity is pH-sensitive and supports their potential involvement in regulating CO₂-mediated blood flow responses.

In addition to their pH-sensitivity and suggested involvement in the functional hyperemic response, K_{ATP} channels have also been linked to other factors related to CO₂; including O₂, adenosine, and NO. Hypoxia-induced increases in cerebral blood flow, vascular conductance, and arteriolar diameter have been shown to be attenuated following selective K_{ATP} channel

blocking (Reid et al., 1993; Taguchi et al., 1994; Bryan & Marshall, 1999; Rocha et al., 2020). In addition, the increased venous K^+ concentration measured during hypoxic conditions was significantly inhibited following administration of GLI (Marshall et al., 1993). These results suggest that K_{ATP} channels could be partially responsible for mediating cerebral vascular responses to hypoxia, including at the microvascular level. Adenosine-induced increases in microvascular blood flow and arteriolar diameter are also significantly attenuated by K_{ATP} channel blocking (Danialou et al., 1997; Bryan & Marshall, 1999; Chen et al., 2000). It has been suggested that adenosine may be involved in the vasodilatory mechanism underlying hypoxic vascular responses and be a link between hypoxia and K_{ATP} channel stimulation (Armstead, 1997; Bryan & Marshall, 1999). Hypoxia-induced arteriolar vasodilation, during both moderate and severe hypoxic conditions, was significantly attenuated following inhibition of adenosine receptors (Armstead, 1997). It has also been shown that adenosine-induced increases in blood flow, arteriolar diameter, and venous K^+ concentration are all significantly decreased following selective K_{ATP} channel blocking (Marshall et al., 1993; Danialou et al., 1997; Bryan & Marshall, 1999; Chen et al., 2000). Inhibition of NO synthesis has also been shown to significantly attenuate both hypoxia and adenosine-induced increases in vascular conductance and arteriolar vasodilation (Armstead, 1997; Danialou et al., 1997; Bryan & Marshall, 1999). Therefore, based on these findings, it has been suggested that hypoxia initiates arteriolar vasodilation through adenosine-induced stimulation of NO synthesis and activation of vascular K_{ATP} channels via a cGMP-dependent mechanism (Armstead, 1997; Danialou et al., 1997; Bryan & Marshall, 1999; Chen et al., 2000).

The presence of pH sensitive K_{ATP} channels in vascular cells and their ability to sense changes in cellular metabolism, initiate local and conducted vascular responses, and their connection to other factors linked to CO₂ (hypoxia, adenosine, and NO) all support the hypothesis that vascular K_{ATP} channels may be involved in mediating CO₂-microvascular blood flow regulation. Some evidence supporting their involvement in CO₂-mediated responses has been provided in the cerebral microcirculation. Selective inhibition of K_{ATP} channels in cerebral arterioles reduced hypercapnia-induced vasodilation and inhibited hypocapnic alkalosis-induced vasoconstriction (Faraci et al., 1994; Wei & Kontos, 1999; Nakahata et al., 2003; Nnorom et al., 2014). In addition, similar to the findings during functional hyperemia outlined above, the degree of attenuation of CO₂-induced responses following GLI administration was dependent on vessel size (Faraci et al., 1994; Nakahata et al., 2003; Nnorom et al., 2014). The vasodilatory response to elevated CO₂ in precapillary arterioles (under 10 µm in diameter) was abolished following K_{ATP} channel blockade, while the response in larger arterioles (above 55 µm in diameter) was only reduced (Faraci et al., 1994; Nakahata et al., 2003; Nnorom et al., 2014). These results suggest that vascular K_{ATP} channels are partially involved in CO₂-mediated cerebral microvascular blood flow regulation and that they have a more significant involvement as vessel size decreases. Although, as mentioned previously, the more pronounced impact on smaller vessels may be due to a greater ability to influence pH across thin-walled microvessels supporting slow, low volume blood flow. The incomplete inhibition of CO₂-induced responses following K_{ATP} channel blockade supports the involvement of K_{ATP}-independent pathways as well. Previous research has also shown that attenuation of hypercapnia-induced arteriolar responses following K_{ATP} channel blockade only occurred when nNOS was also inhibited, which has also been suggested to support the presence of redundant pathways (Wang et al., 1998).

While the role of vascular K_{ATP} -channels in CO_2 -mediated responses has been investigated in the cerebral microcirculation, their involvement in regulating tissue CO_2 in skeletal muscle has not been defined and will be investigated in the current thesis as a potential mechanism underlying CO_2 -mediated blood flow regulation at the capillary level in skeletal muscle tissue, thus addressing objective 2.

1.7 Intravital Video Microscopy (IVVM) and Striated Muscle Tissue Preparations

Intravital video microscopy (IVVM) is an experimental technique commonly used for *in vivo* investigations of both the structure and function of microvascular networks. IVVM combines the use of an inverted or upright microscope with a video recording system to enable simultaneous viewing and recording of microvascular responses to various stimuli, such as increased muscle metabolism and pharmacological interventions, as well as during pathophysiological conditions, such as diabetes (Cohen & Sarelius, 2002; Murrant & Sarelius, 2002; Padilla et al., 2006; Novielli & Jackson, 2014; Corliss et al., 2019). Several measurements quantifying microvascular responses can be obtained through the offline analysis of recorded video sequences, including microvessel diameter and hemodynamic measurements (such as red blood cell (RBC) velocity (V_{RBC}), supply rate (SR), lineal density, and hematocrit (Hct)). There are several advantages associated with using IVVM rather than isolated vessel segments to study microvascular responses; including, the ability to acquire large amounts of microvascular network and flow data per experiment and the ability to directly visualize and quantify microvascular responses *in vivo* with minimal disruption to the overall microvascular system and integrated blood flow responses.

Several types of tissue preparations have been developed for IVVM studies, including a variety of striated muscle tissues such as the cremaster, gluteus maximus, cheek pouch retractor, and extensor digitorum longus (EDL) muscles (Duling, 1973b; Tyml & Budreau, 1991; Bearden et al., 2004; Bagher & Segal, 2011a). Striated muscles are often used to investigate the coordination of microvascular blood flow responses to conditions of increased metabolism and oxygen demand, as well as to identify the mechanism of interaction between active muscle tissue fibers and the microvascular system (Cohen & Sarelius, 2002; Murrant & Sarelius, 2002; Ngo et al., 2010; Riemann et al., 2011). The surgical procedures for each of the preparations mentioned above are similar in that they each involve careful isolation, dissection, and externalization of the muscle tissue of interest to enable visualization with a compound microscope (Duling, 1973b; Tyml & Budreau, 1991; Bearden et al., 2004; Bagher & Segal, 2011a). In addition, they are all accessible thin muscles that can be easily positioned over the microscope objective and transilluminated to allow for optimal visualization of the microcirculation, while maintaining *in situ* dimensions and the endogenous blood supply to ensure minimal disruption to normal microvascular functioning (Duling, 1973b; Tyml & Budreau, 1991; Bearden et al., 2004; Bagher & Segal, 2011a). While there are similarities among muscle preparations, there are also some differences. Experiments involving the cremaster, gluteus maximus, and cheek pouch retractor muscles differ from the muscle preparation used in the current thesis, the EDL muscle, in that they are often continuously perfused with a buffered physiological salt solution (Duling, 1973b; Tyml & Budreau, 1991; Bearden et al., 2004; Bagher & Segal, 2011a). The movement of a superfusion solution over the muscle tissue alters the surface environment, and potentially microvascular responses, by continuously removing trace physiological molecules produced in the muscle tissue that are not included in the buffer formulation (Tyml & Budreau, 1991;

Ghonaim et al., 2011). In addition, using a superfusion solution to alter the gas concentration of tissues or apply pharmacological agents results in the muscle's environment being set for long periods, or even the entire duration of the experiment. The EDL muscle preparation used in the current thesis is not continuously superfused and is instead covered with a stagnant layer of saline that equilibrates with the tissue and maintains moisture, which allows the physiological environment of the muscle surface to remain intact and certain experimental conditions to be more dynamically controlled (Tyml & Budreau, 1991; Fraser et al., 2012). The use of different striated muscle tissue preparations also allows for microvascular responses and their potential underlying mechanisms to be studied in environments with varying muscle fiber compositions and metabolic activity levels, such as skeletal muscles that experience exercise conditions (EDL and gluteus maximus) and those that only experience muscle contraction (cremaster and cheek pouch retractor). Finally, the level of the microvasculature being studied may also vary with different muscle preparations. For example, the EDL is a skeletal muscle tissue preparation that allows for better visualization and quantification of capillary blood flow responses since the distal portion of the muscle is externalized for visualization, compared to the gluteus maximus muscle whose proximal end is externalized and often used to study arteriolar networks (feed artery to terminal arterioles) (Tyml & Budreau, 1991; Bearden et al., 2004; Al-Khazraji et al., 2012).

As briefly mentioned above, several microvascular measurements can be obtained from the offline analysis of recorded intravital video sequences of *in vivo* microvascular networks, including hemodynamic variables that directly describe blood flow (RBC velocity, SR, volume flow, flow distribution, capillary Hct, and RBC distribution) (Ellis et al., 1990; Ellis et al., 1992;

Japee et al., 2004; Al-Khazraji et al., 2012; Ellis et al., 2012; Fraser et al., 2012; McClatchey et al., 2018). Several methods have been developed for measuring RBC hemodynamics in both arteriole and capillary networks, including manual and computational methods. For example, one commonly used method involves the manual tracking of fluorescently labelled RBCs injected into the bloodstream, where RBC velocity and supply rate are measured visually as RBCs pass through each frame of recorded video sequences (Biswal & Hudetz, 1996; Krolo & Hudetz, 2000; Al-Khazraji et al., 2012; Novielli & Jackson, 2014). Another similar method, known as the “Streak Length Method”, enables RBC velocity to be calculated throughout branching arteriolar networks (21 - 115 μm in diameter), where fluorescent streaks created by the movement of labelled RBCs are visualized and measured to calculate RBC velocities ($V_{\text{RBC}} = (\text{RBC streak length} - \text{RBC length}) / \text{Exposure time}$) (Al-Khazraji et al., 2012; Novielli & Jackson, 2014). While these methods have provided valuable information regarding microvascular blood flow, there are some limitations associated with manual hemodynamic measurements; including, the time required to analyze each experiment, the small number of vessels analyzed per experiment, the risk of human error, and variations in measurements among researchers. To address these limitations, computer software systems have since been developed to analyze IVVM video sequences and quantify several microvascular blood flow parameters, such as RBC velocity, RBC SR, lineal density, flow velocity, flow distribution, plasma flow, capillary Hct and capillary Hct heterogeneity (Ellis et al., 1990; Ellis et al., 1992; Japee et al., 2004; Al-Khazraji et al., 2012; Ellis et al., 2012; Fraser et al., 2012; McClatchey et al., 2018; Akerstrom et al., 2020). The use of computer software systems allows for rapid, reliable, and reproducible microvascular blood flow measurements to be made by completing automated or semi-automated quantification of responses in a large number of capillaries and have been shown to yield RBC velocity

measurements similar to those obtained manually (Ellis et al., 1990; Ellis et al., 1992; Japee et al., 2004; Al-Khazraji et al., 2012; Ellis et al., 2012; Fraser et al., 2012; McClatchey et al., 2018).

In the current thesis, a custom MATLAB software was used for semi-automated analysis of recorded IVVM video sequences. The software processes the captured images of microvascular blood flow, compiles them into video sequences and uses them to generate a series of functional images that provide information on the structure of the microvascular network as well as RBC flow (Figure 1.2) (Japee et al., 2004). Measuring light intensity from spatial locations along the centreline of selected capillaries in every frame of the video allows RBCs, which absorb light and appear as dark spots, to be distinguished from the surrounding tissue and plasma, which appear lighter (Ellis et al., 1990; Ellis et al., 1992; Japee et al., 2004; Ellis et al., 2012; Fraser et al., 2012). The fundamental quantitative tool for determining capillary hemodynamics from the light intensity measurements is a space-time image, which are generated for each vessel segment that are manually selected for analysis and plot the light intensity information as a function of time (Figure 1.2) (Ellis et al., 1990; Ellis et al., 1992). Therefore, these images show the location of RBCs flowing through the selected capillaries throughout the entire video sequence and are used to determine hemodynamic measurements for each vessel (Figure 1.2) (RBC velocity ($\mu\text{m/s}$), RBC SR (cells/s), and Hct (%RBC)) (Ellis et al., 1990; Ellis et al., 1992; Japee et al., 2004; Ellis et al., 2012; Fraser et al., 2012). Compared to manual measurements, this software allows for semi-automated, reliable, and reproducible measurements of hemodynamic variables in a large number of in focus capillaries across multiple fields of view (FOV) or focal planes within the muscle. While this semi-automated analysis software is more time consuming and analyzes fewer capillaries than fully automated software's, which can analyze over 100

capillaries per FOV and generate measurements for individual capillaries in approximately 20 seconds (McClatchey et al., 2018), it allows for greater control over selected capillaries to ensure they are suitable for analysis. Also, further experimentation is required to determine the effectiveness of the fully automated software developed by McClatchey et al. (2018) since it only been used to analyze short sequences, has little associated microvascular network geometry data, and has not been widely used experimentally. The software used for this project addresses some of these limitations by providing information on both the microvascular network geometry and blood flow as well as being used to effectively quantify microvascular responses in a variety of experiments. Another advantage to the method used here is that it does not require the use of fluorescently labelled RBCs, exogenous fluorescent probes, or a fluorescent microscope to visualize and quantify RBC flow. In addition, IVVM video sequences were collected simultaneously at two different wavelengths, an oxygen-sensitive (438 nm) and -insensitive (420 nm) wavelength, which enables spectrophotometric RBC oxygen saturation (SO_2) measurements to be made based on the differing light absorptions of oxy- and deoxyhemoglobin proteins (Figure 1.3) (Ellsworth et al., 1987; Ellis et al., 1990; Ellis et al., 1992). Therefore, in addition to capillary hemodynamic measurements, the custom MATLAB software used in the current thesis provides simultaneous RBC SO_2 measurements which allows for convective oxygen transport and SO_2 -dependent regulatory mechanisms of the microvascular system to be investigated *in vivo* (Figure 1.2).

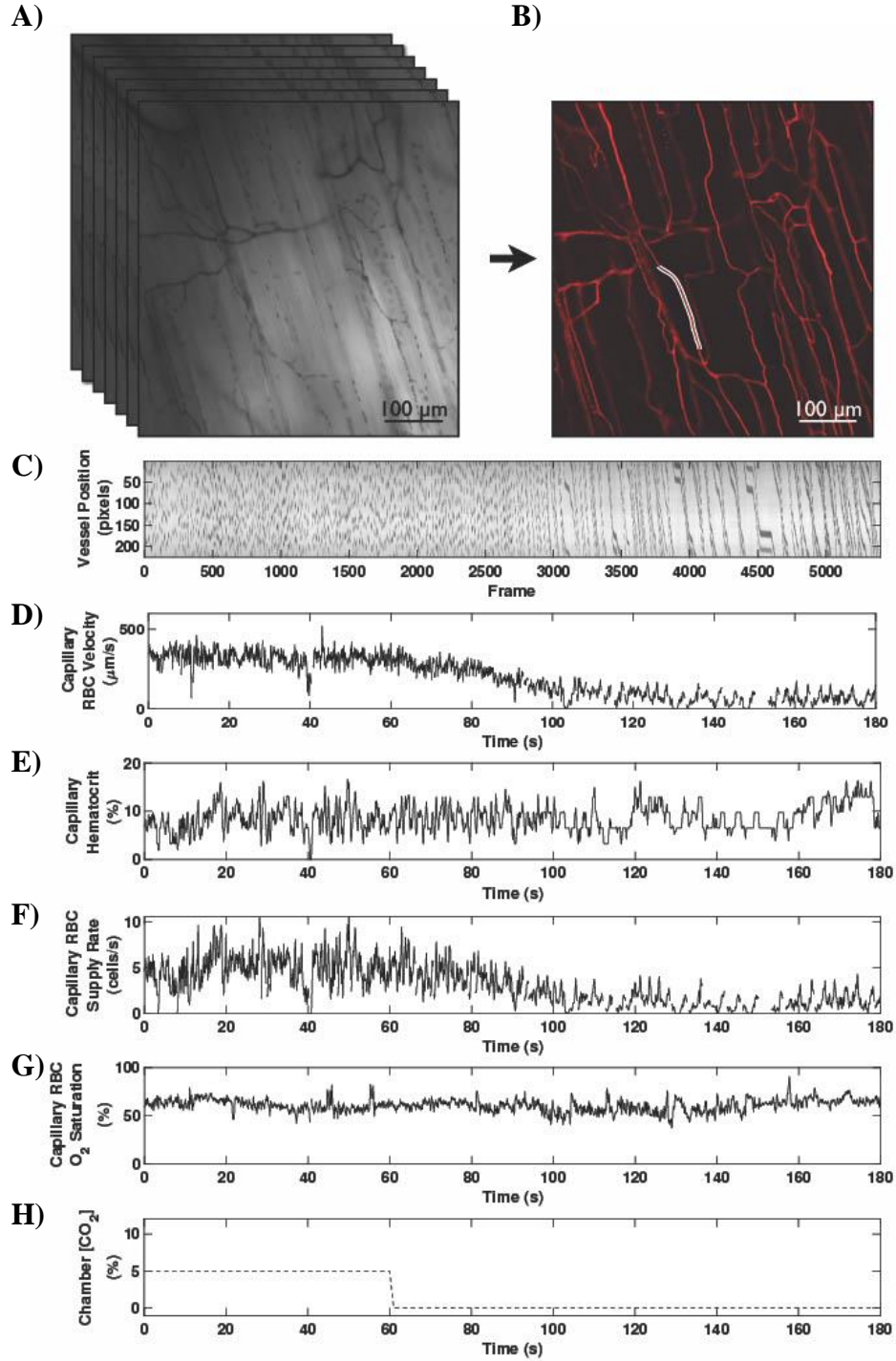


Figure 1. 2. An overview of the analysis process for intravital video microscopy (IVVM) sequences using a custom MATLAB software. A series of images captured during IVVM (A) are compiled into video sequences and used to generate a series of functional images (B). Functional images describe the network geometry, position of individual vessels, and are also used to identify capillary segments to be used for analysis. Space-time images (C) are generated for each capillary selected for analysis, which describe the position of red blood cells (RBC) flowing through the capillary segment in each frame of the video. Space-time images are used to quantify several hemodynamic measurements, such as RBC velocity (D), supply rate (E), hematocrit (F) as well as RBC oxygen saturation (SO_2) (G). The timing of the CO_2 step-change is represented by a dashed line (H).

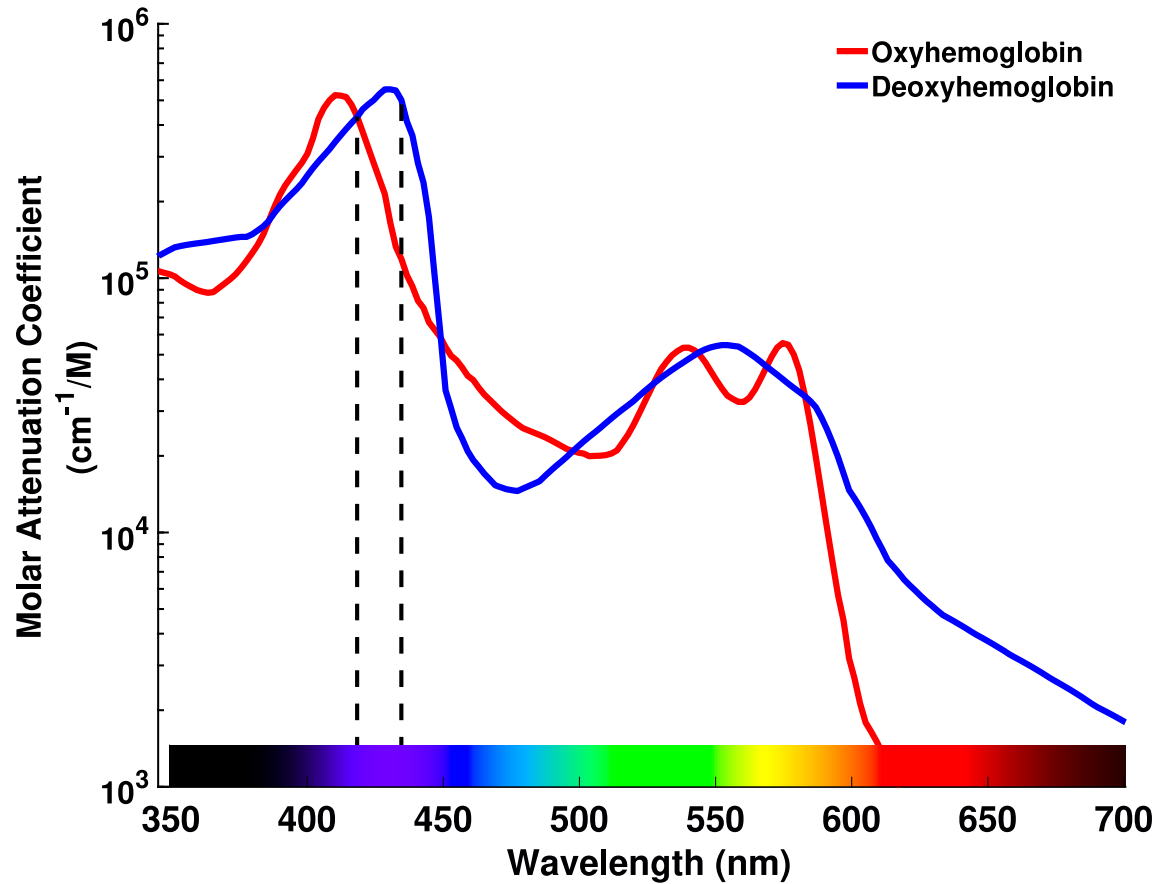


Figure 1. 3. Wavelength dependence of the deoxy- and oxyhemoglobin molar attenuation coefficient. The blue and red lines plot the light absorption of deoxyhemoglobin and oxyhemoglobin across various wavelengths, respectively. The two vertical dashed lines indicate an oxygen independent wavelength (420 nm) where both oxy- and deoxyhemoglobin have the same absorbance, and an oxygen sensitive wavelength (438 nm) where the light absorptions of the two hemoglobin conformations differ, which was used in the present thesis to measure red blood cell oxygen saturation (Adapted from Fraser (2012), based on data from Prahl (1999)).

1.8 Experimental Techniques Used to Alter Arterial and Tissue Gas Concentrations and the Use of a Microfluidic Gas Exchange Chamber

Previous investigations of both O₂- and CO₂-mediated microvascular responses have utilized two main experimental techniques, (i) alterations in inspired gases and (ii) topical superfusion solutions, to impose variations in arterial and tissue gas concentrations, respectively. Systemic changes in blood PO₂ and PCO₂ following either an increase or decrease in the respective inspired gas concentrations have been shown to initiate reliable and significant changes in microvascular tone (Raper et al., 1971; Wei et al., 1980; Morii et al., 1986; Morii et al., 1987; Ibayashi et al., 1988; Simpson & Phillis, 1991; Faraci et al., 1994; Taguchi et al., 1994; Wang et al., 1994; Armstead, 1997; Wang et al., 1998; Rosenblum et al., 2001; Phillis et al., 2004; Miekisiak et al., 2009). However, there are some limitations associated with this method that need to be considered. The main limitation is that systemic hypoxia and hypercapnia both have an impact on the overall systemic circulation, including alterations in cardiac output, heart rate, blood pressure, as well as an impact on sympathetic nerve activity and ventilatory responses (Richardson et al., 1961; Fukuda et al., 1989; Sabino et al., 2013; Jouett et al., 2015). Therefore, systemic changes in blood gas concentrations may have a more widespread impact on overall blood flow, which may influence the response observed at the microvascular level and complicate interpretations of collected data. The widespread influence of systemic changes also makes it difficult to determine the level of the vascular system and the identity of cell types involved in the initiation of the blood flow responses. Another limitation is the amount of time required to initiate maximum microvascular responses (several minutes), which makes it difficult to measure the time transient of the resulting blood flow responses to variations in arterial blood gas concentrations. Understanding the timing and localization of O₂- and CO₂-mediated responses would provide valuable insight regarding potential underlying mechanisms.

Equilibration of superfusion solutions covering externalized muscle tissues with various gas concentrations is another common method used to study O₂- and CO₂-mediated responses that eliminates the risk of systemic changes by altering tissue rather than arterial gas concentrations (Duling, 1973a; Morff et al., 1981; Ngo et al., 2010; Riemann et al., 2011; Charter et al., 2018). While influencing the tissue environment via superfusion solutions resolves the issue regarding the systemic influence of arterial blood gases, there are also limitations associated with this method as well. In addition to the limitations discussed previously (section 1.7) regarding altered muscle surface environments and fixed experimental conditions, since the entire muscle surface is exposed to the gas perturbations in the superfusion solution, it is still difficult to determine the location or locations of CO₂'s impact on the integrated microvascular system. Therefore, the development of another technique for imposing localized changes in tissue microenvironments was necessary to address these limitations and investigate both localized O₂- and CO₂-mediated responses and their underlying mechanisms.

A microfluidic gas exchange chamber (GEC) is a device that has been designed to address these limitations and improve the ability to investigate O₂- and CO₂-mediated microvascular blood flow regulation, and potentially responses to other gaseous stimuli (NO, hydrogen sulfide (H₂S), etc.), by imposing localized and direct changes in tissue microenvironments *in vivo* (Ghonaim et al., 2011; Ghonaim et al., 2013; Sove et al., 2021). The 3D-printed GEC fits into the stage of an inverted microscope and consists of a gas channel that exposes overlying tissues to gas perturbations through a gas permeable polydimethylsiloxane (PDMS) membrane (Figures 1.4 and 1.5) (Ghonaim et al., 2011; Ghonaim et al., 2013; Sove et al., 2021). The PDMS membrane is located within a micro-outlet cut into the channel using microfabrication techniques (Figures

1.4 and 1.5) (Ghonaim et al., 2011; Ghonaim et al., 2013; Sove et al., 2021). The use of a PDMS membrane is one of several gas permeable substrates that can be used to cover the GEC micro-outlet (including polyethylene, hard contact lens material, Tegaderm™, etc.) and was selected due to its high gas permeability ($k_{O_2} = 0.18 \text{ cm}^3 / (\text{cm}^3 \times \text{atm})$, $D_{O_2} = 3.4 \times 10^{-5} \text{ cm}^2 / \text{s}$, $k_{CO_2} = 1.29 \text{ cm}^3 / (\text{cm}^3 \times \text{atm})$, $D_{CO_2} = 2.2 \times 10^{-5} \text{ cm}^2 / \text{s}$) (Merkel et al., 2000) and the ease of fabricating thin, even layers using spin coating techniques. The composition of gas (O₂, N₂, and CO₂) flowing through the channel is set using computer-controlled mass flow meters, which enables the device to impose rapid and dynamic variations in the gas concentrations experienced by the tissue (Ghonaim et al., 2011; Ellis et al., 2012; Ghonaim et al., 2013; Sove et al., 2021). The exteriorized skeletal muscle tissue of interest is reflected on top of the gas permeable membrane positioned above the microscope objective, which enables simultaneous viewing and recording of microvascular blood flow responses during direct gas perturbations using IVVM (Figure 1.5) (Ghonaim et al., 2011; Ghonaim et al., 2013; Sove et al., 2021). Therefore, this device allows a selected region of skeletal muscle tissue to be directly and reversibly exposed to dynamic changes in gas concentrations with minimal disruption to its physiological environment and without impacting the systemic circulation, or tissue and vasculature further than ~200 μm from the membrane surface. Combined with simultaneous visualization of resulting blood flow responses using IVVM, this device can be a powerful tool for studying gas-mediated blood flow responses along with their underlying regulatory mechanisms *in vivo* (Ghonaim et al., 2011; Ghonaim et al., 2013; Sove et al., 2021).

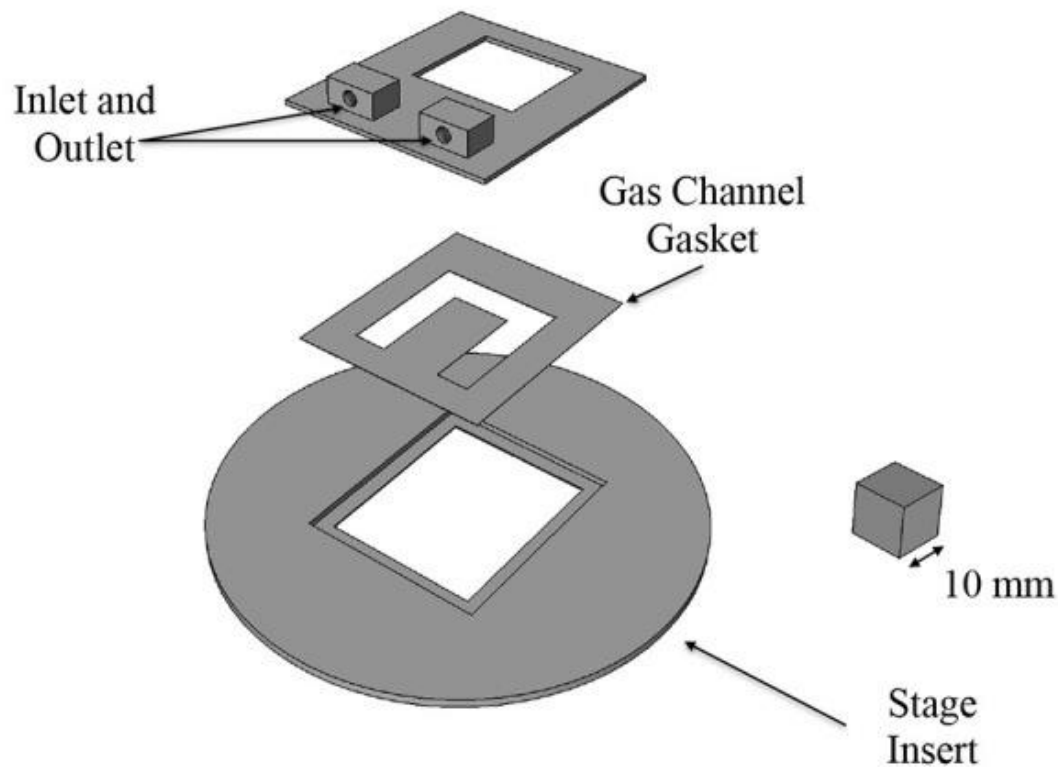


Figure 1. 4. Schematic depicting the multiple components of a three-dimensionally (3D) printed microfluidic gas exchange chamber. The inlet/outlet piece connects to external gas sources (O_2 , CO_2 , N_2), which allows gas to flow through the gas channel gasket component of the device. The outlet cut into the inlet/outlet piece is covered with a gas permeable membrane, which exposes tissues positioned on top of the device to the composition of gases flowing through the chamber. The stage insert is designed to fit into an inverted microscope to enable *in vivo* visualization of blood flow responses to various gas perturbations. Used under Creative Commons license permissions (Sove et al., 2021).

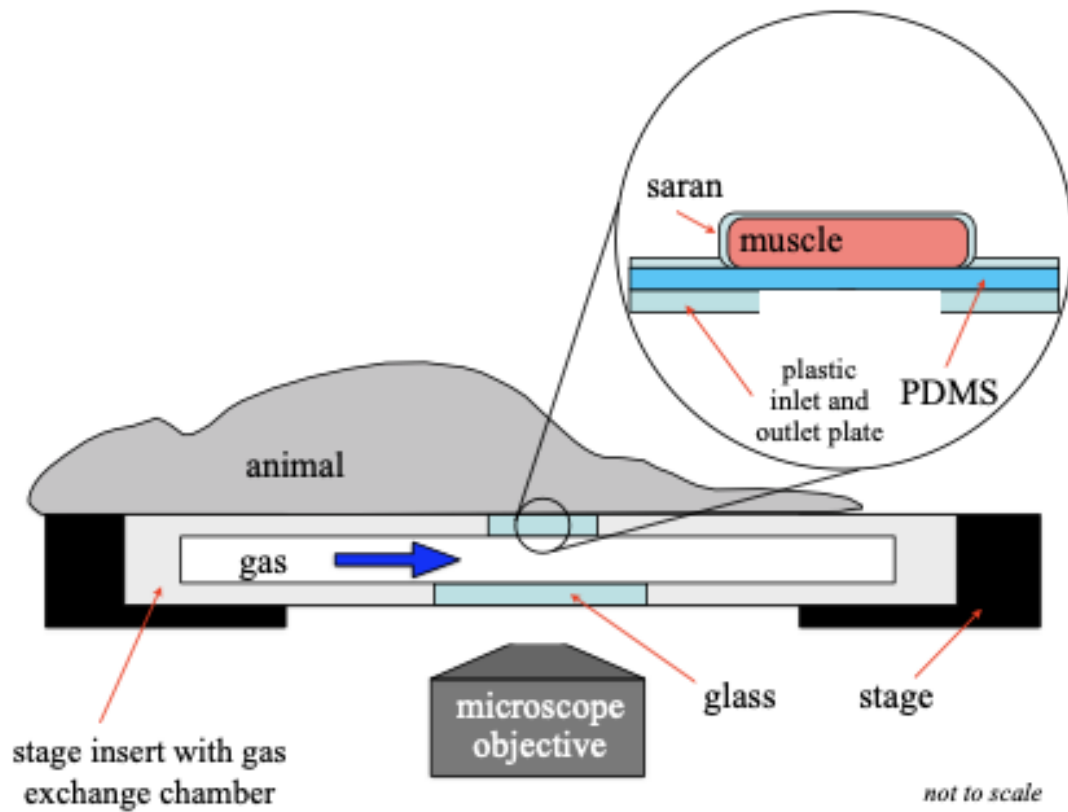


Figure 1. 5. Microfluidic gas exchange chamber. This schematic shows the orientation of a 3D printed gas exchange platform with the reflected skeletal muscle that is used to impose rapid and localized changes in the skeletal muscle tissue CO_2 microenvironment. Computer-controlled flow meters alter the gas concentrations flowing beneath the muscle surface. Adapted from Sove et al. (2021). Used under Creative Commons license permissions.

In addition to imposing direct and reversible changes in the tissue microenvironment, this device can be used to induce highly localized tissue perturbations (Ghonaim et al., 2011; Ghonaim et al., 2013; Sove et al., 2021). Initial investigations involving GECs used full-sized gas exchange surfaces that exposed the entire overlying muscle tissue to variations in gas compositions flowing through the gas channel (Ellis et al., 2012). To increase the spatial specificity of imposed tissue perturbations and improve the ability to investigate gas-mediated responses at specific levels of the microvasculature, GECs with smaller micro-outlets cut into the channel and covered with a gas permeable membrane were developed (Ghonaim et al., 2011; Ghonaim et al., 2013; Sove et al., 2021). The addition of a micro-outlet results in stimulation of only small microscale areas of the muscle being exposed to the gas perturbations within the chamber, which increases the ability to determine the location of the response and potential underlying mechanisms specific to a given level of the microvasculature. Computational modelling and experimentation have been done to determine the micro-outlet size and geometry that impacts enough vessels to generate RBC SO_2 and hemodynamic responses while still maintaining a localized exposure (Ghonaim et al., 2011; Ghonaim et al., 2013; Sove et al., 2021). In these experiments, the O_2 distribution profile was modelled to determine the degree of radial diffusion (distance O_2 travels from the micro-outlet edge) as well as axial diffusion (distance O_2 travels into the tissue from the chamber) to determine spatial specificity of different micro-outlet sizes (Ghonaim et al., 2011; Ghonaim et al., 2013; Sove et al., 2021). The size of micro-outlet used can be varied based on the question being investigated, where small circular (100 μm in diameter) micro-outlets have been shown to be useful for inducing RBC SO_2 but not hemodynamic responses in a small number of capillaries, while larger rectangular outlets (1000 μm wide \times 200 μm long) are useful for stimulating enough vessels to generate both saturation and flow responses while minimizing

the degree of O₂ diffusion from the micro-outlet (Ghonaim et al., 2011; Ghonaim et al., 2013).

The development of a modular GECs enables a variety of micro-outlet designs to be printed and interchanged within a single device, which allows micro-outlets varying in size, geometry, and in number to be used in investigating microvascular blood flow responses *in vivo* (Sove et al., 2021).

In the current thesis, a microfluidic GEC with a single rectangular outlet was used to impose localized perturbations in the tissue CO₂ microenvironment of the EDL muscle to characterize CO₂-mediated microvascular blood flow responses as well as to investigate the potential underlying mechanisms. Similar to the studies investigating O₂-mediated blood flow responses, altering the gas concentrations in the GEC can be used to impose rapid (initiated within 1 – 3 seconds), direct, and reversible alterations to the tissue CO₂ microenvironment; however, this method has not been previously used to investigate CO₂-mediated responses. Therefore, this tool was anticipated to provide novel information to advance our current understanding of CO₂-mediated blood flow regulation in the skeletal muscle microvasculature.

Chapter 2 –

Characterization and Investigation of Potential Mechanisms Underlying CO₂-mediated Microvascular Blood Flow Regulation in Skeletal Muscle Tissue

2.1 Introduction

Microvascular blood flow regulation is a dynamic and highly coordinated process that directs blood flow based on the varying metabolic demands existing among and within tissues (Segal, 2005). The microvascular system integrates a variety of vasoactive signals, including sympathetic nervous activity and the production of vasoactive metabolites, and communicates them into larger upstream vessels to initiate appropriate changes in both the magnitude and distribution of blood flow (Sarelius & Pohl, 2010). Connexin-based gap junctions present along and between the endothelial and vascular smooth muscle cell layers of microvessel walls allow for the rapid transmission of microvascular responses, known as conducted vasomotor responses (Segal et al., 1989; Xia & Duling, 1995; Xia et al., 1995; Welsh & Segal, 1998; de Wit et al., 2000; Segal & Jacobs, 2001; Figueroa et al., 2003; Looft-Wilson et al., 2004; Segal, 2005; Figueroa & Duling, 2008; de Wit, 2010; Milkau et al., 2010). The rapid transmission of electrical signals along the microvessel wall induces a coordinated and spatially specific change in microvascular tone throughout the arteriolar network (Berg et al., 1997; Bagher & Segal, 2011b; Twynstra et al., 2012). Conducted vasomotor responses have been shown to be initiated in response to variations in the local tissue environment of distal arterioles and capillaries, such as increased muscle metabolism and direct exposure to vasoactive metabolites including oxygen (O₂), potassium (K⁺), adenosine, and adenosine triphosphate (ATP) (Song & Tyml, 1993; Ellsworth et al., 1995; McCullough et al., 1997; Collins et al., 1998; Dietrich et al., 2000;

Hungerford et al., 2000; de Wit, 2010; Ngo et al., 2010; Riemann et al., 2011; Lamb & Murrant, 2015; Dora, 2017; Lamb et al., 2018). Therefore, these responses enable vasoactive signals to be rapidly communicated along the microvascular network to initiate effective and efficient coupling of microvascular blood flow with metabolic demand. While several vasoactive molecules associated with increased muscle metabolism have been shown to contribute significantly to local blood flow regulation, the contribution of carbon dioxide (CO₂) has not been well described in the skeletal muscle tissue microcirculation.

The vasoactive property of CO₂ has been established in a variety of vascular beds, including the microvasculature of the highly metabolically active striated muscle and cerebral tissues (Raper et al., 1971; Duling, 1973a; Kontos, Raper, et al., 1977; Kontos, Wei, et al., 1977; Wei et al., 1980; Ward, 1996; Charter et al., 2018). These microvascular beds are sensitive to variations in both systemic and local tissue CO₂ concentrations and experience significant arteriolar vasodilation and vasoconstriction in response to elevated and depressed CO₂, respectively (Raper et al., 1971; Duling, 1973a; Kontos, Raper, et al., 1977; Kontos, Wei, et al., 1977; Wei et al., 1980; Ward, 1996; Charter et al., 2018). The magnitude of CO₂'s impact on microvascular tone has been shown to be inversely related to vessel size, with more profound vasomotor responses being observed in smaller arterioles (Raper et al., 1971; Wei et al., 1980; Ward, 1996)). This vessel size-dependency may be due to a greater ability to influence changes in CO₂ and pH within thin-walled microvessels supporting smaller blood volumes and relatively lower blood flow rates. In addition, microvascular responses to CO₂ also appear to vary between microvascular beds (Kontos, Wei, et al., 1977; Ward, 1996). For example, cerebral pial arterioles experience significant changes in vascular tone between 0 and 60 mmHg of CO₂ and therefore appear to

have a higher sensitivity than the diaphragmatic arterioles, which do not respond until they are exposed to a CO₂ concentration above 80 mmHg (Kontos, Wei, et al., 1977; Ward, 1996). The variability of CO₂-induced blood flow responses both among and within vascular beds highlights the importance of characterizing CO₂-mediated blood flow responses in a variety of tissues, as well as in different levels of the vasculature to develop a complete understanding of blood flow regulation. These findings also demonstrate the high CO₂ sensitivity of microvessels in closest proximity to tissue fibers that experience high and variable levels of metabolic activity, which supports a significant contribution of these vessels in coordinating local blood supply with metabolic demand. Therefore, these findings may also indicate that variations in local CO₂ have a significant role in influencing blood flow responses initiated at the capillary and/or terminal arteriole levels. To date, the magnitude and time transient of capillary blood flow responses across a physiologically relevant range of tissue CO₂ concentrations have not been fully characterized in skeletal muscle tissue. Characterization of the dynamic CO₂-mediated responses under normal conditions is necessary before other questions can be investigated, such as the identification of potential underlying mechanisms.

The mechanism of interaction between CO₂ and the microvascular system has also not been an active area of investigation, especially in skeletal muscle tissue. Carbon dioxide's impact on the vascular system is often attributed to pH-mediated changes in vascular smooth muscle cell contractility and arteriolar tone (Wei et al., 1974; Kontos, Raper, et al., 1977; Toda et al., 1989; You et al., 1994; Tian et al., 1995; Charter et al., 2018). Recently in the striated muscle microcirculation, it has been shown that combined exposure of arterioles to increased CO₂ and hydrogen ion (H⁺) concentration had a synergistic, rather than additive, impact on arteriolar tone,

which supported an interaction between the two vasoactive stimuli (Charter et al., 2018). It has also been shown that while increased striated muscle tissue CO₂ at the arteriolar level stimulates local vasodilation, both independently and in combination with H⁺, the local response was not able to be propagated into larger upstream vessels (Charter et al., 2018). Therefore, it has been suggested that CO₂ does not have a direct role in local blood flow regulation, and it likely influences the activity of other vasodilators and/or regulatory mechanisms (Charter et al., 2018). A few mechanisms underlying CO₂-mediated responses in the cerebral microcirculation have been suggested that may apply to other tissues, including nitric oxide (NO) ((Faraci et al., 1994; Wang et al., 1994; You et al., 1994; Wang et al., 1998; Nakahata et al., 2003; Rosenblum, 2003; Phillis et al., 2004), adenosine (Morii et al., 1986; Morii et al., 1987; Ibayashi et al., 1988; Simpson & Phillis, 1991; Pelligrino et al., 1995; Phillis et al., 2004; Miekisiak et al., 2009), and of interest in the current study, vascular ATP-sensitive potassium (K_{ATP}) channels (Faraci et al., 1994; Wei & Kontos, 1999; Nakahata et al., 2003; Nnorom et al., 2014).

Vascular K_{ATP} channels are one of the many types of ion channels expressed in cell membranes that alter microvascular tone by influencing membrane potential and impacting vascular smooth muscle cell contractility and endothelial production of vasoactive molecules (Jackson, 2000a, 2005; Tykocki et al., 2017). They are activated during conditions of increased cellular metabolism and respond to variations in the intracellular environment, specifically the intracellular concentration of ATP and adenosine diphosphate (ADP) (Jackson, 2000a, 2005; Tykocki et al., 2017). Due to their sensitivity to the metabolic state of their environment and ability to influence vascular tone, K_{ATP} channels have been suggested to have a significant role in blood flow regulation and they have been studied in relation to a variety of factors associated

with increased tissue metabolism; including functional hyperemia/muscle contraction (Saito et al., 1996; Hammer et al., 2001; Cohen & Sarelius, 2002; Murrant & Sarelius, 2002; Farouque & Meredith, 2003; Schrage et al., 2006; Holdsworth et al., 2015; Colburn, Holdsworth, et al., 2020; Schemke & de Wit, 2021), pH changes (Davies, 1990; Xu et al., 2001; Horiuchi et al., 2002; Wang et al., 2003), hypoxia (Marshall et al., 1993; Reid et al., 1993; Taguchi et al., 1994; Bryan & Marshall, 1999; Rocha et al., 2020) and the release of adenosine (Armstead, 1997; Danialou et al., 1997; Bryan & Marshall, 1999; Chen et al., 2000) and nitric oxide (NO) (Armstead, 1997; Bryan & Marshall, 1999). The pH-sensitivity of K_{ATP} channels and their relationship with other factors associated with changes in CO₂ (muscle metabolism, hypoxia, adenosine, and NO) suggests that these channels are a reasonable potential mechanism underlying CO₂-mediated microvascular blood flow regulation. Some evidence supporting this hypothesis has been provided in the cerebral microcirculation, where hypercapnia-induced arteriolar vasodilation and hypocapnic alkalosis-induced vasoconstriction were reduced and inhibited following selective K_{ATP} channel inhibition, respectively (Faraci et al., 1994; Wei & Kontos, 1999; Nakahata et al., 2003; Nnorom et al., 2014). In addition, similar to the vessel-size dependency of CO₂-mediated responses mentioned above, the impact of K_{ATP} channel inhibition on CO₂-mediated responses increases as vessel size decreases, with responses being nearly abolished in small 4th order arterioles (<10 µm in diameter) (Saito et al., 1996; Hammer et al., 2001). This finding suggests that K_{ATP} channels may have a significant role in regulating microvascular responses initiated at the capillary level, which has been supported in the cremaster muscle microvascular response to increased muscle metabolism (Cohen & Sarelius, 2002; Murrant & Sarelius, 2002). Selective inhibition of these channels has also been shown to significantly reduce hypercapnia-induced increases in whole-cell currents when accompanied by a simultaneous change in pH, which

suggests that CO₂ influences membrane potential and microvascular tone through pH-mediated K_{ATP} channel activation (Xu et al., 2001; Wang et al., 2003). Overall, these findings support a significant role for K_{ATP} channels in CO₂-mediated cerebral microvascular responses; however, the role of these channels in regulating capillary blood flow responses to a physiological range of skeletal muscle tissue CO₂ concentrations has not been described.

Another potential mechanism of interest in this study is the involvement of red blood cell (RBC) derived ATP release, which is an important mechanism suggested to be involved in matching microvascular blood flow supply with metabolic demand in skeletal muscle tissue (Ellsworth et al., 2016; Richardson et al., 2020). This mechanism has been studied in relation to O₂-mediated regulation of microvascular tone, where it has been suggested that changes in oxygen saturation (SO₂) and mechanical deformation stimulate RBC-derived ATP release through a G-protein mediated signal transduction pathway, which initiates vascular responses through the action of ATP on vascular purinergic receptors (P_{2Y} and P_{2X}) (Bergfeld & Forrester, 1992; Ellsworth et al., 1995; Sprague et al., 1998; Dietrich et al., 2000; Jagger et al., 2001; Sprague et al., 2001; Sprague et al., 2002; Olearczyk et al., 2004; Sridharan, Adderley, et al., 2010; Sridharan, Sprague, et al., 2010; Ballard, 2014; Racine & Dinunno, 2019). In addition to being sensitive to variations in RBC SO₂, it has been shown that independent pH changes also influence RBC-derived ATP release (Ellsworth et al., 1995). Therefore, due to the saturation and pH dependence of RBC-derived ATP release and the influence of CO₂ and/or pH on the oxygen-dissociation curve (Bohr/Haldane effects), it is reasonable to consider whether variations in SO₂ serve as a potential underlying mechanism for CO₂-mediated microvascular blood flow regulation as well as a link between CO₂- and O₂-mediated responses.

Therefore, the objectives of the current study are as follows: 1) characterize both the magnitude and time transient of dynamic CO₂-mediated microvascular blood flow responses in skeletal muscle tissue, 2) investigate the involvement of vascular K_{ATP} channels in mediating capillary blood flow responses to a physiological range of tissue CO₂ concentrations, and 3) investigate the relationship between CO₂- and O₂-mediated blood flow responses and the presence of a common regulatory mechanism, such as RBC-derived ATP release.

2.2 Methods

2.2.1 Surgical Procedure:

A total of 21 male Sprague-Dawley rats (145-201 g) were anaesthetized using sodium pentobarbital (65 mg/kg) via intraperitoneal injection. Cannulas were introduced into the left common carotid artery (outer cannula diameter = 0.965 mm) and right jugular vein (outer cannula diameter = 1.19 mm) for blood pressure (maintained between 80 – 110 mmHg) and heart rate monitoring, administration of maintenance anaesthetic, and fluid resuscitation. The temperature of anaesthetized animals was maintained at 37 °C throughout the duration of surgical and experimental protocols. Animals were tracheotomized and mechanically ventilated with the initial ventilatory volume and rate determined by weight as per the ventilator manufacturer's instructions (Inspira, Harvard Apparatus, Holliston, MA, USA). The extensor digitorum longus (EDL) muscle of the right hindlimb was isolated, externalized, and reflected over a 3D printed microfluidic gas exchange chamber (Sove et al., 2021) set into the stage of an inverted microscope (IX73, Olympus, Tokyo, Japan) for in vivo visualization of blood flow. The muscle was bathed in warm saline and then isolated from the external environment with a small piece of polyvinylidene film (~ 1 x 1.5 cm) (Saran, Dow Corning, Midland, MI, USA) and a

glass coverslip secured with vacuum grease (high-vacuum silicone grease, Dow Corning, Midland, MI, USA). The space between the muscle and the coverslip was filled with additional warm saline as needed throughout the duration of the experiment to prevent the muscle from drying out. The muscle was allowed to equilibrate on the gas exchange chamber (GEC) for 30 minutes prior to blood sampling for measurement of blood gases and exposure to various experimental protocols detailed below. All protocols were approved by Memorial University of Newfoundland's Animal Care Committee.

2.2.2 Dual Spectrophotometric Intravital Microscopy

Intravital video microscopy (IVVM) was used for simultaneous *in vivo* visualization and quantification of blood flow within the externalized EDL muscle tissue. An inverted microscope (IX73, Olympus, Tokyo, Japan) combined with a video recording system was used to record real-time video sequences of microvascular blood flow responses to imposed changes in the tissue microenvironment. The video recording system consisted of a camera (Hamamatsu Orca Flash4.0 v3 sCMOS Camera) connected to a parfocal beam-splitter (Optosplit II Bypass Beamsplitter, Cairn Research, Faversham, Kent, UK) that directed the image to two bandpass filters at 420 nm and 438 nm wavelengths which were recorded simultaneously on the top and bottom halves of the camera sensor and displayed in real time on a computer monitor. A Xenon light source (Lambda LS-30 Xenon Light Source, Sutter Instrument Company, Novato, CA, USA) was used to transilluminate the EDL muscle on the microscope stage enabling brightfield visualization of the microvascular networks. Video sequences of blood flow responses were recorded at a rate of 30 frames per second and were processed using a custom MATLAB software to generate a series of images that describe both the structure of the microvascular

network and capillary RBC perfusion, as described previously (Ellis et al., 1990; Ellis et al., 1992; Japee et al., 2004; Ellis et al., 2012; Fraser et al., 2012; Ghonaim et al., 2021). In addition to structural and blood flow measurements, the simultaneous viewing and recording of microvascular responses using oxygen-sensitive (438 nm) and oxygen-insensitive (420 nm) wavelengths allows for the simultaneous spectrophotometric measurement of RBC oxygen saturation (SO₂) due to differences in light absorption by oxy- and deoxyhemoglobin molecules, which enables the study of convective oxygen transport and SO₂-dependent vasomotor responses (Ellis et al., 1992).

2.2.3 Microfluidic Gas Exchange Chamber

A microfluidic gas exchange chamber (GEC) was used to impose localized and direct changes to tissue gas microenvironments *in vivo* (Ghonaim et al., 2011; Ghonaim et al., 2013; Sove et al., 2021). A 3D-printed GEC was fabricated as described by Sove et al. (2021) and fit into the stage of an inverted microscope where the exteriorized EDL muscle was reflected over the microscope objective for visualization using IVVM (Figures 1.4 and 1.5). While on the stage, the muscle was covered with a small piece of polyvinylidene film (Saran wrap, Dow Corning, MI, USA) and a coverslip to isolate it from the external environment. The space between the coverslip and the muscle was also filled with warm saline to maintain moisture. Running beneath the surface of the muscle was a gas channel where the composition of the gas (O₂, N₂, and CO₂) flowing through the channel was set using computer-controlled mass flow meters (SmartTrack100, Sierra Instruments, CA, USA). The skeletal muscle was then directly interfaced with channel environment through a gas permeable membrane fabricated with polydimethylsiloxane (PDMS) similar to technologies described previously (Ghonaim et al., 2011; Ghonaim et al., 2013; Sove

et al., 2021). Flow meters were computer-controlled using a custom MATLAB interface to impose rapid, dynamic, and precisely timed gas perturbations on the EDL tissue microenvironment and expose the muscle to various experimental protocols as described in sections 2.2.4 and 2.2.5.

2.2.4 Experimental Protocols 1A, 1B, 1C, and 1D: Characterization of CO₂-mediated microvascular blood flow response.

Protocol 1A: Quantification of graded CO₂-mediated blood flow response.

To quantify the steady state blood flow of graded CO₂-induced microvascular responses, the EDL muscles of 13 male Sprague-Dawley rats (145-197 g) were directly exposed to incremental levels of CO₂ (0, 2, 4, 5, 6, 8, 10%) at a constant O₂ concentration (5%) using a microfluidic gas exchange chamber and computer-controlled CO₂, O₂, and N₂ mass flow meters (SmartTrak100, Sierra Instruments, Monterey, CA, USA). One-minute IVVM sequences of the microcirculation were recorded at each CO₂ level using the dual-wavelength video microscopy system described above. The muscle was allowed to equilibrate to each CO₂ level for 1-minute before recording video sequences to allow for a steady-state to be reached. In between each CO₂ level, the muscle was equilibrated with a physiological concentration of CO₂ (5%) and O₂ (5%) while captured IVVM data was saved to disk. This was done to avoid any confounding effects of prolonged exposure to high and low tissue CO₂. The CO₂ staircase protocol was repeated in 2 to 4 fields of view (FOVs) in the EDL muscle of each animal. Bright FOVs containing the largest number of perfused, in-focus vessels with plasma gaps between red blood cells (RBCs) were selected for data acquisition and analysis.

Protocol 1B: Dynamics of CO₂ mediated blood flow response

To provide insight into the time course of CO₂-mediated blood flow responses, a microfluidic GEC and computer-controlled mass flow meters (SmartTrak100, Sierra Instruments, Monterey, CA, USA) were used to directly expose the EDL muscle of 7 male Sprague-Dawley rats (168-201 g) to dynamic tissue CO₂ perturbations. EDL muscles were exposed to 5% CO₂ for 1-minute followed by 2-minutes at either 10 or 0% CO₂ while maintaining a constant O₂ state (5%). Three-minute IVVM sequences of the microvascular blood flow response to the high CO₂ challenge followed by the low CO₂ challenge were recorded using the dual-wavelength video microscopy system described above. The muscle was equilibrated with 5% CO₂ and 5% O₂ for 5 minutes in between the high/low CO₂ challenges. Each high and low CO₂ challenge was repeated in 3 to 4 FOVs in the EDL muscle of each animal. Bright FOVs containing the largest number of perfused, in-focus vessels with plasma gaps between RBCs were selected for data acquisition and analysis.

Protocol 1C: Simultaneous determination of the magnitude and time transient of CO₂-mediated blood flow response: CO₂ Oscillation

A microfluidic GEC and computer-controlled flow meters (SmartTrak100, Sierra Instruments, Monterey, CA, USA) were used to directly expose the EDL muscle of 9 male Sprague-Dawley rats (149-201 g) to oscillating CO₂ levels (5-0-10-5%) while maintaining a constant O₂ concentration (5%) to provide simultaneous measurements of both the magnitude and time course of blood flow responses to dynamic tissue CO₂ perturbations. Four-minute IVVM sequences (1-minute at each CO₂ level) of the microcirculation were recorded. The CO₂ oscillation protocol was repeated in 2 or 3 FOVs in the EDL muscle of each animal. Bright

FOVs containing the largest number of perfused, in-focus vessels with plasma gaps between RBCs were selected for data acquisition and analysis.

Protocol 1D: Simultaneous determination of the magnitude and time transient of O₂-mediated blood flow response: O₂ Oscillation

A microfluidic GEC and computer-controlled flow meters (SmartTrak100, Sierra Instruments, Monterey, CA, USA) were used to directly expose the EDL muscle of 9 male Sprague-Dawley rats (149-201 g) to oscillating O₂ levels (7-12-2-7%) while maintaining a constant CO₂ concentration (5%). Four-minute IVVM sequences (1-minute at each O₂ level) of the microcirculation were recorded. The O₂ oscillation protocol was repeated in 2 - 3 FOVs in the EDL muscle of each animal. O₂ oscillations were conducted to allow for comparison between CO₂- and O₂-mediated microvascular blood flow responses and to provide insight into potential overlapping mechanisms between the two vasoactive stimuli.

2.2.5 Experimental Protocol 2: Investigation of the role of ATP-sensitive K⁺ ion (K_{ATP}) channels in CO₂-mediated blood flow regulation.

A microfluidic GEC and computer-controlled flow meters (SmartTrak100, Sierra Instruments, Monterey, CA, USA) were used to directly expose the EDL muscles of 4 male Sprague-Dawley rats (150-197 g) to incremental levels of CO₂ (0, 2, 4, 5, 6, 8, 10%) while maintaining a constant O₂ concentration (5%). One-minute IVVM video sequences of the microvasculature were recorded during baseline conditions. Following completion of baseline captures, a glibenclamide (GLI) stock solution was prepared daily for each experiment by dissolving 20 mg of GLI in 1 mL of dimethyl sulfoxide (DMSO). A 0.25 mL portion of the GLI stock solution was then diluted with 0.75 mL of a sodium hydroxide (NaOH) and distilled water (dH₂O) mixture (990 µL

dH₂O and 10 μ L 1M NaOH) to minimize the amount of DMSO administered systemically. A 5 mg/kg dose was then drawn from the GLI/DMSO/dH₂O/NaOH mixture and was administered intravenously via the jugular vein to block ATP-sensitive K⁺ (K_{ATP}) channels. This dose is a well-established concentration of GLI that corresponds to a systemic GLI concentration between 2-3 μ mol/L and has been shown to be selective for K_{ATP} channels below 5 μ mol/L (Beech et al., 1993b, 1993a; Sadraei & Beech, 1995; Holdsworth et al., 2016b). The muscle was allowed to rest for 10 minutes in between GLI administration and repetition of the CO₂ staircase protocol and IVVM recordings in the same FOV's as during the baseline condition. A quarter dose of GLI was administered 1 hour after the initial dose to maintain a systemic GLI concentration between 2-3 μ mol/L to ensure blockage of K_{ATP} channels throughout the duration of data collection (Li et al., 2012). In addition to the CO₂ Staircase, the EDL muscles were exposed to oscillating CO₂ (5-0-10-5%) and O₂ (7-12-2-7%) concentrations, as described in protocols 1C and 1D, before and after the intravenous administration of GLI. The CO₂ staircase, CO₂ oscillation, and O₂ oscillation protocols were each completed in 2 FOVs in the EDL muscle of each animal during both baseline and GLI conditions.

2.2.6 Data Analysis and Statistical Tests:

IVVM video sequences for each experimental protocol were analyzed offline for hemodynamic variables (capillary RBC velocity, supply rate (SR), and hematocrit (Hct)) as well as oxygen saturation (SO₂) using a custom MATLAB software (Ellis et al., 1990; Ellis et al., 1992; Japee et al., 2004; Ellis et al., 2012; Fraser et al., 2012; Ghonaim et al., 2021). FOVs and/or individual vessels within FOVs that were not in-focus, supported a hyperemic flow state without plasma gaps, and/or exhibited vasomotion were not selected for analysis. All capillary hemodynamic and

saturation measurements were averaged and presented as per animal means. Each CO₂ concentration of the CO₂ staircase was calculated as 1-minute averages per animal. For the CO₂ and O₂ oscillation protocols, an average of the full first minute and of the last 15 seconds of each of the remaining 3 minutes were calculated for each step-change. Repeated measures one-way ANOVAs and Tukey's multiple comparisons tests were used to determine statistical significance between different gas perturbations during the CO₂ staircases, CO₂ oscillations, and O₂ oscillations (p-value < 0.05). Paired parametric t-tests were used to determine statistical significance between the baseline response and the response to high/low gas perturbations during the CO₂ challenges by comparing an average of the first and last minutes (p-value < 0.05).

2.3 Results

Systemic circulatory and respiratory conditions were monitored and measured throughout the duration of each experiment. Collected measurements from each animal were averaged and presented as mean measurements (Table 2.1). Blood gas samples acquired from each animal prior to data collection were also analyzed, averaged, and presented as mean measurements (Table 2.1).

Table 2. 1. Mean measurements of systemic circulatory, respiratory, and blood gas conditions (n = 21 animals).

| | | | | | | | |
|--------------------------------------|-------------|----------------------------|---------|----------------------------------|--------------|---|-------------|
| Heart rate (bpm) | 407 ± 17 | Mean BP (mmHg) | 96 ± 7 | pH | 7.403 ± 0.04 | HCO₃⁻ (mmol/L) | 29.7 ± 2.0 |
| Ventilatory rate (cycles/min) | 84 ± 1.8 | Systolic BP (mmHg) | 100 ± 7 | PCO₂ (mmHg) | 47.9 ± 6.0 | TCO₂ (mmol/L) | 31 ± 2.2 |
| Stroke volume (cc) | 1.16 ± 0.09 | Diastolic BP (mmHg) | 88 ± 7 | PO₂ (mmHg) | 115 ± 17 | SO₂ (%) | 98 ± 1 |
| FiO₂ (%) | 31.2 ± 6.0 | | | BE_{ecf} (mmol/L) | 5 ± 1.8 | Lac (mmol/L) | 0.83 ± 0.33 |

Note. The systemic circulatory, respiratory, and blood gas conditions presented in this table were quantified using the following measurements and units. The animals heart rate was measured in beats per minute (bpm). The ventilatory rate was measured in cycles per minute (cycles/min) and the stroke volume was measured in cubic centimeters (cc). The partial pressure of carbon dioxide (PCO₂), partial pressure of oxygen (PO₂), mean blood pressure (BP), systolic BP, and diastolic BP were all measured in millimetres of mercury (mmHg). The base excess in the extracellular fluid compartment (BEecf), bicarbonate (HCO₃⁻), total CO₂ (TCO₂), and lactate (Lac) were measured in millimoles per liter (mmol/L).

2.3.1 Experimental Protocols 1A, 1B, 1C, and 1D: Characterization of CO₂-mediated microvascular blood flow response.

Protocol 1A: Quantification of graded CO₂ mediated blood flow response

The imposed CO₂ perturbations in the skeletal muscle tissue microenvironment yielded a graded increase in both RBC velocity and SR, as shown in Figure 2.1. Significant differences in RBC velocity were observed between several CO₂ concentrations, most notably between 0 and 5% CO₂ ($145 \pm 81 \mu\text{m/s}$ and $340 \pm 117 \mu\text{m/s}$, $p < 0.0001$), 0 and 10% CO₂ ($145 \pm 81 \mu\text{m/s}$ and $488 \pm 133 \mu\text{m/s}$, $p < 0.0001$) and 5 and 10% CO₂ ($340 \pm 117 \mu\text{m/s}$ and $488 \pm 133 \mu\text{m/s}$, $p < 0.0001$). Similarly changes in RBC supply rate was also observed and significant differences between 0 and 5% CO₂ ($5 \pm 3 \text{ cells/s}$ and $22 \pm 10 \text{ cells/s}$, $p < 0.0001$), 0 and 10% CO₂ ($5 \pm 3 \text{ cells/s}$ and $36 \pm 11 \text{ cells/s}$, $p < 0.0001$) and 5 and 10% CO₂ ($22 \pm 10 \text{ cells/s}$ and $36 \pm 11 \text{ cells/s}$, $p = 0.0016$) were measured (Figure 2.1). An incremental increase in CO₂ yielded a similar graded increase in Hct which was more responsive to low (0%) CO₂ rather than high CO₂ concentrations (Figure 2.1). Finally, there was no significant change in RBC SO₂ across the various CO₂ concentrations (Figure 2.1).

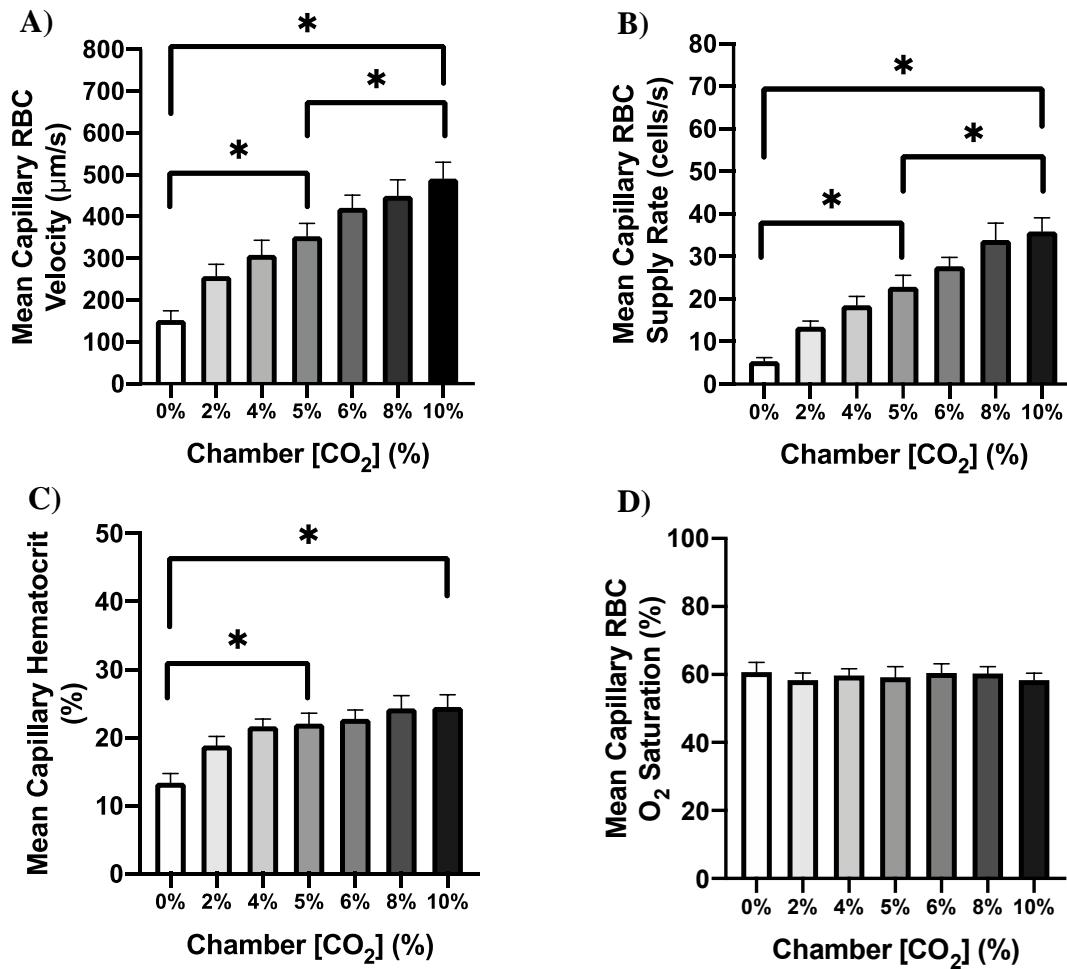


Figure 2. 1. Capillary hemodynamics in rat skeletal muscle at a range of tissue CO₂ concentrations. The muscle was exposed to each concentration (0, 2, 4, 5, 6, 8, 10% CO₂) for one-minute while maintaining a constant O₂ level (5%). Capillary red blood cell (RBC) velocity (A), RBC supply rate (B), hematocrit (C), and RBC oxygen saturation (D) were measured after allowing the muscle to equilibrate with each concentration. The average value of each parameter at each concentration was calculated per animal. The bars represent the average of all included animals. Error bars show SEM. A repeated measures one-way ANOVA and a Tukey's multiple comparisons test were used to determine statistical significance. Note. * = p-value < 0.05 (N = 13, 673 capillaries (A-C) and 586 capillaries (D)).

Protocol 1B: Dynamics of CO₂ mediated blood flow response

Direct EDL muscle exposure to a step-change from 5% CO₂ to 0% CO₂ using a microfluidic gas exchange chamber induced hemodynamic responses that were consistent with the dynamic changes present in the CO₂ staircase data previously described. The mean values of each variable (RBC velocity, SR, Hct, and SO₂) during the 60 s baseline period were compared against the last 60 s of each step-change. The mean RBC velocity during baseline was found to be significantly different during the low CO₂ perturbation with mean values of $415 \pm 100 \mu\text{m/s}$ and $199 \pm 75 \mu\text{m/s}$, respectively ($p < 0.0001$) (Figure 2.2). The mean RBC SR during baseline was found to be significantly different during the low CO₂ perturbation with mean values of $26 \pm 6 \text{ cells/s}$ and $9 \pm 4 \text{ cells/s}$, respectively ($p = 0.0003$) (Figure 2.3). The mean Hct during baseline was also found to be significantly different during the low CO₂ perturbation with mean values of $23 \pm 2\%$ and $14 \pm 3\%$, respectively ($p = 0.0008$) (Figure 2.4). The apparent time to a steady state of the blood flow response to tissue CO₂ perturbations is approximately 70, 65, and 60 seconds for RBC velocity, SR, and Hct, respectively. In addition, a significant decrease in RBC SO₂ was observed in response to the low step-change from 5 to 0% CO₂ ($61 \pm 3\%$ versus $54 \pm 6\%$, $p = 0.0355$) and a new steady state was achieved approximately 75 second after the imposed step-change (Figure 2.5).

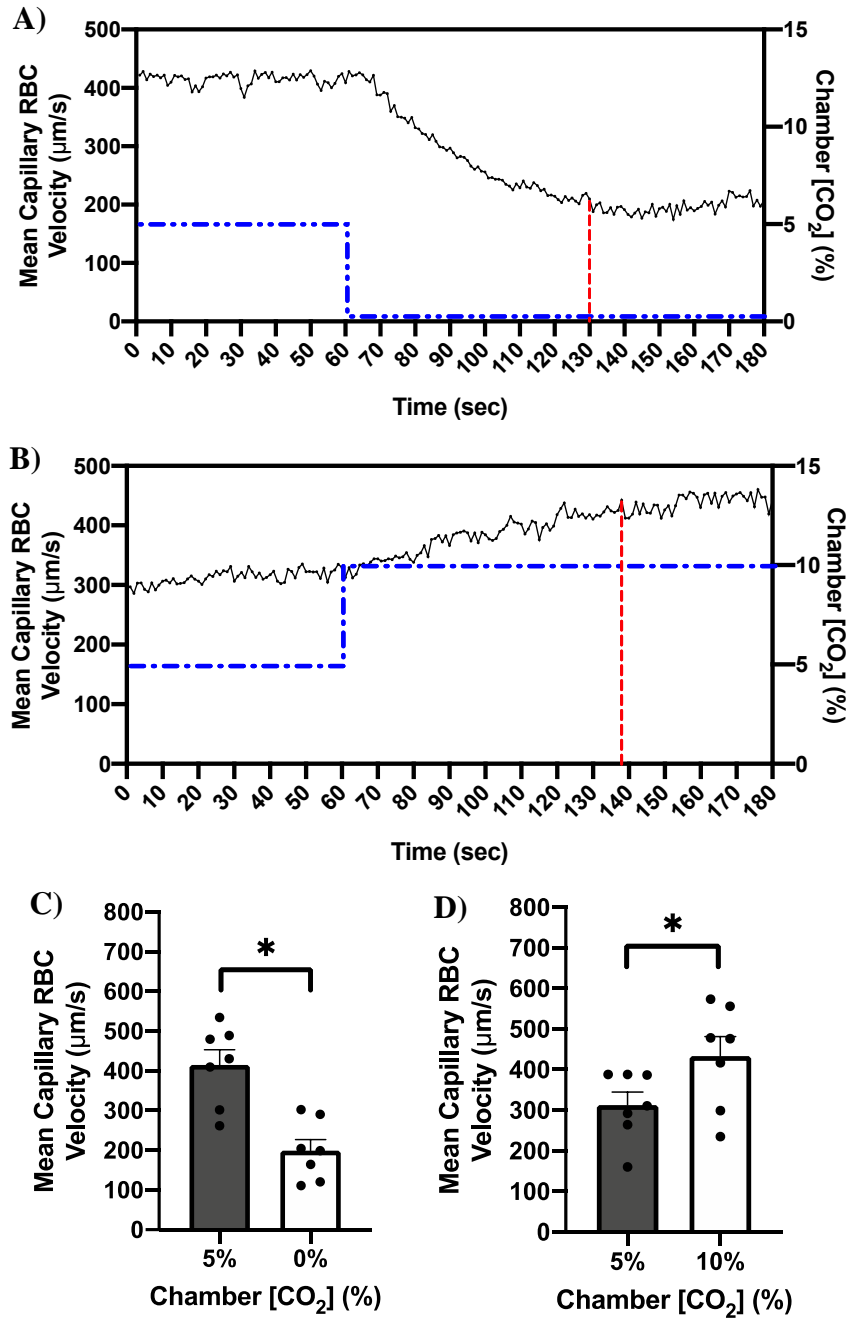


Figure 2. 2. Mean time series plots demonstrating the change in RBC velocity in response to low (A) and high (B) tissue CO_2 perturbations over a 2-minute period. The muscle was equilibrated with 5% CO_2 and 5% O_2 for 5 minutes in between the low and high CO_2 perturbations. Step-changes in the chamber CO_2 concentrations are represented by blue dashed lines. The apparent time to a steady state of the blood flow response to tissue CO_2 perturbations is indicated by a red dashed line. Error bars show SEM. A paired parametric t-test was used to determine statistical significance. *Note.* * = p-value < 0.05 (N = 7, 230 capillaries (A) and 224 capillaries (B)).

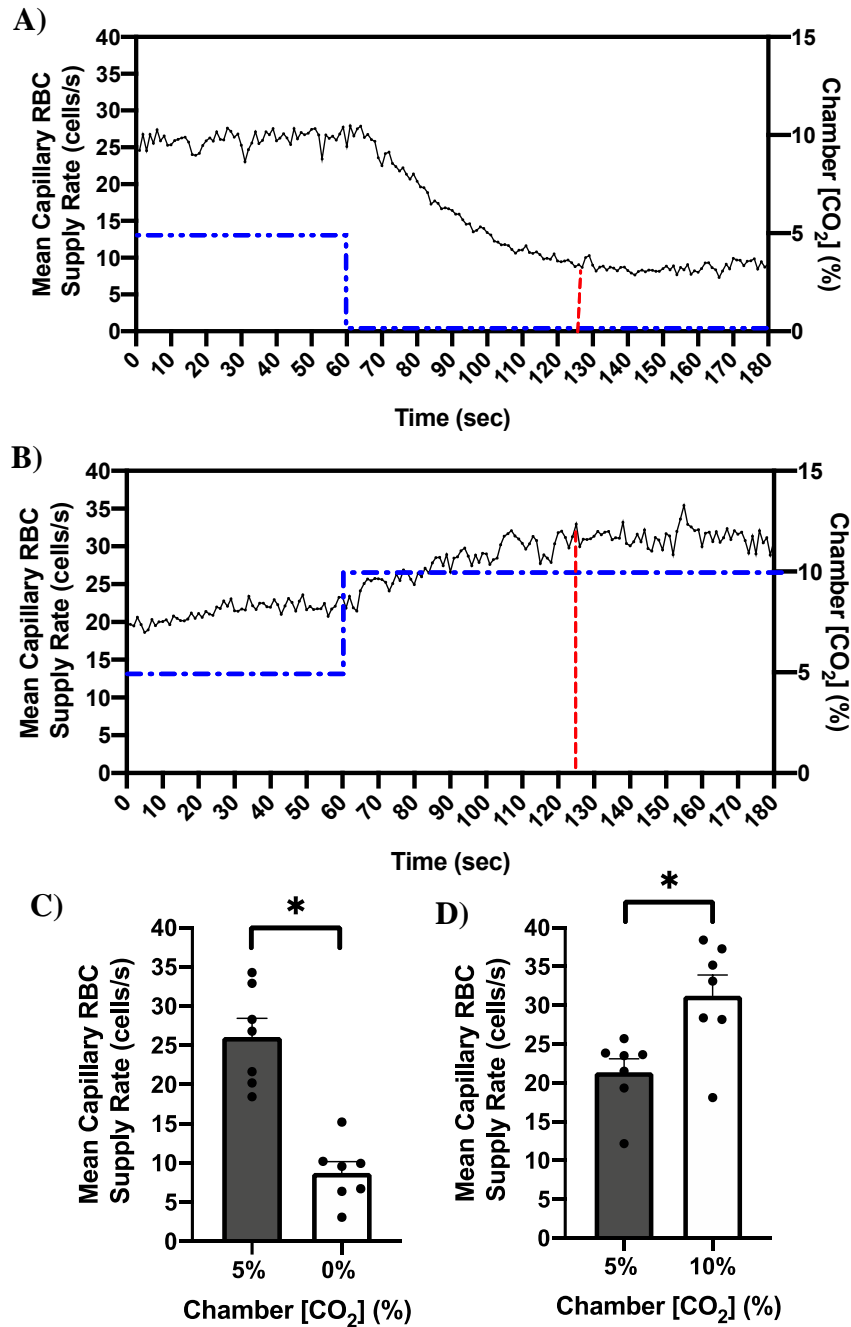


Figure 2. 3. Time series plots demonstrating the change in RBC supply rate in response to low (A) and high (B) tissue CO₂ perturbations over a 2-minute period. The muscle was equilibrated with 5% CO₂ and 5% O₂ for 5 minutes in between the low (0%) and high (10%) CO₂ perturbations. Step-changes in the chamber CO₂ concentrations are represented by blue dashed lines. The apparent time to a steady state of the blood flow response to tissue CO₂ perturbations is indicated by a red dashed line. Error bars show SEM. A paired parametric t-test was used to determine statistical significance. *Note.* * = p-value < 0.05 ((N = 7, 230 capillaries (A) and 224 capillaries (B)).

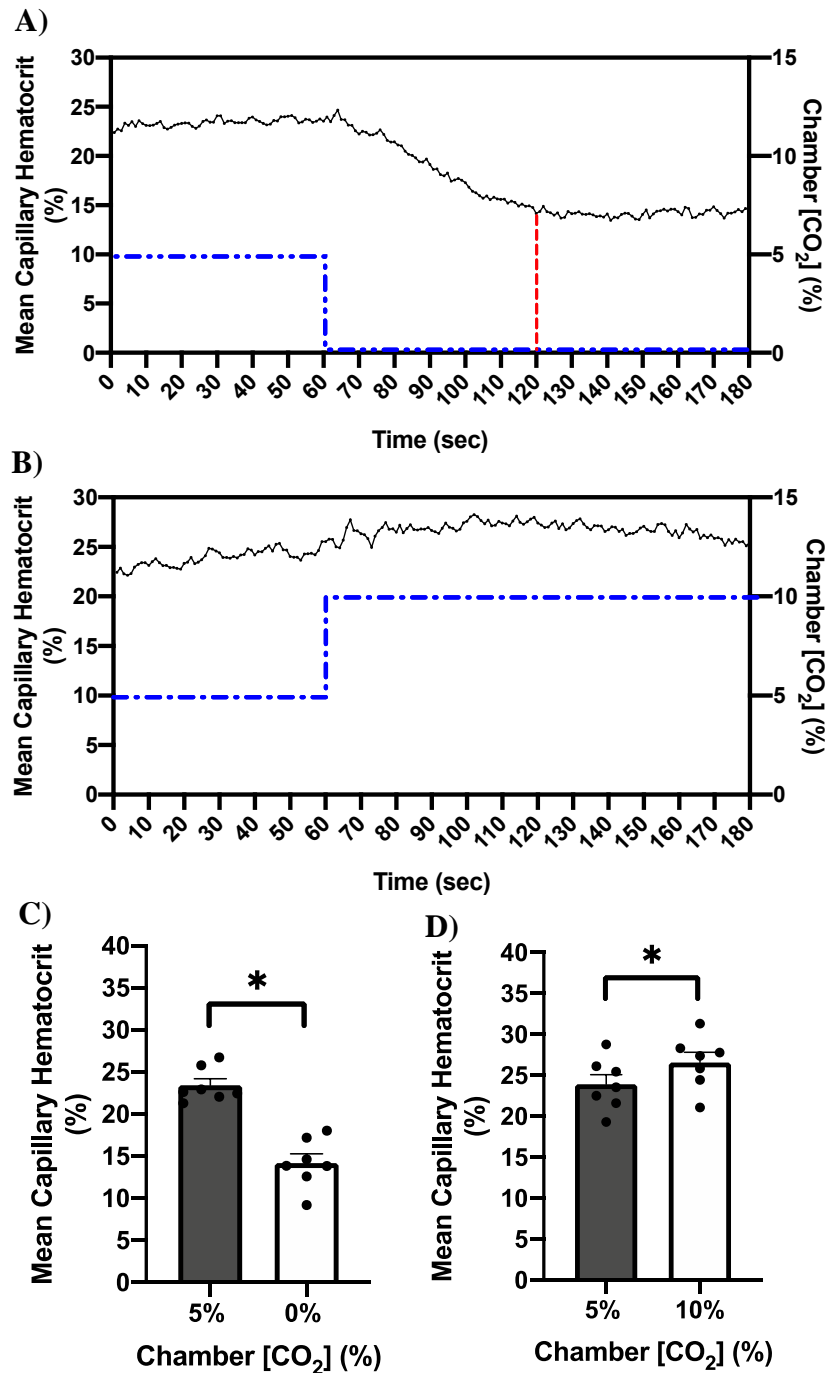


Figure 2. 4. Time series plots demonstrating the change in capillary hematocrit in response to low (A) and high (B) tissue CO₂ perturbations over a 2-minute period. The muscle was equilibrated with 5% CO₂ and 5% O₂ for approximately 5 minutes in between the low (0%) and high (10%) CO₂ perturbations. Step-changes in the chamber CO₂ concentrations are represented by blue dashed lines. The apparent time to a steady state of the blood flow response to tissue CO₂ perturbations is indicated by a red dashed line. Error bars show SEM. A paired parametric t-test was used to determine statistical significance. *Note.* * = p-value < 0.05 (N = 7, 230 capillaries (A) and 224 capillaries (B)).

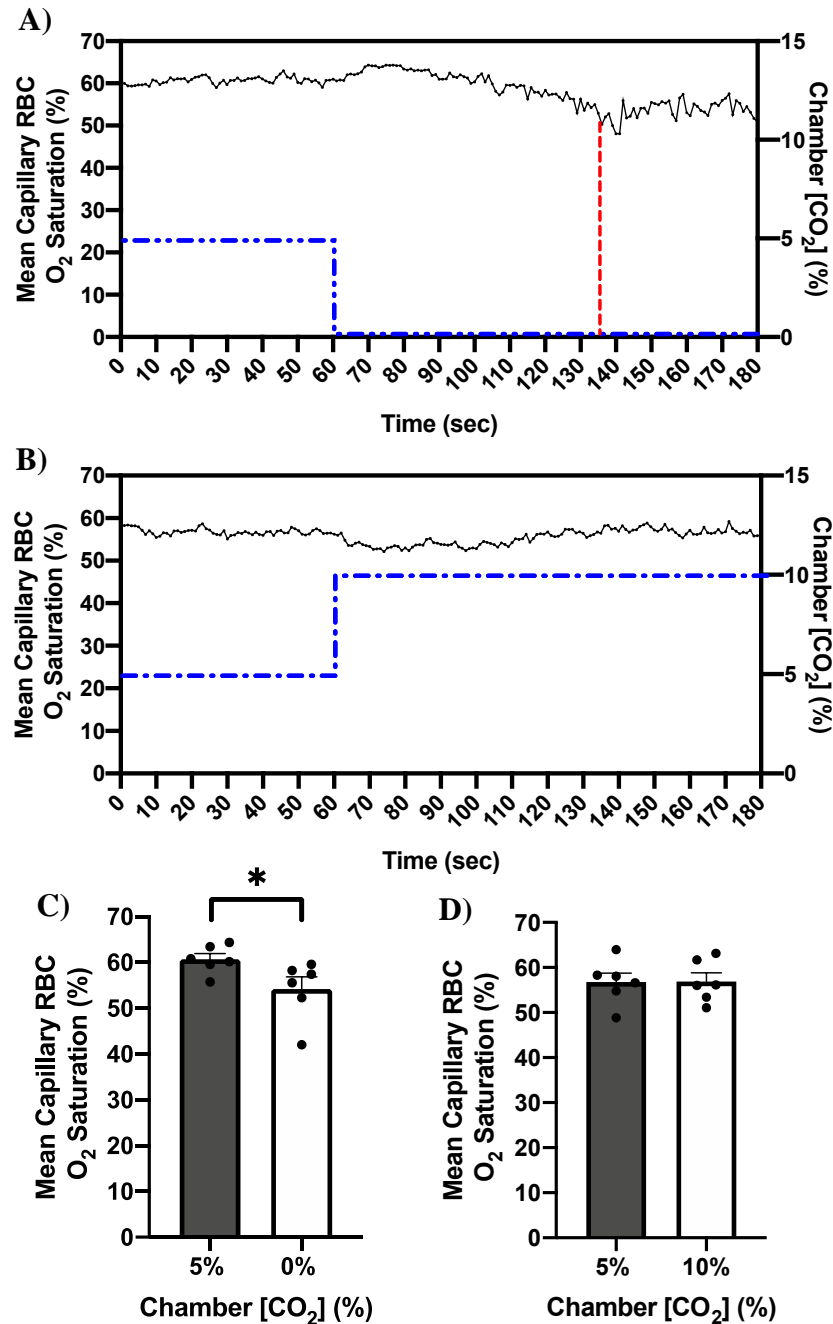


Figure 2. 5. Time series plots demonstrating the change in RBC oxygen saturation in response to low (A) and high (B) tissue CO₂ perturbations over a 2-minute period. The muscle was equilibrated with 5% CO₂ and 5% O₂ for approximately 5 minutes in between the low (0%) and high (10%) CO₂ perturbations. Step-changes in the chamber CO₂ concentrations are represented by blue dashed lines. The apparent time to a steady state of the blood flow response to tissue CO₂ perturbations is indicated by a red dashed line. Error bars show SEM. A paired parametric t-test was used to determine statistical significance. *Note.* * = p-value < 0.05 (N = 7, 125 capillaries (A) and 128 capillaries (B)).

Direct EDL muscle exposure to a step-change from 5% CO₂ to 10% CO₂ using a microfluidic gas exchange chamber induced hemodynamic responses that were consistent with the steady state changes present in the CO₂ staircase data previously described. The mean values of each variable (RBC velocity, SR, Hct, and SO₂) during the 60 s baseline period were compared against the last 60 s of each step-change. The mean RBC velocity during baseline was found to be significantly different during the high CO₂ perturbation with mean values of $313 \pm 85 \mu\text{m/s}$ and $433 \pm 127 \mu\text{m/s}$, respectively ($p = 0.002$) (Figure 2.2). The mean RBC SR during baseline was found to be significantly different during the high CO₂ perturbation with mean values of $21 \pm 5 \text{ cells/s}$ and $31 \pm 7 \text{ cells/s}$, respectively ($p = 0.001$) (Figure 2.3). The mean Hct during baseline was also found to be significantly different during the high CO₂ perturbation with mean values of $24 \pm 3\%$ and $27 \pm 3\%$, respectively ($p = 0.0006$) (Figure 2.4). The apparent time to a steady state of the blood flow response to tissue CO₂ perturbations is approximately 80 and 65 seconds for RBC velocity and SR, respectively. In addition, no significant changes in RBC SO₂ were observed in response to the high CO₂ step-change (Figure 2.5).

Protocol 1C: Simultaneous determination of the magnitude and dynamics of CO₂-mediated blood flow response

Direct EDL muscle exposure to oscillating CO₂ levels using a microfluidic gas exchange chamber resulted in changes in RBC velocity, SR, and Hct that were consistent with the CO₂-induced blood flow responses previously described with the CO₂ staircase data. A significant decrease in RBC velocity was observed as CO₂ decreased from 5 to 0% ($281 \pm 97 \mu\text{m/s}$ to $125 \pm 66 \mu\text{m/s}$, $p = 0.0002$) followed by a significant increase above the baseline level as CO₂ was increased from 0 to 10% ($125 \pm 66 \mu\text{m/s}$ to $359 \pm 123 \mu\text{m/s}$, $p = 0.0002$) (Figure 2.6). A significant decrease in RBC SR was also observed as CO₂ decreased from 5 to 0% ($13 \pm 3 \text{ cells/s}$

to 3 ± 2 cells/s, $p < 0.0001$) followed by a significant increase above the baseline level as CO₂ was increased from 0 to 10% (3 ± 2 cells/s to 18 ± 5 cells/s, $p < 0.0001$) (Figure 2.6). However, significant changes in both RBC velocity and SR were not observed when CO₂ was returned to 5% from 10% CO₂ and both variables remained elevated (352 ± 129 μ m/s and 17 ± 6 cells/s, respectively) (Figure 2.6). A significant decrease in Hct was also observed as CO₂ decreased from 5 to 0% ($18 \pm 3\%$ to $8 \pm 3\%$, $p = 0.0005$) followed by a significant increase as CO₂ increased from 0 to 10% CO₂ ($8 \pm 3\%$ to $20 \pm 4\%$, $p < 0.0001$) (Figure 2.6). However, there was no significant difference in Hct between either of the 5% CO₂ conditions ($18 \pm 3\%$ and $19 \pm 4\%$) and the 10% CO₂ condition ($20 \pm 4\%$) (Figure 2.6). This result is consistent with the CO₂ staircase response. In addition, RBC SO₂ remained unchanged across the various CO₂ concentrations.

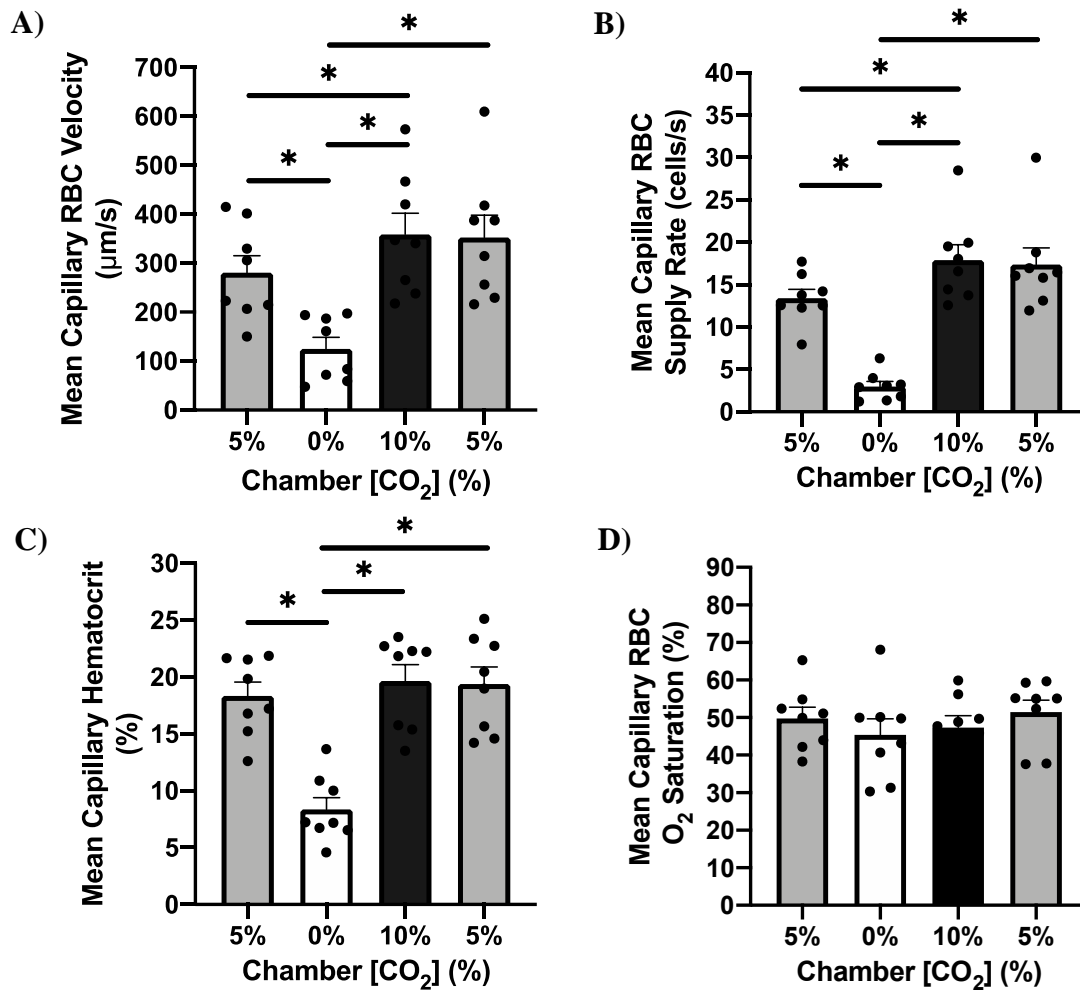


Figure 2. 6. Capillary hemodynamics and RBC oxygen saturation in rat skeletal muscle in response to oscillating tissue CO₂ concentrations using a gas exchange chamber. The muscle was exposed to each CO₂ concentration (5, 0, 10, 5%) for one-minute while maintaining a constant oxygen level (5%). Capillary red blood cell (RBC) velocity (A), RBC supply rate (B), hematocrit (C), and RBC oxygen saturation (D) were measured from recorded intravital video microscopy sequences. The average value of each variable was calculated per animal. The bars represent the average of all included animals. Error bars indicate SEM. A repeated measures one-way ANOVA and a Tukey's multiple comparisons test were used to determine statistical significance. *Note.* * = p-value < 0.05 (N= 8 animals, 242 capillaries (A-C) and 121 capillaries (D)).

In addition to measuring the change in magnitude, the dynamic microvascular blood flow response to oscillating CO₂ was observed and measured. The decreases in RBC velocity, SR, and Hct were initiated quickly (< 10 seconds) in response to decreasing CO₂; however, the maximum response and new apparent steady state were not reached for each hemodynamic variable until at least 60 seconds after the imposed step-change (Figure 2.7). A similar dynamic response was observed for RBC velocity and SR as CO₂ was increased from 0 to 10% (Figure 2.7). The change in Hct in response to increasing CO₂ from 0 to 10% appears quicker, with the maximum response and new steady state being reached approximately 30 seconds after the imposed step-change (Figure 2.7). In addition, there was no significant change in RBC SO₂ as CO₂ decreased from 5 to 0% (Figure 2.7). A slight decrease in RBC SO₂ was observed as CO₂ was increased from 0 to 10%; however, this decrease was very brief and oxygen saturation values quickly returned to baseline levels for the remainder of the oscillation (Figure 2.7).

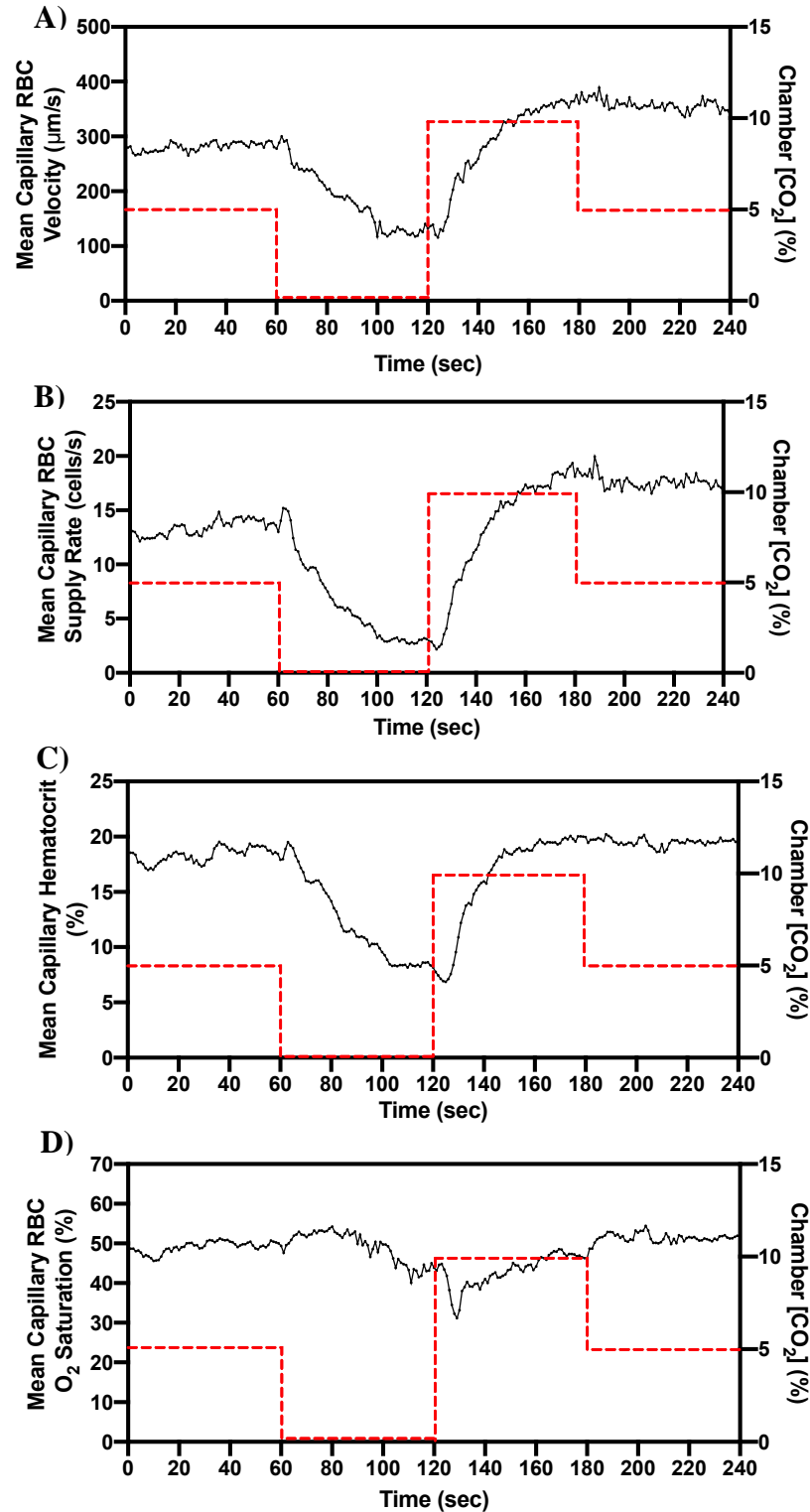


Figure 2. 7. Time series plots demonstrating the change in mean RBC velocity (A), RBC supply rate (B), hematocrit (C), and RBC oxygen saturation (D) in response oscillating tissue CO₂ perturbations over a 4-minute period. Step-changes in the chamber CO₂ concentrations are represented by red dashed lines. (N= 8 animals, 242 capillaries (A-C) and 121 capillaries (D)).

Protocol 1D: Simultaneous determination of the magnitude and dynamics of O₂-mediated blood flow response

Direct EDL muscle exposure to oscillating O₂ levels using a microfluidic gas exchange chamber resulted in dynamic changes in RBC velocity, SR, Hct, and SO₂. A significant decrease in RBC velocity was observed as O₂ increased from 7 to 12% ($317 \pm 70 \mu\text{m/s}$ to $275 \pm 77 \mu\text{m/s}$, $p = 0.0270$) followed by a significant increase above the baseline level as O₂ decreased from 12 to 2% ($275 \pm 77 \mu\text{m/s}$ to $355 \pm 82 \mu\text{m/s}$, $p = 0.0031$) (Figure 2.8). There were no significant differences in RBC velocity observed between either of the 7% O₂ conditions ($317 \pm 70 \mu\text{m/s}$ and $327 \pm 91 \mu\text{m/s}$) and the 2% O₂ condition ($355 \pm 82 \mu\text{m/s}$) (Figure 2.8). Significant changes in RBC SR were observed between several O₂ concentrations, including 7% and 12% O₂ (20 ± 5 cells/s and 13 ± 4 cells/s, $p = 0.0045$), 12% and 2% O₂ (13 ± 4 cells/s and 24 ± 5 cells/s, $p = 0.0008$), and 7% and 2% O₂ (20 ± 5 cells/s and 24 ± 5 cells/s, $p = 0.0042$) (Figure 2.8). A significant increase in Hct was also observed as O₂ decreased from 12 to 2% ($17 \pm 6\%$ to $23 \pm 4\%$, $p = 0.0040$) followed by a significant decrease as O₂ increased from 2 to 7% O₂ ($23 \pm 4\%$ to $20 \pm 3\%$, $p = 0.0033$) (Figure 2.8). However, there was no significant difference in Hct between either of the 7% O₂ conditions ($22 \pm 4\%$ and $20 \pm 3\%$) and the 12% O₂ condition ($17 \pm 6\%$) (Figure 2.8). Finally, significant changes in RBC SO₂ were observed between each 7% O₂ condition (64 ± 5 and 62 ± 6) and 12% O₂ (77 ± 4 , $p < 0.003$), 12% and 2% O₂ (77 ± 4 to 43 ± 8 , $p < 0.0001$), and each 7% O₂ condition (64 ± 5 and 62 ± 6) and 2% O₂ (43 ± 8), $p < 0.0001$) (Figure 2.8).

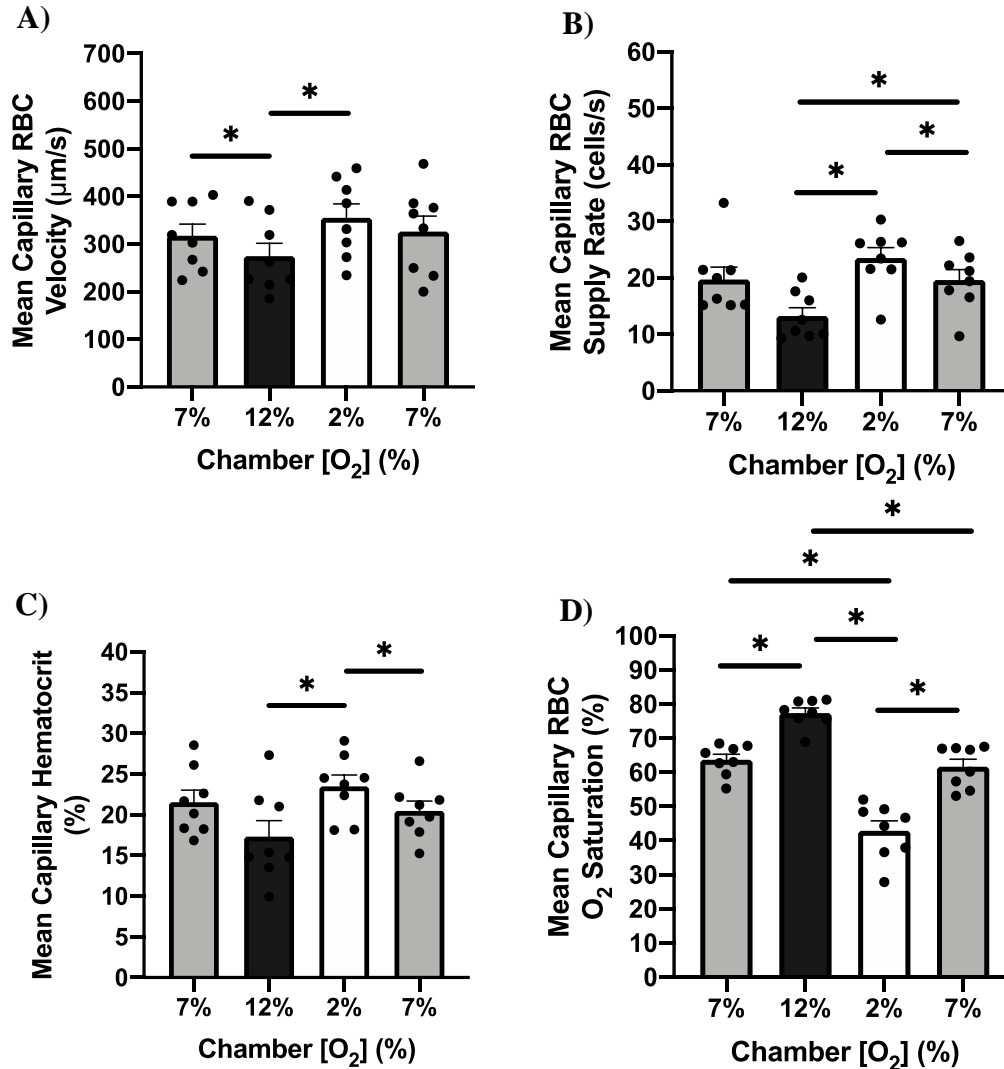


Figure 2. 8. Capillary hemodynamics in rat skeletal muscle in response to oscillating tissue O₂ concentrations using a gas exchange chamber. The muscle was exposed to each O₂ concentration (7, 12, 2, 7%) for one-minute while maintaining a constant CO₂ level (5%). Capillary red blood cell (RBC) velocity (A), RBC supply rate (B), hematocrit (C), and RBC oxygen saturation (D) were measured from recorded intravital video microscopy sequences. The average value of each variable was calculated per animal. The bars represent the average of all included animals. Error bars show SEM. A repeated measures one-way ANOVA and a Tukey's multiple comparisons test were used to determine statistical significance. (N= 8, 242 capillaries (A-C) and 113 capillaries (D)).

In addition to measuring the change in magnitude, the dynamic microvascular blood flow response to oscillating O_2 was observed and measured. The decrease in RBC velocity, SR, and Hct was initiated quickly in response to increasing O_2 and occurred within approximately 10 seconds (Figure 2.9). However, the maximum response and new apparent steady state were not reached for each hemodynamic variable until at least 30 seconds after the imposed step-change (Figure 2.9). A more rapid dynamic response was observed for RBC velocity, SR, and Hct as O_2 decreased from 12 to 2% and a new apparent steady state was achieved approximately 10 seconds after the imposed change (Figure 2.9). Each hemodynamic variable quickly returned to baseline levels as O_2 increased from 2 to 7%, again with this change occurring within approximately 10 seconds after the imposed change in the tissue microenvironment (Figure 2.9). Finally, near instantaneous changes in RBC SO_2 were observed as O_2 concentrations oscillated across 7, 12, 2, and 7% O_2 (Figure 2.9).

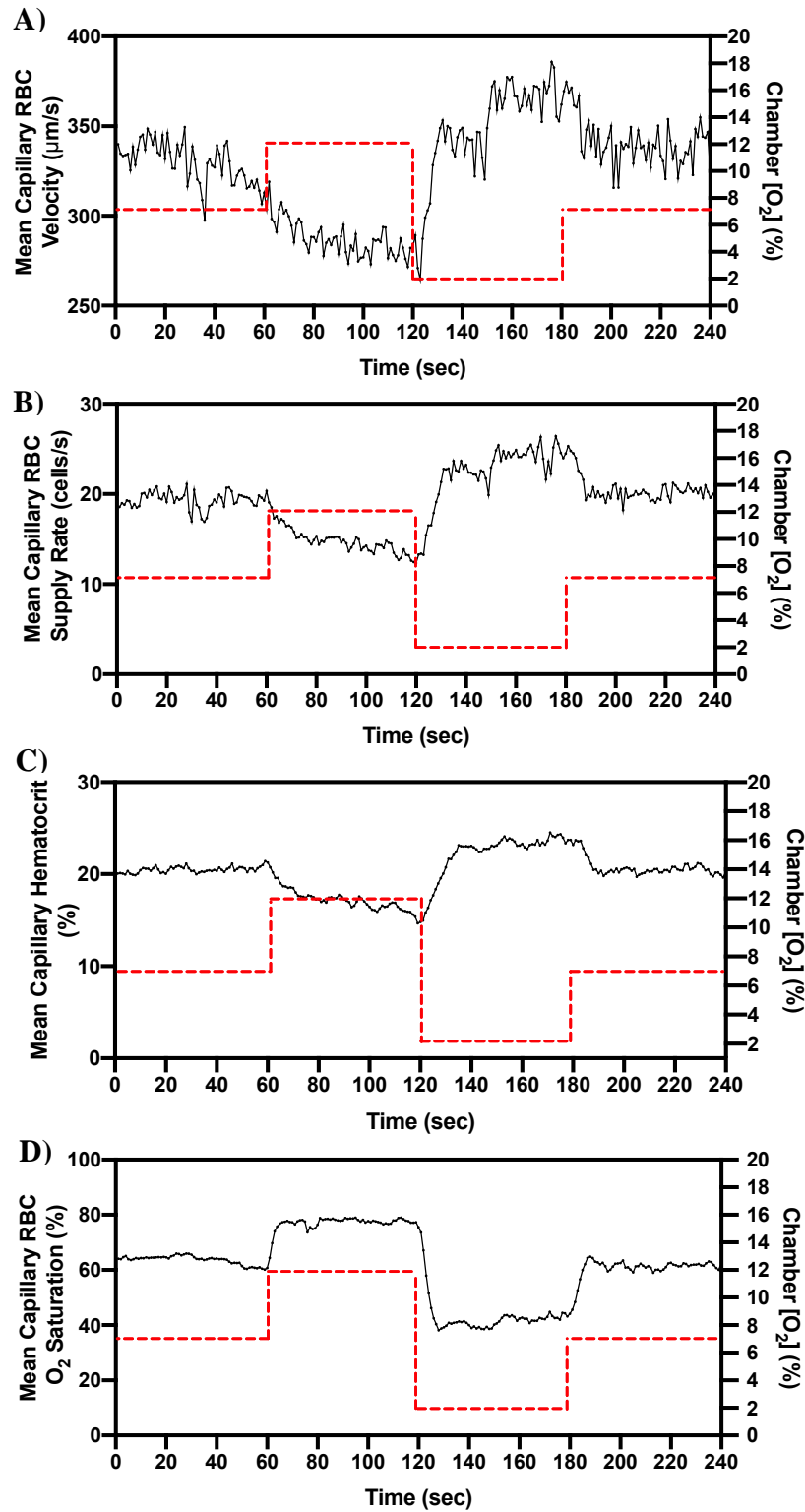


Figure 2. 9. Time series plots demonstrating the change in mean RBC velocity (A), RBC supply rate (B), hematocrit (C), and RBC oxygen saturation (D) in response oscillating tissue O_2 perturbations over a 4-minute period. Step-changes in the chamber O_2 concentrations are represented by red dashed lines. (N = 8, 242 capillaries (A-C) and 113 capillaries (D)).

2.3.2 Experimental Protocol 2: Investigation of the role of ATP-sensitive K⁺ ion (K_{ATP}) channels in CO₂-mediated blood flow regulation.

Direct, incremental changes in CO₂ within the EDL muscle tissue microenvironment following the administration of GLI yielded a graded increase in both RBC velocity and SR. However, the response did not appear to be as pronounced as during the baseline condition. It is important to note that the overall flow state of the tissue was elevated during GLI data collection compared to baseline conditions, due to either the gradual increase in flow observed over time or due to the systemic administration of GLI. Significant differences in RBC velocity were observed between 0 and 6% CO₂ ($415 \pm 151 \mu\text{m/s}$ and $555 \pm 170 \mu\text{m/s}$, $p = 0.037$) as well as between 5 and 10% CO₂ ($530 \pm 193 \mu\text{m/s}$ and $587 \pm 195 \mu\text{m/s}$, $p = 0.0465$) (Figure 2.10). Significant differences in RBC SR were observed between several CO₂ concentrations, including between 2 and 6% CO₂ ($28 \pm 10 \text{ cells/s}$ and $45 \pm 11 \text{ cells/s}$, $p = 0.0295$), 2 and 10% CO₂ ($28 \pm 10 \text{ cells/s}$ and $53 \pm 12 \text{ cells/s}$, $p = 0.0059$), 4 and 10% CO₂ ($34 \pm 17 \text{ cells/s}$ and $53 \pm 12 \text{ cells/s}$, $p = 0.0272$), and 5 and 10% CO₂ ($43 \pm 14 \text{ cells/s}$ and $53 \pm 12 \text{ cells/s}$, $p = 0.0419$) (Figure 2.10). An incremental increase in CO₂ also yielded a similar graded increase in Hct; however, the response was more subtle and significant differences were only found between 4 and 6% CO₂ ($22 \pm 7\%$ and $26 \pm 8\%$, $p = 0.0062$), as shown in Figure 2.10. In addition, there was no significant change in RBC SO₂ across the various CO₂ concentrations (Figure 2.10).

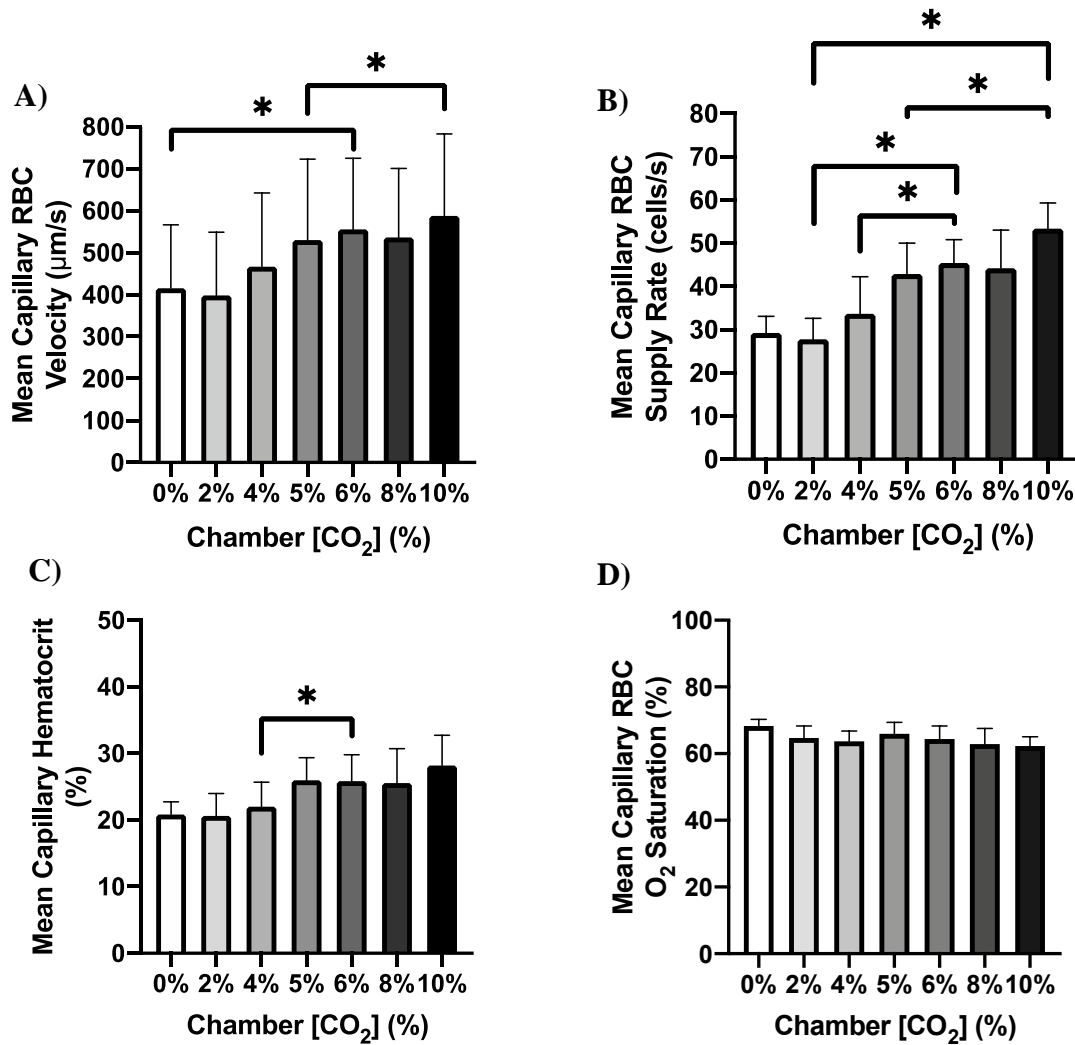


Figure 2. 10. Capillary hemodynamics in rat skeletal muscle at a range of tissue CO_2 concentrations following intravenous administration of glibenclamide (GLI, 5 mg/kg). The muscle was exposed to each concentration (0, 2, 4, 5, 6, 8, 10% CO_2) for one-minute while maintaining a constant O_2 level (5%). Capillary red blood cell (RBC) velocity (A), RBC supply rate (B), hematocrit (C), and capillary RBC oxygen saturation (D) were measured after allowing the muscle to equilibrate with each concentration. The average value of each variable at each concentration was calculated per animal. The bars represent the average of all included animals. Error bars show SEM. A repeated measures one-way ANOVA and a Tukey's multiple comparisons test were used to determine statistical significance. (N = 4 animals, 130 capillaries (A-C) and 92 capillaries (D)).

Direct muscle exposure to oscillating CO₂ levels following the administration of GLI also resulted in changes in both RBC velocity and SR that were similar to the baseline responses, although less pronounced. A significant decrease in RBC velocity was observed as CO₂ decreased from 5 to 0% ($372 \pm 67 \mu\text{m/s}$ to $281 \pm 85 \mu\text{m/s}$, $p = 0.0423$) followed by a significant increase above the baseline level as CO₂ was increased from 0 to 10% ($281 \pm 85 \mu\text{m/s}$ to $461 \pm 102 \mu\text{m/s}$, $p = 0.0338$) (Figure 2.11). A significant decrease in RBC SR was also observed as CO₂ decreased from 5 to 0% ($22 \pm 1 \text{ cells/s}$ to $12 \pm 1 \text{ cells/s}$, $p = 0.0320$) followed by a significant increase above the baseline level as CO₂ was increased from 0 to 10% ($12 \pm 1 \text{ cells/s}$ to $28 \pm 3 \text{ cells/s}$, $p = 0.0299$) (Figure 2.11). However, significant changes in both RBC velocity and SR were not observed when CO₂ was returned to 5% from 10% CO₂ and both variables remained elevated ($477 \pm 82 \mu\text{m/s}$ and $28 \pm 3 \text{ cells/s}$, respectively) (Figure 2.11). A small decrease in Hct was also observed as CO₂ decreased from 5 to 0% followed by a small increase above the baseline levels as CO₂ increased from 0 to 10%; however, these responses were not significant (Figure 2.11). The time transient associated with changes in each of these variables (RBC velocity, SR, and Hct) were similar (Figure 2.12). The decrease in each hemodynamic variable was initiated quickly as CO₂ decreased from 5 to 0%; however, the maximum responses did not appear to be reached for each variable until at least 60 seconds after the imposed step-change (Figure 2.12). Similar dynamic responses for each variable were also observed as CO₂ increased from 0 to 10%; however, the response appeared to be quicker, and a new steady-state was achieved approximately 30 seconds after the imposed step-change (Figure 2.12). Finally, RBC SO₂ remained unchanged across the various CO₂ concentrations (Figure 2.11).

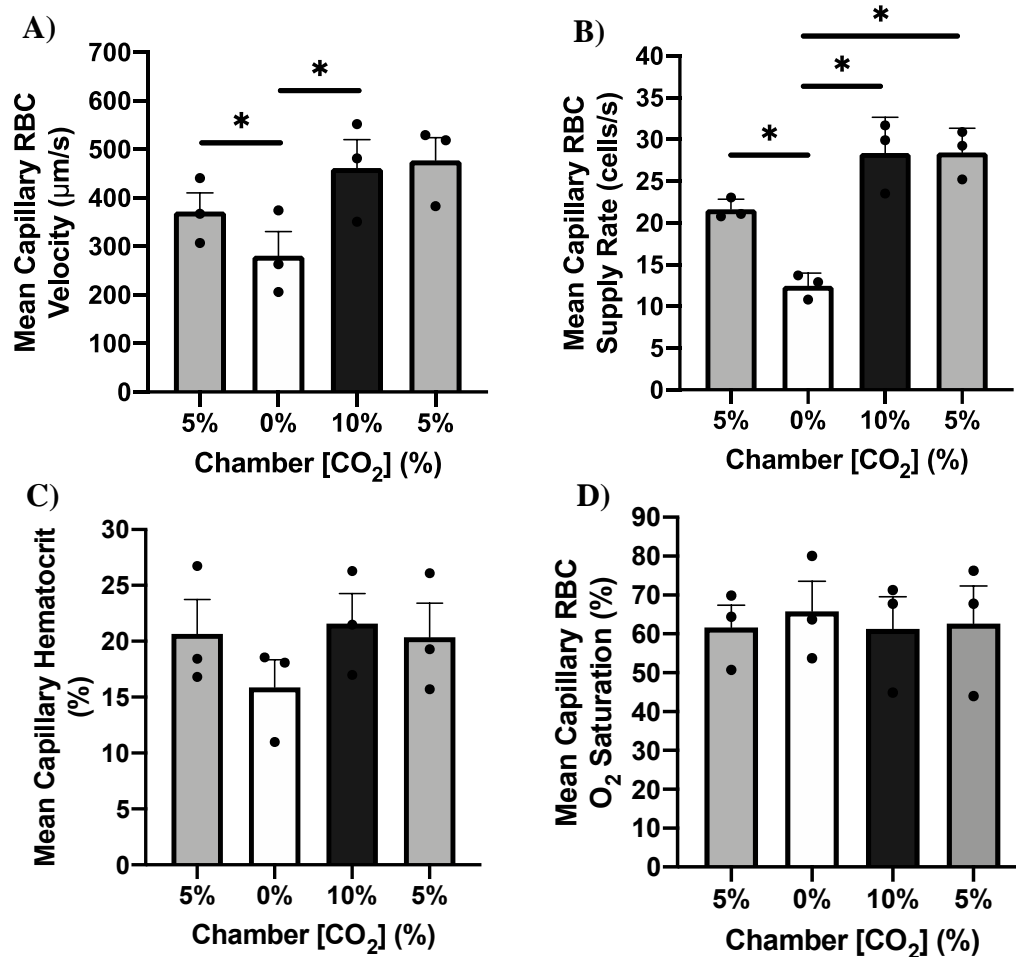


Figure 2. 11. Capillary hemodynamics in rat skeletal muscle in response to oscillating tissue CO_2 concentrations following intravenous administration of glibenclamide (5 mg/kg). The muscle was exposed to each CO_2 concentration (5, 0, 10, 5%) for one-minute while maintaining a constant O_2 level (5%). Capillary red blood cell (RBC) velocity (A), RBC supply rate (B), hematocrit (C), and RBC oxygen saturation (D) were measured from recorded intravital video microscopy sequences. The average value of each variable was calculated per animal. The bars represent the average of all included animals. Error bars show SEM. A repeated measures one-way ANOVA and a Tukey's multiple comparisons test were used to determine statistical significance. (N = 3 animals, 57 capillaries (A-C) and 28 capillaries (D)).

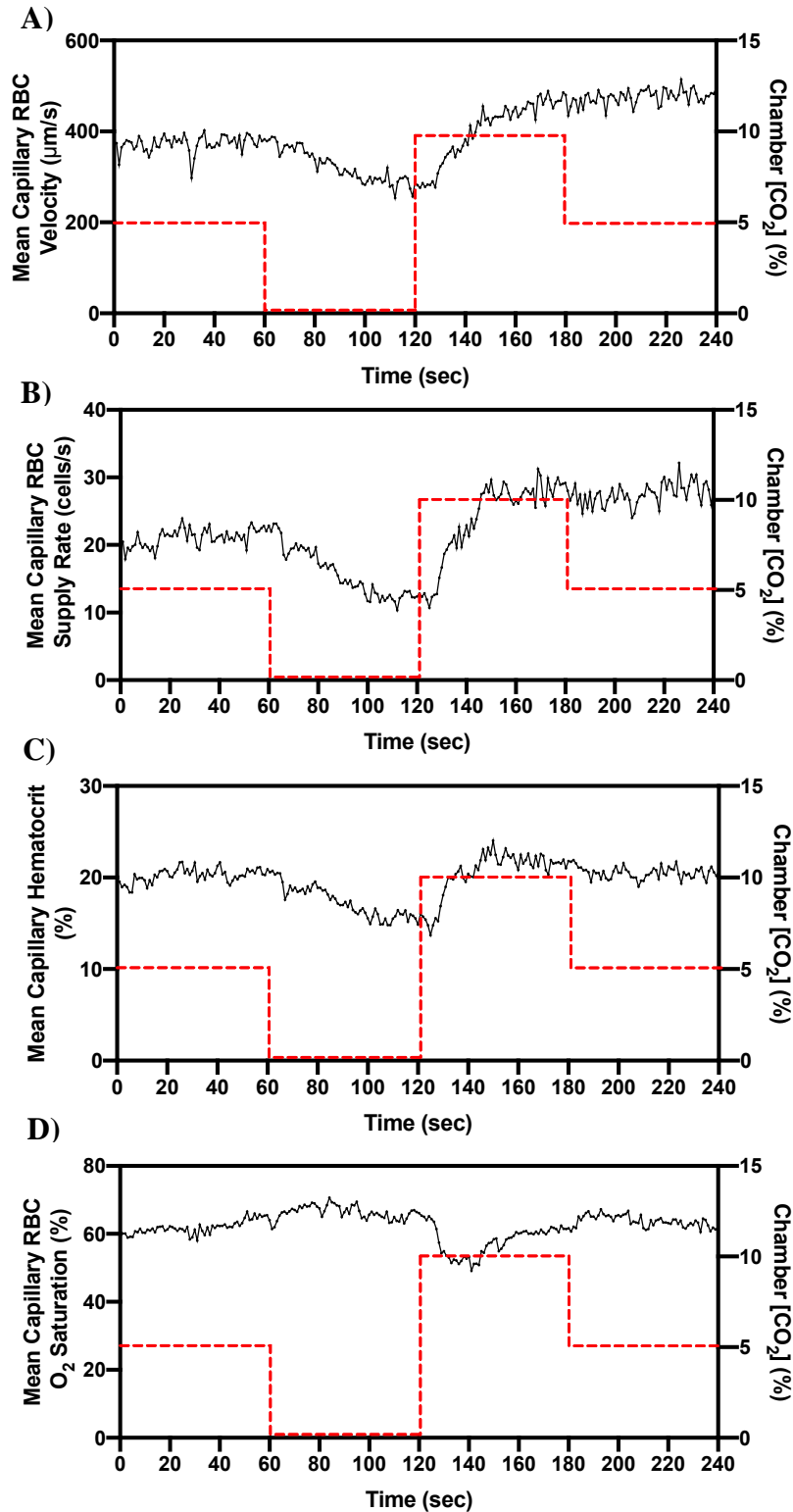


Figure 2. 12. Time series plots demonstrating the change in mean RBC velocity (A), RBC supply rate (B), hematocrit (C), and RBC oxygen saturation (D) in response oscillating tissue CO_2 perturbations following intravenous administration of glibenclamide (5 mg/kg). Step-changes in the chamber CO_2 concentrations are represented by red dashed lines. (N = 3 animals, 57 capillaries (A-C) and 28 capillaries (D)).

In contrast to the CO₂ oscillations, the administration of GLI appeared to alter microvascular blood flow responses to direct EDL muscle exposure to oscillating O₂ levels. There was no significant difference in RBC velocity as O₂ was increased from 7 to 12% or as it was decreased from 12 to 2% (Figure 2.13 and 2.14). However, a gradual increase in capillary RBC velocity was observed over the course of the 4-minute period and there was a significant difference between 12% O₂ and the second 7% O₂ conditions ($391 \pm 163 \mu\text{m/s}$ and $470 \pm 160 \mu\text{m/s}$, $p = 0.0088$). A similar response occurred with capillary RBC SR as no significant differences were observed as O₂ increased from 7 to 12% or decreased from 12 to 2% (Figure 2.13 and 2.14). A slight gradual increase in RBC SR was also observed throughout the 4-minute period; however, unlike RBC velocity, this was not significant (Figure 2.13 and 2.14). A small decrease in Hct was also observed as O₂ increased from 7 to 12% followed by a small increase as O₂ decreased from 12 to 2% O₂; however, these responses were also not significant (Figure 2.13 and 2.14). Hct also returned to baseline levels as O₂ increased from 2 to 7%, although the response was not significant (Figure 2.13 and 2.14). In addition, changes in capillary RBC SO₂ were observed in response to oscillating O₂ levels. However, the responses were not as pronounced as during baseline conditions and significant differences were only observed as O₂ decreased from 12 to 2% (80 ± 9 to 47 ± 15 , $p = 0.0324$) and as it increased from 2 to 7% (47 ± 15 to 69 ± 14 , $p = 0.0194$) (Figure 2.13 and 2.14). Similar to baseline responses, the capillary RBC SO₂ response to O₂ step-changes following GLI administration occurred immediately following the imposed change in chamber [O₂] (Figure 2.14).

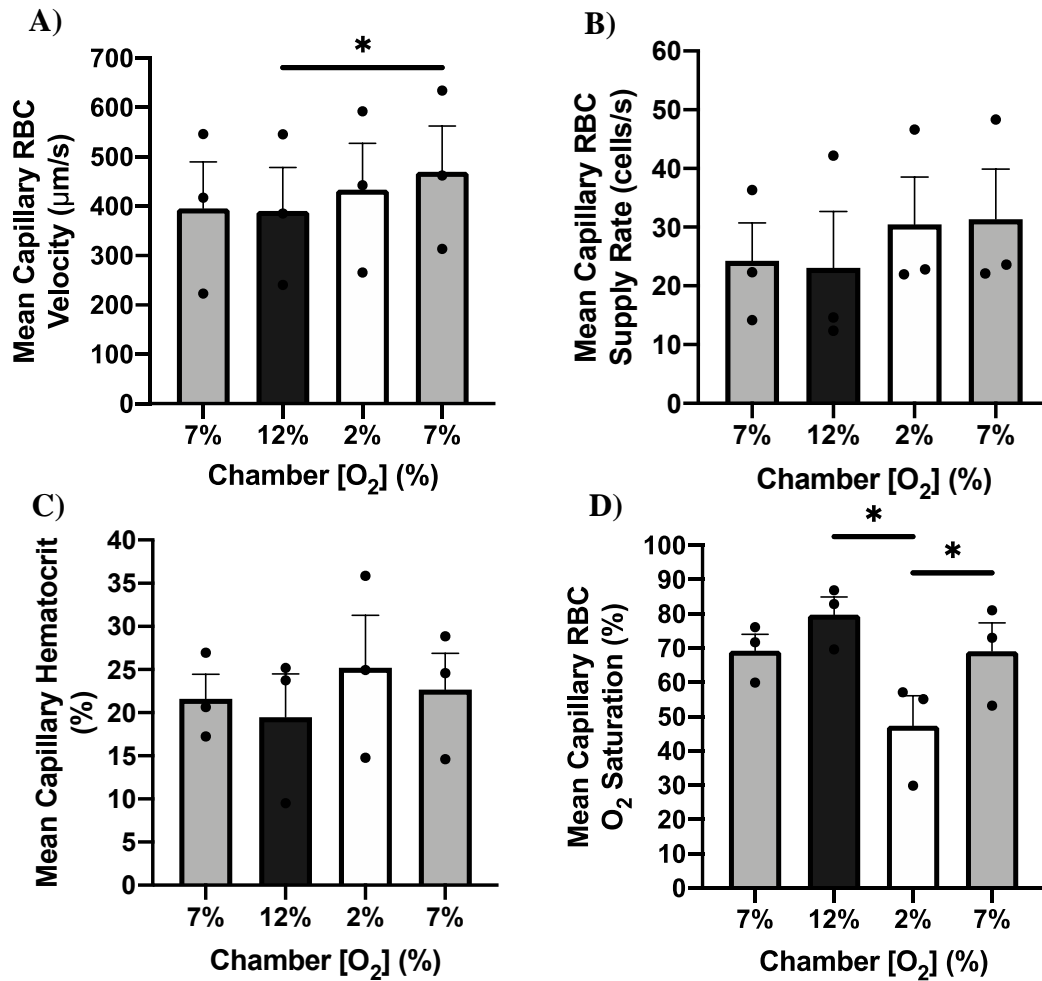


Figure 2. 13. Capillary hemodynamics in rat skeletal muscle in response to oscillating tissue O_2 concentrations following intravenous administration of glibenclamide (5 mg/kg). The muscle was exposed to each O_2 concentration (7, 12, 2, 7%) for one-minute while maintaining a constant CO_2 level (5%). Capillary red blood cell (RBC) velocity (A), RBC supply rate (B), hematocrit (C), and RBC oxygen saturation (D) were measured from recorded intravital video microscopy sequences. The average value of each variable was calculated per animal. The bars represent the average of all included animals. Error bars show SEM. A repeated measures one-way ANOVA and a Tukey's multiple comparisons test were used to determine statistical significance. (N = 3 animals, 35 capillaries (A-C) and 16 capillaries (D)).

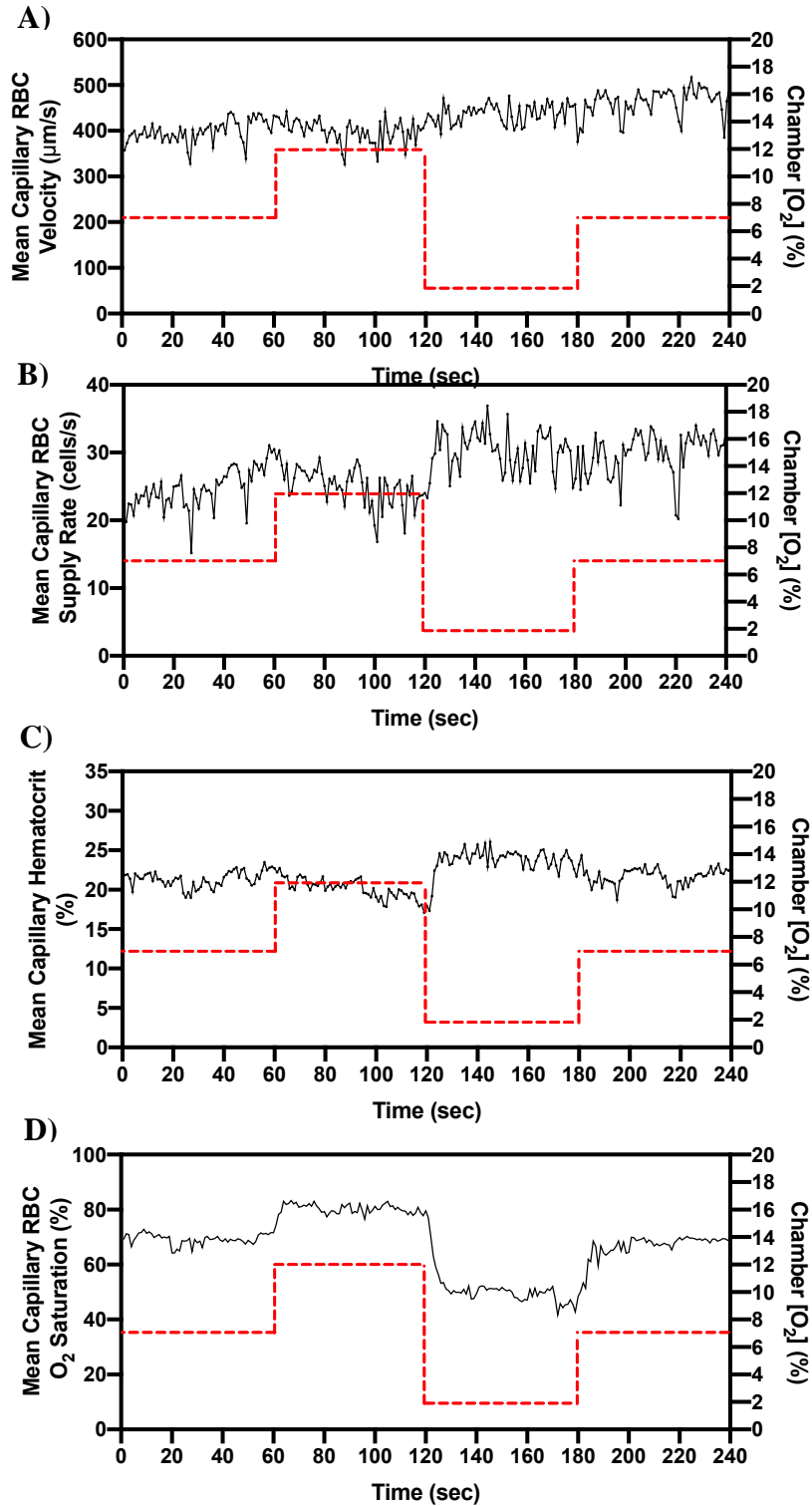


Figure 2. 14. Time series plots demonstrating the change in mean RBC velocity (A), RBC supply rate (B), hematocrit (C), and RBC oxygen saturation (D) in response oscillating tissue O₂ perturbations following intravenous administration of glibenclamide (5 mg/kg). Step-changes in the chamber O₂ concentrations are represented by red dashed lines. (N = 3, 35 capillaries (A-C) and 16 capillaries (D)).

2.4 Discussion

The objectives of the current study were to advance our understanding of CO₂-mediated microvascular blood flow regulation in skeletal muscle tissue through the characterization of the dynamic response under physiological conditions as well as the investigation of potential underlying mechanisms. Our findings demonstrate that localized changes in skeletal muscle tissue CO₂ concentrations initiate rapid (order of seconds) and significant microvascular blood flow responses at the capillary level. We have also provided evidence supporting a partial involvement of vascular K_{ATP} channels in CO₂-mediated microvascular blood flow regulation. Finally, we have provided evidence against a role for CO₂-induced changes in oxygen saturation in regulating CO₂-mediated blood flow responses, which supports the presence of independent vasoactive pathways underlying CO₂-mediated and O₂-mediated microvascular blood flow regulation.

Although evidence supporting CO₂-mediated microvascular blood flow regulation has been provided in several vascular beds, the blood flow response across a physiological range of CO₂ concentrations has not been well described. There are some studies that have measured microvascular responses to a wide range of tissue CO₂ concentrations in both the cerebral and striated muscle tissue microcirculations (Kontos, Wei, et al., 1977; Ward, 1996). In the cerebral microcirculation, changes in arteriolar diameter have been observed in response to a wide range of tissue CO₂ perturbations (0 to 275 mmHg), with the most pronounced changes occurring within a physiological range of tissue CO₂ concentrations (0 and ~60 mmHg) that is similar to the range used in the current study (Kontos, Wei, et al., 1977). However, CO₂-induced responses also appear to differ between microvascular beds (Ward, 1996; Charter et al., 2018). In contrast

to the cerebral microcirculation, diaphragmatic microvessels have been shown to be less sensitive to tissue CO₂ perturbations and do not experience significant microvascular responses until a CO₂ concentration above 80 mmHg is reached (Ward, 1996). In the cremaster muscle microcirculation, significant arteriolar vasodilation has been observed in response to moderate increases in tissue CO₂ (from 43 to 62 mmHg CO₂), which is similar to responses observed in the cerebral microcirculation as well as those presented in the current study. However, increasing the cremaster muscle tissue CO₂ to 74 mmHg shifted the microvascular response from vasodilation to vasoconstriction, which differs from our results and the results presented in cerebral tissue (Kontos, Wei, et al., 1977; Charter et al., 2018). In addition, the microvascular response to a stepwise decrease in striated muscle tissue CO₂ has not been measured (Ward, 1996; Charter et al., 2018). The variation of CO₂-induced microvascular responses across different vascular beds demonstrates that conclusions drawn from one region of study cannot always be translated into another and highlights the need to characterize responses in different vascular beds to gain a complete understanding of blood flow regulation across tissues. While information regarding the magnitude of CO₂-induced arteriolar diameter responses has been provided in several vascular beds, direct measurements of the microvascular blood flow responses were not made in these studies. In addition, previous research has primarily investigated the influence of CO₂ on arteriolar tone and the contribution of CO₂ in local blood flow regulation at the capillary level, especially in skeletal muscle tissue, is not well-defined.

In the present study, we measured a graded increase in several capillary hemodynamic variables (RBC velocity, RBC supply rate, and hematocrit) in response to rapid, incremental, and localized changes in the tissue CO₂ concentration (0 to 76 mmHg) of the EDL muscle *in vivo*. Significant

changes in both capillary RBC velocity and supply rate were observed between several CO₂ concentrations, most notably between 0 and 5% CO₂ (0 and 38 mmHg), 0 and 10% CO₂ (0 and ~76 mmHg) and 5 and 10% CO₂ (Figure 2.1 and 2.6). A graded increase in capillary hematocrit was also observed as tissue CO₂ was increased; however, the response was more subtle and appeared to be more responsive to low (0%) rather than high CO₂ concentrations (Figure 2.1 and 2.6). The lack of significant change in hematocrit during various CO₂ perturbations suggests that the influence of elevated CO₂ on capillary RBC SR is more so driven by changes in RBC velocity rather than Hct. Overall, the significant capillary hemodynamic responses to tissue CO₂ perturbations support a significant role for CO₂ in coordinating local microvascular blood flow with metabolic demand in skeletal muscle tissue. These findings are consistent with previous studies that investigated CO₂-induced responses in the cerebral microcirculation, where evidence supporting a significant role for tissue CO₂ in local blood flow regulation was provided and significant changes in arteriolar diameter were observed when exposed to a similar range of CO₂ concentrations (0-60 mmHg) (Kontos, Wei, et al., 1977; Wei et al., 1980; Pelligrino et al., 1995). In addition, by demonstrating significant changes in capillary hemodynamics in response to small, incremental CO₂ perturbations within a physiological range, our findings support a high sensitivity of the smallest microvessels to variations in local CO₂ in skeletal muscle tissue. In addition, the ability for local CO₂ to induce strong microvascular blood flow responses initiated at the capillaries and/or terminal arterioles suggests that the resulting blood flow response has potential high spatial specificity and only increases blood flow towards metabolically active regions of muscle fibers, which enables local CO₂ to ensure tight coupling between blood supply with metabolic demand (Berg et al., 1997; Twynstra et al., 2012). The pronounced capillary responses described here are also consistent with previous research conducted in both the

cerebral and diaphragmatic microcirculations, where the magnitude of CO₂-induced microvascular responses depended on vessel size and more profound arteriolar responses to CO₂ were measured in smaller vessels (Raper et al., 1971; Wei et al., 1980; Ward, 1996)). The strong microvascular responses in smaller vessels, especially in capillaries, may be due to a higher CO₂ permeability across thinner vessel walls or due to the presence of smaller volumes of blood flowing through the vessels causing capillaries to experience more dramatic changes in PCO₂. The impact of vessel diameter and/or flow on the ability to alter blood gas conditions following tissue perturbations is supported by modelling data presented by Ghonaim et al. (2013), where arterioles displayed some resistance to changes in RBC SO₂ following surface O₂ perturbations compared to capillaries. While the presented findings are consistent with studies conducted in the cerebral microcirculation, they also contrast with previous work presented by Charter et al. (2018), where direct application of CO₂ on cremaster muscle capillaries causes modest increases in diameter of upstream arterioles and it was suggested that CO₂ was not significantly involved in local blood flow regulation (Charter et al., 2018). However, blood flow measurements in the downstream capillary networks were not made in this study (Charter et al., 2018). While arteriolar diameter measurements provide valuable information regarding microvascular responses to vasoactive stimuli, changes in arteriolar diameter, and therefore vascular resistance, can only be determined in individual vessel segments and not throughout the contiguous vascular networks. Therefore, arteriolar diameter measurements do not necessarily correspond to the expected change in vascular resistance and blood flow, which necessitates the direct measurement of variations in microvascular blood flow to fully understand the impact of CO₂ on local blood flow regulation. The data presented in the current study demonstrates significant capillary hemodynamic responses to variations in local tissue CO₂ concentrations, which

suggests that the upstream arteriolar networks experience a large enough change in diameter to influence significant blood flow responses and supports the significant contribution of CO₂ in local blood flow regulation.

In addition to the novelty associated with characterizing the magnitude of capillary hemodynamic responses to a physiological range of tissue CO₂ concentrations in the EDL muscle, the method employed in the current study is a unique way to alter tissue microenvironments *in vivo* and it addresses some of the limitations associated with other experimental techniques. The most common methods for investigating CO₂-induced responses in the microcirculation involve either inhalation-induced systemic changes in arterial CO₂ or topical exposure of tissues to superfusion solutions equilibrated with various CO₂ gas concentrations. While these methods reliably induce significant microvascular responses to both variations in tissue and arterial CO₂, there are several limitations to be considered. The first limitation associated with both methods involves the localization of CO₂-induced blood flow responses. Altering arterial CO₂, either by increasing the concentration of inhaled CO₂ or by decreasing the ventilatory rate, results in systemic changes (such variations in heart rate, blood pressure, cardiac output, cardiac contractility, etc) that can potentially lead to a more widespread impact on overall blood flow and influence the response observed at the microvascular level (Rothe et al., 1990). It is also difficult to determine the level of the vascular tree, as well as the identity of the specific cell types involved in the initiation of CO₂-mediated blood flow responses when multiple levels of the vasculature are being exposed to the change in CO₂. The same issue arises when using a superfusion technique to influence changes in the tissue CO₂ concentration as it is difficult to identify the location of CO₂'s interaction with the vascular system when the entire tissue surface,

and hence vascular networks, are being exposed to the experimental perturbation. The microfluidic GEC employed in this study allows for localized changes in the tissue microenvironment surrounding only the microcirculation under direct observation without impacting the systemic circulation and with minimal disruption to other areas within the muscle. Another limitation associated with inhalation-induced CO₂ alterations is the amount of time required to significantly change the CO₂ concentration and initiate blood flow responses, which can take several minutes to occur (Kontos et al., 1968; Raper et al., 1971). Therefore, it is difficult to accurately measure the timing of CO₂-mediated blood flow responses using this method. The microfluidic GEC alleviates this issue by imposing rapid changes in the gas composition flowing through the device using computer-controlled mass flow meters, which creates rapid changes in the tissue microenvironment and allows us to measure the time transient of the resulting blood flow responses. Developing a clear understanding of both the location and timing of CO₂'s action on the vascular system is important because it provides valuable insight regarding potential underlying mechanisms.

Due to a combination of method related limitations and an overall lack of measurements, the timing of CO₂'s impact on the microvascular system has not been well defined. In several studies conducted in the cerebral microcirculation, data was not collected immediately following the imposed CO₂ perturbations and the arteriolar responses were not measured until after a new steady state was achieved (Kontos, Raper, et al., 1977; Kontos, Wei, et al., 1977; Iadecola, 1992; Wang et al., 1992; Faraci et al., 1994; Wang et al., 1994; Ma et al., 1996; Okamoto et al., 1997). In the few studies that did measure the timing of CO₂-induced microvascular responses, it took several minutes for a significant response to occur (Raper et al., 1971; Minamiyama &

Yamamoto, 2010; Charter et al., 2018). In the cerebral microcirculation, arteriolar responses to elevated inspired CO₂ (7 and 10%) have been shown to require between 1.5 - 2.5 minutes to be initiated and between 5 – 8 minutes for maximum responses to be observed, depending on the magnitude of the imposed CO₂ perturbation (Raper et al., 1971). Fabricius et al. (1996) reported a much quicker response to inhalation-induced hypercapnia in the cerebral microcirculation where they observed a maximum increase in arteriolar diameter between 1 and 1.5 minutes after the imposed CO₂ change; however, the data supporting this claim was not published. A similar response was recorded in the cremaster muscle microcirculation, where a significant increase in arteriolar diameter (~1-2 μ m above baseline) began to occur 1 minute following an increase in tissue CO₂, with the maximal response (7 μ m above baseline) being observed within 2 minutes of the imposed CO₂ change (0 to 43 mmHg) (Charter et al., 2018). In the subcutaneous microcirculation, a longer response time following topical CO₂ exposure was observed, with initial increases in arteriolar diameter and venular blood flow occurring within 5 minutes of exposure and maximum responses requiring 15 minutes to be observed (Minamiyama & Yamamoto, 2010). The variability in the findings of previous studies and the amount of time required to observe maximal microvascular responses to CO₂ may be due to differences between the vascular beds being studied, the animal models used, the anaesthetics used, and/or the methods used to alter CO₂ concentrations. Also, while some information has been provided regarding the time transient of the microvascular blood flow responses to both elevated tissue and arterial CO₂ concentrations, the timing of the response to lowered CO₂ is yet to be described.

As briefly discussed previously, we were able to study dynamic microvascular blood flow responses by imposing rapid variations in the tissue CO₂ concentration using a microfluidic gas

exchange chamber. The increase in both capillary RBC velocity and supply rate were initiated quickly following an increase in tissue CO₂ from 5 to 10%, occurring within 10-15 seconds of the imposed CO₂ step-change (Figures 2.2 and 2.3). The maximum blood flow response to elevated tissue CO₂ and apparent new steady state was achieved in approximately 80 and 65 seconds for RBC velocity and SR, respectively (Figures 2.2 and 2.3). The faster time transient for RBC SR compared to velocity indicates that CO₂-induced changes in RBC SR also involve changes in capillary Hct. These findings demonstrate that high CO₂ conditions in skeletal muscle tissue have a much quicker impact on microvascular blood flow responses than previously described in a variety of vascular beds, where responses were observed at least several minutes after CO₂ concentrations were increased (Kontos et al., 1968; Raper et al., 1971; Minamiyama & Yamamoto, 2010; Charter et al., 2018). The time transient of the capillary hemodynamic response during high CO₂ conditions described in the current study was most similar to the response presented by Fabricius et al. (1996), where the maximal hypercapnia-induced cerebral arteriolar vasodilation was observed within 60 to 90 seconds. In addition to measuring capillary hemodynamic responses during high CO₂ conditions, we described the time transient of these responses during low CO₂ conditions as well. Capillary RBC velocity, supply rate, and hematocrit each experienced a steep decline following a decrease in tissue CO₂ from 5 to 0%, occurring within 5-10 seconds of the imposed CO₂ step-change (Figures 2.2, 2.3, 2.4 and 2.7). There are a few studies that have provided quantitative evidence supporting a significant decrease in the magnitude of cerebral blood flow as well as arteriolar vasoconstriction in response to lowered tissue and arterial CO₂ concentrations (Kontos, Wei, et al., 1977; Ibayashi et al., 1988; Wang et al., 1992). However, the time transient of the microvascular responses was not measured in these studies (Kontos, Wei, et al., 1977; Ibayashi et al., 1988; Wang et al., 1992).

Therefore, the rapid hemodynamic responses to low tissue CO₂ measured in the current study provide novel information regarding the dynamic response to local variations in CO₂ and further support a high local sensitivity to a physiological range of tissue CO₂ concentrations in skeletal muscle.

Investigating the time transient of dynamic microvascular blood flow responses provides valuable information regarding potential underlying mechanisms, such as the likelihood of a conducted or pH-mediated response. The conduction of vasomotor responses along microvessel walls is a very rapid process (average propagation velocity = 0.02 cm s⁻¹) that enables vasoactive signals generated near distal arteriole and capillary networks to rapidly communicate and coordinate downstream capillary blood flow responses to ensure tight coupling with tissue metabolic demand (Berg et al., 1997; Cohen & Sarelius, 2002; Murrant & Sarelius, 2002; Twynstra et al., 2012). While both the initial and maximum changes in capillary hemodynamic variables were observed quickly after the imposed tissue CO₂ perturbations (within 15 and 90 seconds of the imposed change, respectively), the time frame of the observed responses was much slower than expected if a conducted vasomotor response was involved. This finding agrees with work completed by Charter et al. (2018), where direct application of CO₂ on striated muscle capillaries was unable to elicit an upstream increase in arteriolar diameter. Therefore, the findings presented in the current study as well as those presented by Charter et al. (2018) provide evidence against the involvement of a purely conducted vasomotor response underlying CO₂-mediated microvascular blood flow regulation in striated muscle tissue. The slower time transient of the CO₂-mediated response presented here may be indicative of a pH-mediated response, which is consistent with previous work conducted in the cerebral circulation where it

has been suggested that impact of CO₂ on vascular tone is primarily mediated by the impact of pH on vascular smooth muscle contractility (Kontos, Raper, et al., 1977; Toda et al., 1989; You et al., 1994; Tian et al., 1995; Xu et al., 2001; Wang et al., 2003). However, the role of pH in mediating CO₂-induced responses in the skeletal muscle microcirculation is yet to be fully described. Work completed by Charter et al. (2018) has provided some evidence supporting a synergistic interaction between CO₂ and pH while influencing arteriolar diameter in striated muscle tissue. In addition, they demonstrated that independent changes in pH were able to initiate significant changes in arteriolar diameter in under 2 minutes (Charter et al., 2018). Although simultaneous pH measurements were not made in the current study, the similar time scale of the pH-induced arteriolar responses presented by Charter et al. (2018) and the time transient of the CO₂-mediated capillary hemodynamic responses presented here provides some indirect evidence suggesting the presence of pH-dependent mechanism. However, it is also important to note the absence of RBC SO₂ changes that would be expected due to pH's influence on the oxygen-dissociation curve. Therefore, future experiments recording simultaneous pH measurements during CO₂-induced microvascular blood flow responses are required to directly determine if pH has a role in this response.

To further investigate the mechanism underlying CO₂-mediated microvascular blood flow regulation, we studied the potential involvement of vascular ATP-sensitive potassium ion (K_{ATP}) channels in this response. Due to their ability to influence microvascular tone and respond to changes in cellular metabolism, the involvement of K_{ATP} channels in coordinating blood flow responses has been an active area of research and they have been studied in relation to several factors associated with increased muscle metabolism, including functional (or active) hyperemia

and muscle contraction (Saito et al., 1996; Hammer et al., 2001; Cohen & Sarelius, 2002; Murrant & Sarelius, 2002). Selective inhibition of K_{ATP} channels has been shown to significantly attenuate muscle contraction-induced increases in arteriolar diameter and capillary blood flow (Saito et al., 1996; Hammer et al., 2001; Cohen & Sarelius, 2002; Murrant & Sarelius, 2002). Similar to the vessel-size dependency of CO_2 -induced responses discussed above, the impact of K_{ATP} channel inhibition on muscle-contraction induced arteriolar responses increases with decreasing vessel size, with arteriolar vasodilation being nearly abolished following K_{ATP} channel inhibition in 4th order arterioles (Saito et al., 1996; Hammer et al., 2001). In addition, increases in arteriolar diameter and capillary blood flow in response to muscle fiber stimulation under selected capillary beds were inhibited following the direct application of GLI onto capillaries (Cohen & Sarelius, 2002; Murrant & Sarelius, 2002). These findings support a significant role for K_{ATP} channels in communicating vasoactive signals produced near the smallest microvessels into larger upstream vessels that have the capacity to significantly alter the magnitude and distribution of blood flow directed towards active muscle fibers. While K_{ATP} channels have been shown to be involved in coordinating arteriolar responses and increased capillary blood flow with increased muscle metabolism, their role in coordinating microvascular blood flow responses to specific vasoactive metabolites, such as CO_2 , is yet to be fully described in the skeletal muscle microcirculation.

Findings presented here demonstrate a less profound graded increase in the capillary hemodynamic responses (RBC velocity and supply rate) to incremental and dynamic tissue CO_2 perturbations following the systemic administration of GLI (Figures 2.10, 2.11, and 2.12). Significant changes in capillary RBC velocity were observed in response to larger differences in

tissue CO₂ concentrations, such as between 0 and 6% CO₂ and 5 and 10% CO₂ (Figure 2.10). A similar change in capillary RBC supply rate was also observed, with significant differences occurring between several tissue CO₂ concentrations including 2 and 6% CO₂, 2 and 10% CO₂, and 5 and 10% CO₂ (Figure 2.10). While significant CO₂-induced changes in capillary RBC velocity and supply rate were still measured following the systemic administration of GLI, the magnitude of the responses were smaller than those observed during baseline conditions. For example, under GLI conditions RBC velocity decreased by 24% and RBC SR decreased by 45% when tissue CO₂ decreased from 5 to 0% (Figure 2.11). The percent decrease in both variables was smaller than those observed under baseline conditions, where RBC velocity decreased by 56% and RBC SR decreased by 77% in response to the same tissue CO₂ perturbation (Figure 2.6). The change in RBC velocity and SR in response to an increase in tissue CO₂ was also blunted following the systemic administration of GLI. Under GLI conditions, RBC velocity increased by 11% and RBC SR increased by 23% as tissue CO₂ increased from 5 to 10% (Figure 2.10). The response was more profound under baseline conditions, where RBC velocity increased by 44% and RBC SR increased by 64% in response to the same tissue CO₂ perturbation (Figure 2.1). Therefore, these findings may support at least a partial involvement of vascular K_{ATP} channels in coordinating microvascular blood flow responses to local variations in tissue CO₂. This finding would be consistent with previous evidence presented in the cerebral microcirculation, where changes in arteriolar diameter in response to a similar range of CO₂ concentrations (16-75 mmHg) were significantly attenuated, but not abolished, following selective K_{ATP} channel inhibition via topical application of GLI (Faraci et al., 1994; Wei & Kontos, 1999; Nakahata et al., 2003; Nnorom et al., 2014). One mechanism CO₂ may utilize to influence K_{ATP} channel activation involves CO₂-induced changes in pH. Previous research has

indicated that K_{ATP} channel activation is sensitive to intracellular acidification and that K_{ATP} channels are involved in acidosis-induced arteriolar vasodilation (Davies, 1990; Horiuchi et al., 2002). In addition, hypercapnia-induced increases in whole-cell currents were only significantly reduced following K_{ATP} channel inhibition when hypercapnia was accompanied by a change in pH (Xu et al., 2001; Wang et al., 2003). These findings indicate that CO_2 -mediated changes in pH are responsible for enhanced K_{ATP} channel activation and membrane current during hypercapnic conditions (Xu et al., 2001; Wang et al., 2003). Therefore, the blunted capillary hemodynamic responses following K_{ATP} channel inhibition, along with the slow time transient discussed previously, indicate that CO_2 may influence skeletal muscle tissue microvascular blood flow through pH-mediated changes in K_{ATP} channel activity. However, further experimentation measuring simultaneous changes in both pH and membrane potential, verification and quantification of K_{ATP} channel expression in the skeletal muscle tissue microcirculation, and completion of a GLI dose-response curve to confirm accurate dosage would be required to further investigate this hypothesis. Alternatively, the blunted CO_2 -induced capillary hemodynamic response following systemic administration of GLI may be a powering issue due to the small sample size ($N \leq 4$ animals). Therefore, interpretations and conclusions drawn from these results should be done with caution and additional animals should be tested to ensure adequate power and to clarify the role of these channels in CO_2 -mediated blood flow regulation. In addition, a gradual increase in flow state was observed throughout the duration of all experiments due to prolonged tissue CO_2 exposure, which also decreased the number of vessels available for analysis during GLI conditions. Therefore, additional investigation is also required where baseline and GLI data are collected further apart in time, or collected in separate animals,

to minimize the risk of having an elevated flow state during GLI conditions and to further clarify the role of K_{ATP} channels in this response.

In addition to characterizing the dynamic microvascular blood flow response to variations in skeletal muscle tissue CO_2 , the present study also began to investigate the relationship between CO_2 - and O_2 -mediated blood flow regulation. It is well known that a simultaneous and opposite change in O_2 consumption and CO_2 production occurs in response to variations in cellular metabolism, such as during exercise. However, the potential interaction between the two vasoactive stimuli, including the presence of overlapping vasoactive mechanisms, is not well understood in the skeletal muscle microcirculation. There are a couple of studies that have investigated the potential interaction between CO_2 and O_2 in the cremaster and diaphragmatic microcirculations (Morff et al., 1981; Ward, 1996). Morff et al. (1981) demonstrated that alterations in tissue CO_2 were unable to overcome systemic hypoxia-induced arteriolar vasoconstriction, which suggests that CO_2 has no influence or involvement in the mechanism controlling this response. The lack of interaction between CO_2 and O_2 in initiating microvascular responses was also supported by work completed by Ward (1996), which showed that the combined impact of hypoxia and hypercapnia on arteriolar diameter was additive rather than synergistic. These findings indicate that variations in local CO_2 and O_2 concentrations likely utilize independent mechanisms to initiate appropriate microvascular blood flow responses. The present study provides some evidence which further supports this conclusion in the skeletal muscle tissue microcirculation.

First, we demonstrated that CO₂'s influence on capillary hemodynamics does not appear to depend on changes in RBC oxygen saturation (SO₂) (Figures 2.1 and 2.7). Carbon dioxide's impact on the oxygen dissociation curve, known as the Bohr effect, is of relevance since it not only demonstrates the direct impact of CO₂ on tissue O₂ concentrations, but also highlights a potential shared vasoactive mechanism between the two molecules, such as oxygen saturation-dependent (SO₂) RBC-derived ATP release. Altering microvascular blood flow by increasing extracellular ATP and initiating vasodilatory responses via purinergic receptor activation has been studied as a potential underlying mechanism for O₂-mediated blood flow regulation (Ellsworth et al., 2016; Richardson et al., 2020). However, CO₂'s ability to influence RBC-derived ATP release through an SO₂-dependent mechanism has not been an active area of investigation. Previous research has shown that simultaneous exposure to both hypoxia and hypercapnia, as well as independent changes in pH, were able to increase extracellular RBC-derived ATP (Bergfeld & Forrester, 1992; Ellsworth et al., 1995). However, these studies have yet to be completed *in vivo* and the independent role of CO₂ in RBC-derived ATP release has not been determined.

In the present study, no significant changes in capillary RBC SO₂ were observed in response to incremental increases in tissue CO₂ concentrations (0 to 10%) or during dynamic CO₂ oscillations (5-0-10-5%) (Figures 2.1, 2.6 and 2.7). A small decline in RBC SO₂ was observed as CO₂ increased from 0 to 10% during the CO₂ oscillations; however, the decline was very brief and SO₂ values quickly returned to baseline levels (Figure 2.7). This brief decline may be explained by CO₂'s impact on the tissues flow state. Capillary RBC velocity and supply rate, and therefore the amount of blood directed towards the tissue, are either significantly decreased or

stopped in response to low CO₂ conditions. However, the metabolic rate and oxygen demand of the surrounding tissue remains constant. Therefore, during conditions of slow or stopped microvascular blood flow, the tissue may increase O₂ extraction from RBCs present in the capillaries and/or upstream arterioles to ensure adequate O₂ delivery to the tissue. When CO₂ is increased from 0 to 10%, capillary RBC supply rate and velocity rapidly increase in response to the perturbation and therefore, directs the potentially deoxygenated blood through the capillaries which results in a brief decrease in the RBC SO₂ values. This possible explanation suggests that the transient decline in RBC SO₂ occurred because of CO₂'s influence on local microvascular blood flow and does not initiate the response. This could also explain the decrease in RBC SO₂ observed during the low CO₂ challenge as well (Figure 2.5). Overall, these findings suggest that unlike O₂-mediated responses, CO₂-induced microvascular blood flow responses do not appear to be initiated by an SO₂-dependent mechanism, such as RBC-derived ATP release, which supports the presence of an independent CO₂-mediated blood flow regulation mechanism.

Second, the data presented here indicates a different degree of K_{ATP} channel involvement between CO₂- and O₂-mediated microvascular blood flow regulation. As discussed previously, we provided evidence suggesting a partial dependence of CO₂-mediated responses on K_{ATP} channel activation by demonstrating a blunted increase in capillary RBC velocity and supply rate in response to incremental increases in tissue CO₂ as well as dynamic CO₂ oscillations following the systemic administration of GLI (Figures 2.10-2.12). In contrast to the CO₂-mediated response, selective K_{ATP} channel inhibition had a more profound impact on the microvascular response to oscillating tissue O₂ concentrations (Figures 2.13 and 2.14). During baseline conditions, we observed a significant change in both the capillary hemodynamic (RBC velocity,

RBC supply rate, hematocrit) and RBC SO₂ responses to oscillating tissue O₂ concentrations (7-12-2-7% O₂) (Figures 2.8 and 2.9). These capillary hemodynamic responses were profoundly blunted following systemic administration of GLI and no significant changes in either capillary RBC supply rate or hematocrit were observed in response to O₂ oscillations (Figures 2.13 and 2.14). A gradual increase in capillary RBC velocity was observed throughout the duration of the 4-minute oscillation (Figure 2.14). This increase may represent a delayed blood flow response or may be due to the systemic administration of GLI. Future experiments designed to collect baseline and GLI data in separate animals may help clarify this finding. Overall, these findings suggest that vascular K_{ATP} channels have a significant role in regulating O₂-mediated capillary hemodynamic responses in skeletal muscle tissue.

These findings are consistent with previous studies that investigated the role of K_{ATP} channels in hypoxia-induced blood flow responses in cerebral tissue (Reid et al., 1993; Taguchi et al., 1994; Bryan & Marshall, 1999; Rocha et al., 2020). In these studies, hypoxia-induced increases in cerebral blood flow, vascular conductance, and arteriolar diameter were all significantly attenuated following selective K_{ATP} channel inhibition and therefore, also supported a significant role for these channels in the hypoxic response (Reid et al., 1993; Taguchi et al., 1994; Bryan & Marshall, 1999; Rocha et al., 2020). However, there is also evidence against the presence of a K_{ATP} channel-dependent pathway underlying O₂-mediated blood flow regulation. Jackson (2000a) also provided evidence supporting impaired oxygen sensitivity of isolated cremaster arteriolar muscle cells to low O₂ bath solutions (15 mmHg) following GLI application; however, they did not measure a change in membrane potential during hypoxic conditions. Therefore, they suggested that hypoxia-induced arteriolar responses were not due to the activation of K_{ATP}

channels and the impact of GLI on the response was likely due to nonspecific effects of the pharmacological agent (Jackson, 2000a). There are some alternative explanations for the lack of significant capillary hemodynamic responses to oscillating tissue O₂ concentrations following K_{ATP} channel inhibition observed in the current study. First, the tissue experienced a gradual increase in the overall flow state throughout the duration of the experiments. Since the microvascular blood flow responses to oscillating CO₂ and O₂ concentrations were recorded following baseline measurements, a higher flow state was present during these measurements. A higher flow state would indicate a higher O₂ supply to the tissue, which could decrease the O₂ concentration gradient present between the blood and the surrounding tissue. Therefore, the imposed tissue O₂ perturbations might not have been profound enough to elicit a blood flow response. However, since oscillating tissue CO₂ concentrations were still able to influence a blood flow response during the same high flow conditions and significant variations in RBC SO₂ were observed during the O₂ oscillations (Figures 2.11-2.14), the lack of flow response to O₂ is not likely due to the high flow conditions or the inability to induce a profound change in the O₂ concentration. Second, the lack of significant capillary hemodynamic responses could be simply attributed to the small sample size included. Therefore, additional experiments would be required to further elucidate the role of K_{ATP} channels in O₂-mediated blood flow regulation, especially in striated muscle tissue.

In summary, significant capillary blood flow responses were observed in response to a physiological range of tissue CO₂ concentrations, which supports a high CO₂ sensitivity and significant contribution of the smallest microvessels in local blood flow regulation in skeletal muscle tissue. We presented novel information regarding the timing of CO₂-induced

microvascular blood flow responses, which provided indirect evidence against the initiation of a conducted vasomotor response and indicated that CO₂ likely utilizes a pH-dependent mechanism. In addition, the preliminary findings presented here suggest a partial dependence of CO₂-mediated microvascular blood flow responses on vascular K_{ATP} channel activation in skeletal muscle tissue, potentially through a pH-dependent mechanism. However, further experimentation is required to clarify the role of K_{ATP} channels in this response. Finally, we provided evidence against the involvement of a SO₂-dependent vasodilatory mechanism, such as RBC-derived ATP release, in mediating CO₂-induced blood flow responses, which supports the presence of independent mechanisms underlying CO₂-mediated and O₂-mediated blood flow regulation.

Chapter 3 – Summary

Conclusion:

The distribution of blood flow throughout and among tissues is a dynamic and highly regulated process that ensures effective and efficient coupling of O₂ and nutrient supply with metabolic demand, while simultaneously removing of metabolic waste products, such as CO₂. The microvascular system is composed of an extensive and densely branched network of the smallest vessels in the body. The close proximity of microvessels to active muscle tissue fibers as well as their ability to sense and communicate changes in their environment enables the microvascular system to have a significant role in coordinating both the magnitude and distribution of local blood flow. Blood flow regulation is a complex process that requires distal microvessels to integrate a wide variety of vasoactive stimuli, including local metabolic factors and extrinsic neural activity, to induce appropriate changes in microvascular tone and blood flow. Several vasoactive molecules associated with increased muscle metabolism have been shown to interact with distal microvessels to initiate rapid and spatially specific changes in microvascular tone, including O₂, adenosine, K⁺, and ATP. However, the involvement of other vasoactive metabolites, such as CO₂, in local blood flow regulation as well as the mechanism of interaction between CO₂ and the microvascular system, have not been well described. Therefore, the objectives of this thesis were to characterize both the magnitude and time transient of CO₂-mediated microvascular blood flow regulation in skeletal muscle tissue, as well as to investigate potential underlying mechanisms such as the involvement of vascular K_{ATP} channels and SO₂-dependent RBC ATP release.

Using a novel experimental technique to impose rapid, direct, and localized changes in the skeletal muscle tissue microenvironment, we provided evidence supporting a high CO₂ sensitivity of the smallest vessels in the microvascular system as well as a significant role for tissue CO₂ in local microvascular blood flow regulation. We achieved our first objective by characterizing the magnitude and time transient of the expected graded increases of several capillary hemodynamic variables (RBC velocity, supply rate, and hematocrit) in response to incremental increases in tissue CO₂ concentrations within a physiologically relevant range. We also directly quantified capillary blood flow responses as opposed to measuring changes in microvascular tone, which directly supports the ability of CO₂ to coordinate the local blood supply with metabolic demand. The use of a microfluidic gas exchange chamber (GEC) allowed for direct and dynamic changes in tissue CO₂ concentrations without impacting the systemic circulation or the deeper muscle tissue microenvironment. Therefore, this method addressed some limitations associated with other methods that are commonly used to influence arterial and tissue CO₂, such as variations in inspired gases and equilibration of superfusion solutions, respectively. The use of a GEC to impose rapid and dynamic variations in the tissue microenvironment also enabled us to provide novel information regarding the time transient of CO₂-mediated blood flow responses as well as valuable insight into potential underlying mechanisms. Capillary hemodynamic responses to tissue CO₂ perturbations occurred rapidly with maximum responses being observed within 90 seconds; however, they were too slow to support the presence of an underlying conducted vasomotor response and indirectly supported the possible dependence on a pH-mediated mechanism. One possible mechanism involves the activation of pH sensitive vascular K_{ATP} channels expressed in endothelial cell membranes and our second objective was to investigate the involvement of these channels in CO₂-mediated

blood flow regulation in the skeletal muscle microcirculation. This objective was achieved by providing preliminary evidence supporting at least a partial dependence of CO₂-mediated blood flow responses on K_{ATP} channel activity and demonstrated blunted capillary hemodynamic responses to tissue CO₂ perturbations following selective K_{ATP} channel inhibition with glibenclamide (GLI). Finally, our last objective was to investigate the relationship between CO₂- and O₂-mediated blood flow regulation and the presence of overlapping regulatory mechanisms, such as oxygen saturation (SO₂) dependent ATP release from RBCs and vascular K_{ATP} channel activity. Red blood cell SO₂ measurements remained constant across various tissue CO₂ concentrations during both baseline and GLI conditions, which supported the presence of an SO₂-independent pathway underlying CO₂-mediated responses as well as the presence of separate mechanisms for CO₂- and O₂-mediated blood flow regulation. This was further supported by the varying degrees of K_{ATP} channel involvement in regulating variations in both tissue CO₂ and O₂ concentrations, where capillary hemodynamic responses to CO₂ were blunted and the responses to O₂ were abolished.

Limitations:

While the data presented in this thesis has provided valuable information to improve our understanding of CO₂-mediated microvascular blood flow regulation, some limitations must be considered and addressed with future experimentation. Over the duration of the experimental protocol, repeated exposure to high tissue CO₂ perturbations seemed to provoke an elevated flow state over time. The gradual increase in blood flow is somewhat confounding as the shifting flow state makes comparisons with baseline data difficult. The elevated flow state also decreased the number of capillaries that could be selected for analysis due to the limitations of the analysis software, which requires the presence of plasma gaps between RBCs flowing through selected,

in-focus capillaries. The hyperemic flow state and the smaller number of capillaries suitable for analysis had a greater impact on experiments investigating the involvement of K_{ATP} channels. Since tissues were exposed to baseline CO_2 perturbations prior to administration of GLI, a higher flow state was present during the recording and measurement of capillary hemodynamic responses following selective K_{ATP} channel inhibition. Therefore, future experiments designed to collect capillary blood flow responses during baseline and GLI conditions in separate animals are required to clarify the role of K_{ATP} channels in CO_2 -mediated blood flow responses and determine whether the observed responses were impacted by a higher flow state. Alternatively, to reduce the risk of introducing significant variation by completing baseline and GLI experiments in separate animals, the protocol could be modified to include longer wait times between baseline and GLI conditions. However, it is important to consider when increasing the duration of experiments that the muscle condition, and therefore the quality of the data collected, could begin to deteriorate over time.

There are also other limitations associated with our investigation of K_{ATP} channels as a potential site of action for CO_2 -mediated blood flow regulation. While the preliminary findings suggested a partial dependence of CO_2 -induced blood flow responses on K_{ATP} channel activation, potentially through changes in pH, some pieces of information were not addressed in the current thesis in order to have a complete understanding of their role in CO_2 -mediated responses. First, direct evidence supporting the presence of K_{ATP} channels in skeletal muscle capillaries needs to be provided. The molecular expression of K_{ATP} channels has been described in different capillary beds, such as in the heart and brain, and their presence has been indirectly shown in striated muscle capillaries through pharmacological interventions. However, the expression and

quantification of K_{ATP} channels in skeletal muscle capillaries have not been described and are therefore required to confirm their presence and potential involvement in microvascular blood flow regulation. In addition, while previous research has also shown that the GLI dosage used here is selective for K_{ATP} channels and has been widely used in investigations involving K_{ATP} channel, a dose-response curve for systemic GLI is also required to ensure accurate dosage for our experiments as well. And finally, simultaneous changes in pH and membrane potential were not measured during capillary blood flow responses to variations in tissue CO_2 concentrations. While both the time-transient of CO_2 -induced responses and the blunted changes in capillary hemodynamic variables following administration of GLI may indicate the involvement of pH-mediated K_{ATP} channel activity in CO_2 -mediated blood flow regulation, direct pH and membrane potential measurements are needed to confirm the pH-dependence and the involvement of electrical signals.

Perspectives:

In addition to addressing the limitations discussed above, there are several directions for future experiments to further advance our understanding of the impact of tissue CO_2 on the skeletal muscle microvascular system. The development and use of a gas exchange chamber (GEC) with an array of smaller micro-outlets would allow the level of vasculature involved in CO_2 -mediated responses to be more clearly defined. The GEC used for this thesis induced localized changes in only the tissue microenvironments under direct observation; however, the field of observation was large enough to expose both capillaries and terminal arterioles to variations in tissue CO_2 concentrations. Therefore, a GEC with small micro-outlets overlying a limited number of vessels could be used to control the level of vasculature being exposed to tissue perturbations and to

determine the location of CO₂'s interaction with the microvascular system. The relationship between CO₂- and O₂-mediated blood flow responses and the potential interaction between the two vasoactive stimuli can also be investigated further. Experiments designed to investigate capillary blood flow responses during both independent and simultaneous variations in tissue CO₂ and O₂ concentrations can be conducted to determine the presence of either a synergistic or additive impact on microvascular blood flow responses. This would provide valuable information regarding the blood flow response observed during simultaneous changes in CO₂ and O₂ that occur during conditions of increased metabolism, such as exercise. The molecular mechanism underlying CO₂-mediated blood flow regulation can also be investigated further. In addition to the potential involvement of vascular K_{ATP} channels, several possible targets may be directly or indirectly impacted by variations in tissue CO₂ and/or pH, such as other ion and/or voltage-gated channels expressed in vascular cell membranes, gap junctions, and enzymatic activity. Investigation of several, potentially redundant mechanisms responsible for regulating tissue CO₂ concentrations is necessary to gain a complete understanding of CO₂-mediated microvascular blood flow regulation. Finally, characterization of capillary blood flow responses to a physiologically relevant range of tissue CO₂ concentrations under normal conditions can serve as a control for investigating CO₂-mediated blood flow regulation in disease or exercise models and for determining if the regulatory mechanisms are altered. Investigations of CO₂-mediated blood flow responses in diseases associated with microvascular dysfunction, such as diabetes, this could also provide valuable information regarding the identity of mechanisms underlying the response and how those mechanisms could be impaired in relevant pathologies.

List of References

- Akerstrom, T., Goldman, D., Nilsson, F., Milkovich, S. L., Fraser, G. M., Brand, C. L., Hellsten, Y., & Ellis, C. G. (2020). Hyperinsulinemia does not cause de novo capillary recruitment in rat skeletal muscle. *Microcirculation*, 27(2), e12593. <https://doi.org/10.1111/micc.12593>
- Al-Khazraji, B. K., Novielli, N. M., Goldman, D., Medeiros, P. J., & Jackson, D. N. (2012). A simple "streak length method" for quantifying and characterizing red blood cell velocity profiles and blood flow in rat skeletal muscle arterioles. *Microcirculation*, 19(4), 327-335. <https://doi.org/10.1111/j.1549-8719.2012.00165.x>
- Ali Akbar, S., & Brown, P. R. (1996). Measurement of human erythrocyte CAI and CAII in adult, newborn, and fetal blood. *Clin Biochem*, 29(2), 157-164. [https://doi.org/10.1016/0009-9120\(95\)02021-7](https://doi.org/10.1016/0009-9120(95)02021-7)
- Armstead, W. M. (1997). Role of Nitric Oxide, Cyclic Nucleotides, and the Activation of ATP-Sensitive K⁺ Channels in the Contribution of Adenosine to Hypoxia-Induced Pial Artery Dilation. *Journal of Cerebral Blood Flow & Metabolism*, 17(1), 100-108. <https://doi.org/10.1097/00004647-199701000-00013>, note = PMID: 8978392
- Arthurs, G. J., & Sudhakar, M. (2005). Carbon dioxide transport. *Continuing education in anaesthesia, critical care & pain*, 5(6), 207-210. <https://doi.org/10.1093/bjaceaccp/mki050>
- Aziz, Q., Li, Y., Anderson, N., Ojake, L., Tsisanova, E., & Tinker, A. (2017). Molecular and functional characterization of the endothelial ATP-sensitive potassium channel. *J Biol Chem*, 292(43), 17587-17597. <https://doi.org/10.1074/jbc.M117.810325>
- Aziz, Q., Li, Y., & Tinker, A. (2018). Endothelial biology and ATP-sensitive potassium channels. *Channels (Austin)*, 12(1), 45-46. <https://doi.org/10.1080/19336950.2017.1412151>
- Bagher, P., & Segal, S. S. (2011a). The mouse cremaster muscle preparation for intravital imaging of the microcirculation. *J Vis Exp*(52). <https://doi.org/10.3791/2874>
- Bagher, P., & Segal, S. S. (2011b). Regulation of blood flow in the microcirculation: role of conducted vasodilation. *Acta Physiol (Oxf)*, 202(3), 271-284. <https://doi.org/10.1111/j.1748-1716.2010.02244.x>
- Baldwin, J., & Chothia, C. (1979). Haemoglobin: the structural changes related to ligand binding and its allosteric mechanism. *J Mol Biol*, 129(2), 175-220. [https://doi.org/10.1016/0022-2836\(79\)90277-8](https://doi.org/10.1016/0022-2836(79)90277-8)
- Ballard, H. (2014). ATP and adenosine in the regulation of skeletal muscle blood flow during exercise. *Sheng li xue bao : [Acta physiologica Sinica]*, 66, 67-78. <https://doi.org/10.13294/j.aps.2014.0009>
- Beach, J. M., McGahren, E. D., & Duling, B. R. (1998). Capillaries and arterioles are electrically coupled in hamster cheek pouch. *American Journal of Physiology-Heart and Circulatory Physiology*, 275(4), H1489-H1496. <https://doi.org/10.1152/ajpheart.1998.275.4.H1489>
- Bearden, S. E., Payne, G. W., Chisty, A., & Segal, S. S. (2004). Arteriolar network architecture and vasomotor function with ageing in mouse gluteus maximus muscle. *The Journal of Physiology* 561(2), 535-545. <https://doi.org/10.1113/jphysiol.2004.068262>
- Beech, D. J., Zhang, H., Nakao, K., & Bolton, T. B. (1993a). K channel activation by nucleotide diphosphates and its inhibition by glibenclamide in vascular smooth muscle cells. *Br J Pharmacol*, 110(2), 573-582. <https://doi.org/10.1111/j.1476-5381.1993.tb13849.x>

- Beech, D. J., Zhang, H., Nakao, K., & Bolton, T. B. (1993b). Single channel and whole-cell K⁺ currents evoked by levcromakalim in smooth muscle cells from the rabbit portal vein. *Br J Pharmacol*, 110(2), 583-590. <https://doi.org/10.1111/j.1476-5381.1993.tb13850.x>
- Berg, B. R., Cohen, K. D., & Sarelius, I. H. (1997). Direct coupling between blood flow and metabolism at the capillary level in striated muscle. *Am J Physiol*, 272(6 Pt 2), H2693-2700. <https://doi.org/10.1152/ajpheart.1997.272.6.H2693>
- Berg, B. R., & Sarelius, I. H. (1995). Functional capillary organization in striated muscle. *American Journal of Physiology-Heart and Circulatory Physiology*, 268(3), H1215-H1222. <https://doi.org/10.1152/ajpheart.1995.268.3.H1215>, note = PMID: 7900875
- Bergfeld, G. R., & Forrester, T. (1992). Release of ATP from human erythrocytes in response to a brief period of hypoxia and hypercapnia. *Cardiovascular Research*, 26(1), 40-47. <https://doi.org/10.1093/cvr/26.1.40>
- Biswal, B. B., & Hudetz, A. G. (1996). Synchronous Oscillations in Cerebrocortical Capillary Red Blood Cell Velocity after Nitric Oxide Synthase Inhibition. *Microvascular Research*, 52(1), 1-12. <https://doi.org/10.1006/mvre.1996.0039>
- Bohr, C., Hasselbalch, K., & Krogh, A. (1904). Ueber einen in biologischer Beziehung wichtigen Einfluss, den die Kohlensäurespannung des Blutes auf dessen Sauerstoffbindung übt1. *Skandinavisches Archiv Für Physiologie*, 16(2), 402-412. <https://doi.org/10.1111/j.1748-1716.1904.tb01382.x>
- Bryan, P. T., & Marshall, J. M. (1999). Cellular mechanisms by which adenosine induces vasodilatation in rat skeletal muscle: significance for systemic hypoxia. *The Journal of Physiology*, 514(1), 163-175. <https://doi.org/10.1111/j.1469-7793.1999.163af.x>
- Cartheuser, C.-F. (1993). Standard and pH-affected hemoglobin-O₂ binding curves of Sprague-Dawley rats under normal and shifted P50 conditions. *Comparative Biochemistry and Physiology Part A: Physiology*, 106(4), 775-782. [https://doi.org/10.1016/0300-9629\(93\)90396-L](https://doi.org/10.1016/0300-9629(93)90396-L)
- Charter, M. E., Lamb, I. R., & Murrant, C. L. (2018). Arteriolar and capillary responses to CO. *Microcirculation*, 25(7), e12494. <https://doi.org/10.1111/micc.12494>
- Chen, C.-W., Chang, H.-Y., & Hsiue, T.-R. (2000). Mechanism of adenosine-induced vasodilation in rat diaphragm microcirculation. *American Journal of Physiology-Heart and Circulatory Physiology*, 279(5), H2210-H2217. <https://doi.org/10.1152/ajpheart.2000.279.5.H2210>
- Christiansen, J., Douglas, C. G., & Haldane, J. S. (1914). The absorption and dissociation of carbon dioxide by human blood. *The Journal of Physiology*, 48(4), 244-271. <https://doi.org/10.1113/jphysiol.1914.sp001659>
- Chu, A. H., & Ackers, G. K. (1981). Mutual effects of protons, NaCl, and oxygen on the dimer-tetramer assembly of human hemoglobin. The dimer Bohr effect. *Journal of Biological Chemistry*, 256(3), 1199-1205. [https://doi.org/10.1016/s0021-9258\(19\)69949-7](https://doi.org/10.1016/s0021-9258(19)69949-7)
- Clifford, P. S., & Hellsten, Y. (2004). Vasodilatory mechanisms in contracting skeletal muscle. *Journal of Applied Physiology*, 97(1), 393-403. <https://doi.org/10.1152/japplphysiol.00179.2004>, note = PMID: 15220322
- Cohen, K. D., & Sarelius, I. H. (2002). Muscle contraction under capillaries in hamster muscle induces arteriolar dilatation via K(ATP) channels and nitric oxide. *J Physiol*, 539(Pt 2), 547-555. <https://doi.org/10.1113/jphysiol.2001.013388>
- Colburn, T. D., Holdsworth, C. T., Craig, J. C., Hirai, D. M., Montgomery, S., Poole, D. C., Musch, T. I., & Kenney, M. J. (2020). ATP-sensitive K(+) channel inhibition in rats

- decreases kidney and skeletal muscle blood flow without increasing sympathetic nerve discharge. *Respir Physiol Neurobiol*, 278, 103444.
<https://doi.org/10.1016/j.resp.2020.103444>
- Colburn, T. D., Weber, R. E., Hageman, K. S., Caldwell, J. T., Schulze, K. M., Ade, C. J., Behnke, B. J., Poole, D. C., & Musch, T. I. (2020). Vascular ATP-sensitive K(+) channels support maximal aerobic capacity and critical speed via convective and diffusive O₂ transport. *J Physiol*, 598(21), 4843-4858. <https://doi.org/10.1113/JP280232>
- Collins, D. M., McCullough, W. T., & Ellsworth, M. L. (1998). Conducted vascular responses: communication across the capillary bed. *Microvasc Res*, 56(1), 43-53.
<https://doi.org/10.1006/mvre.1998.2076>
- Corliss, B. A., Mathews, C., Doty, R., Rohde, G., & Peirce, S. M. (2019). Methods to label, image, and analyze the complex structural architectures of microvascular networks. *Microcirculation*, 26(5), e12520. <https://doi.org/10.1111/micc.12520>
- Danialou, G., Vicaut, E., Sambe, A., Aubier, M., & Boczkowski, J. (1997). Predominant role of A₁ adenosine receptors in mediating adenosine induced vasodilatation of rat diaphragmatic arterioles: involvement of nitric oxide and the ATP-dependent K⁺ channels. *British Journal of Pharmacology*, 121(7), 1355-1363.
<https://doi.org/10.1038/sj.bjp.0701247>
- Dash, R. K., & Bassingthwaite, J. B. (2010). Erratum to: Blood HbO₂ and HbCO₂ dissociation curves at varied O₂, CO₂, pH, 2,3-DPG and temperature levels. *Ann Biomed Eng*, 38(4), 1683-1701. <https://doi.org/10.1007/s10439-010-9948-y>
- Davies, N. W. (1990). Modulation of ATP-sensitive K⁺ channels in skeletal muscle by intracellular protons. *Nature*, 343(6256), 375-377. <https://doi.org/10.1038/343375a0>
- Davis, M. J. (1993). Myogenic response gradient in an arteriolar network. *American Journal of Physiology-Heart and Circulatory Physiology*, 264(6), H2168-H2179.
<https://doi.org/10.1152/ajpheart.1993.264.6.H2168>
- Davis, M. J., Ferrer, P. N., & Gore, R. W. (1986). Vascular anatomy and hydrostatic pressure profile in the hamster cheek pouch. *Am J Physiol*, 250(2 Pt 2), H291-303.
<https://doi.org/10.1152/ajpheart.1986.250.2.H291>
- de Wit, C. (2010). Different pathways with distinct properties conduct dilations in the microcirculation in vivo. *Cardiovasc Res*, 85(3), 604-613.
<https://doi.org/10.1093/cvr/cvp340>
- de Wit, C., Roos, F., Bolz, S.-S., Kirchhoff, S., Krüger, O., Willecke, K., & Pohl, U. (2000). Impaired Conduction of Vasodilation Along Arterioles in Connexin40-Deficient Mice. *Circulation Research*, 86(6), 649-655. <https://doi.org/10.1161/01.RES.86.6.649>
- Decker, B., Sender, S., & Gros, G. (1996). Membrane-associated carbonic anhydrase IV in skeletal muscle: subcellular localization. *Histochemistry and Cell Biology*, 106(4), 405-411. <https://doi.org/10.1007/BF02473299>
- Delashaw, J. B., & Duling, B. R. (1988). A study of the functional elements regulating capillary perfusion in striated muscle. *Microvascular Research*, 36(2), 162-171.
[https://doi.org/10.1016/0026-2862\(88\)90016-7](https://doi.org/10.1016/0026-2862(88)90016-7)
- Dietrich, H. H., Ellsworth, M. L., Sprague, R. S., & Dacey, R. G. (2000). Red blood cell regulation of microvascular tone through adenosine triphosphate. *American Journal of Physiology-Heart and Circulatory Physiology*, 278(4), H1294-H1298.
<https://doi.org/10.1152/ajpheart.2000.278.4.H1294> , note = PMID: 10749727

- Dietrich, H. H., & Tynl, K. (1992a). Capillary as a communicating medium in the microvasculature. *Microvascular Research*, 43(1), 87-99. [https://doi.org/10.1016/0026-2862\(92\)90008-D](https://doi.org/10.1016/0026-2862(92)90008-D)
- Dietrich, H. H., & Tynl, K. (1992b). Microvascular flow response to localized application of norepinephrine on capillaries in rat and frog skeletal muscle. *Microvascular Research*, 43(1), 73-86. [https://doi.org/10.1016/0026-2862\(92\)90007-C](https://doi.org/10.1016/0026-2862(92)90007-C)
- Dora, K. A. (2017). Conducted dilatation to ATP and K. *Acta Physiol (Oxf)*, 219(1), 202-218. <https://doi.org/10.1111/apha.12656>
- Duling, B. R. (1973a). Changes in microvascular diameter and oxygen tension induced by carbon dioxide. *Circ Res*, 32(3), 370-376. <https://doi.org/10.1161/01.res.32.3.370>
- Duling, B. R. (1973b). The preparation and use of the hamster cheek pouch for studies of the microcirculation. *Microvascular Research*, 5(3), 423-429. [https://doi.org/10.1016/0026-2862\(73\)90059-9](https://doi.org/10.1016/0026-2862(73)90059-9)
- Duling, B. R., & Berne, R. M. (1970). Propagated Vasodilation in the Microcirculation of the Hamster Cheek Pouch. *Circulation Research*, 26(2), 163-170. <https://doi.org/10.1161/01.RES.26.2.163>
- Ellis, C. G., Ellsworth, M. L., & Pittman, R. N. (1990). Determination of red blood cell oxygenation in vivo by dual video densitometric image analysis. *American Journal of Physiology-Heart and Circulatory Physiology*, 258(4), H1216-H1223. <https://doi.org/10.1152/ajpheart.1990.258.4.H1216>
- Ellis, C. G., Ellsworth, M. L., Pittman, R. N., & Burgess, W. L. (1992). Application of image analysis for evaluation of red blood cell dynamics in capillaries. *Microvascular Research*, 44(2), 214-225. [https://doi.org/10.1016/0026-2862\(92\)90081-Y](https://doi.org/10.1016/0026-2862(92)90081-Y)
- Ellis, C. G., Milkovich, S., & Goldman, D. (2012). What is the efficiency of ATP signaling from erythrocytes to regulate distribution of O₂ supply within the microvasculature? *Microcirculation*, 19(5), 440-450. <https://doi.org/10.1111/j.1549-8719.2012.00196.x>
- Ellsworth, M. L., Ellis, C. G., & Sprague, R. S. (2016). Role of erythrocyte-released ATP in the regulation of microvascular oxygen supply in skeletal muscle. *Acta Physiol (Oxf)*, 216(3), 265-276. <https://doi.org/10.1111/apha.12596>
- Ellsworth, M. L., Forrester, T., Ellis, C. G., & Dietrich, H. H. (1995). The erythrocyte as a regulator of vascular tone. *American Journal of Physiology-Heart and Circulatory Physiology*, 269(6), H2155-H2161. <https://doi.org/10.1152/ajpheart.1995.269.6.H2155>
- Ellsworth, M. L., Pittman, R. N., & Ellis, C. G. (1987). Measurement of hemoglobin oxygen saturation in capillaries. *American Journal of Physiology-Heart and Circulatory Physiology*, 252(5), H1031-H1040. <https://doi.org/10.1152/ajpheart.1987.252.5.H1031>
- Emerson, T. E., & Raymond, R. M. (1981). Involvement of adenosine in cerebral hypoxic hyperemia in the dog. *American Journal of Physiology-Heart and Circulatory Physiology*, 241(2), H134-H138. <https://doi.org/10.1152/ajpheart.1981.241.2.H134>
- Enns, T. (1967). Facilitation by Carbonic Anhydrase of Carbon Dioxide Transport. *Science*, 155(3758), 44-47. <https://doi.org/10.1126/science.155.3758.44>
- Estevez, A. Y., & Phillis, J. W. (1997). Hypercapnia-induced increases in cerebral blood flow: roles of adenosine, nitric oxide and cortical arousal. *Brain Research*, 758(1), 1-8. [https://doi.org/10.1016/S0006-8993\(97\)00154-6](https://doi.org/10.1016/S0006-8993(97)00154-6)
- Fabricsius, M., Rubin, I., Bundgaard, M., & Lauritzen, M. (1996). NOS activity in brain and endothelium: relation to hypercapnic rise of cerebral blood flow in rats. *American*

- Journal of Physiology-Heart and Circulatory Physiology*, 271(5), H2035-H2044.
<https://doi.org/10.1152/ajpheart.1996.271.5.H2035>
- Faraci, F. M., Breese, K. R., & Heistad, D. D. (1994). Cerebral vasodilation during hypercapnia. Role of glibenclamide-sensitive potassium channels and nitric oxide. *Stroke*, 25(8), 1679-1683. <https://doi.org/10.1161/01.STR.25.8.1679>
- Faraci, F. M., Taugher, R. J., Lynch, C., Fan, R., Gupta, S., & Wemmie, J. A. (2019). Acid-Sensing Ion Channels: Novel Mediators of Cerebral Vascular Responses. *Circ Res*, 125(10), 907-920. <https://doi.org/10.1161/CIRCRESAHA.119.315024>
- Farouque, H. M. O., & Meredith, I. T. (2003). Relative contribution of vasodilator prostanoids, NO, and KATP channels to human forearm metabolic vasodilation. *American Journal of Physiology-Heart and Circulatory Physiology*, 284(6), H2405-H2411.
<https://doi.org/10.1152/ajpheart.00879.2002>
- Fathi, A. R., Yang, C., Bakhtian, K. D., Qi, M., Lonser, R. R., & Pluta, R. M. (2011). Carbon dioxide influence on nitric oxide production in endothelial cells and astrocytes: cellular mechanisms. *Brain Res*, 1386, 50-57. <https://doi.org/10.1016/j.brainres.2011.02.066>
- Figueroa, X. F., Chen, C.-C., Campbell, K. P., Damon, D. N., Day, K. H., Ramos, S., & Duling, B. R. (2007). Are voltage-dependent ion channels involved in the endothelial cell control of vasomotor tone? *American Journal of Physiology-Heart and Circulatory Physiology*, 293(3), H1371-H1383. <https://doi.org/10.1152/ajpheart.01368.2006>
- Figueroa, X. F., & Duling, B. R. (2008). Dissection of two Cx37-independent conducted vasodilator mechanisms by deletion of Cx40: electrotonic versus regenerative conduction. *Am J Physiol Heart Circ Physiol*, 295(5), H2001-2007.
<https://doi.org/10.1152/ajpheart.00063.2008>
- Figueroa, X. F., Paul, D. L., Simon, A. M., Goodenough, D. A., Day, K. H., Damon, D. N., & Duling, B. R. (2003). Central role of connexin40 in the propagation of electrically activated vasodilation in mouse cremasteric arterioles in vivo. *Circ Res*, 92(7), 793-800.
<https://doi.org/10.1161/01.RES.0000065918.90271.9A>
- Fraser, G. M. (2012). Modeling Oxygen Transport in Three-Dimensional Capillary Networks. *Electronic Thesis and Dissertation Repository*, 500.
- Fraser, G. M., Milkovich, S., Goldman, D., & Ellis, C. G. (2012). Mapping 3-D functional capillary geometry in rat skeletal muscle in vivo. *Am J Physiol Heart Circ Physiol*, 302(3), H654-664. <https://doi.org/10.1152/ajpheart.01185.2010>
- Friend, S. H., Matthew, J. B., & Gurd, F. R. (1981). Protein-protein interactions: nature of the electrostatic stabilization of deoxyhemoglobin tetramer formation. *Biochemistry*, 20(3), 580-586. <https://doi.org/10.1021/bi00506a021>
- Fry, B. C., Roy, T. K., & Secomb, T. W. (2013). Capillary recruitment in a theoretical model for blood flow regulation in heterogeneous microvessel networks. *Physiol Rep*, 1(3), e00050. <https://doi.org/10.1002/phy2.50>
- Fukuda, Y., Sato, A., Suzuki, A., & Trzebski, A. (1989). Autonomic nerve and cardiovascular responses to changing blood oxygen and carbon dioxide levels in the rat. *Journal of the Autonomic Nervous System*, 28(1), 61-74. [https://doi.org/10.1016/0165-1838\(89\)90008-8](https://doi.org/10.1016/0165-1838(89)90008-8)
- Geers, C., & Gros, G. (2000). Carbon Dioxide Transport and Carbonic Anhydrase in Blood and Muscle. *Physiological Reviews*, 80(2), 681-715.
<https://doi.org/10.1152/physrev.2000.80.2.681>

- Ghonaim, N. W., Fraser, G. M., Ellis, C. G., Yang, J., & Goldman, D. (2013). Modeling steady state SO₂-dependent changes in capillary ATP concentration using novel O₂ micro-delivery methods. *Front Physiol*, 4, 260. <https://doi.org/10.3389/fphys.2013.00260>
- Ghonaim, N. W., Fraser, G. M., Goldman, D., Milkovich, S., Yang, J., & Ellis, C. G. (2021). Evidence for role of capillaries in regulation of skeletal muscle oxygen supply. *Microcirculation*, 28(6), e12699. <https://doi.org/10.1111/micc.12699>
- Ghonaim, N. W., Lau, L. W., Goldman, D., Ellis, C. G., & Yang, J. (2011). A micro-delivery approach for studying microvascular responses to localized oxygen delivery. *Microcirculation*, 18(8), 646-654. <https://doi.org/10.1111/j.1549-8719.2011.00132.x>
- Goadsby, P. J., Kaube, H., & Hoskin, K. L. (1992). Nitric oxide synthesis couples cerebral blood flow and metabolism. *Brain Research*, 595(1), 167-170. [https://doi.org/10.1016/0006-8993\(92\)91470-Y](https://doi.org/10.1016/0006-8993(92)91470-Y)
- Gorczynski, R. J., Klitzman, B., & Duling, B. R. (1978). Interrelations between contracting striated muscle and precapillary microvessels. *American Journal of Physiology-Heart and Circulatory Physiology*, 235(5), H494-H504. <https://doi.org/10.1152/ajpheart.1978.235.5.H494>
- Greco, F. A., & Solomon, A. K. (1997). Kinetics of Chloride-Bicarbonate Exchange Across the Human Red Blood Cell Membrane. *The Journal of Membrane Biology*, 159(3), 197-208. <https://doi.org/10.1007/s002329900283>
- Gros, G., Rollema, H. S., & Forster, R. E. (1981). The carbamate equilibrium of alpha- and epsilon-amino groups of human hemoglobin at 37 degrees C. *Journal of Biological Chemistry*, 256(11), 5471-5480. [https://doi.org/10.1016/s0021-9258\(19\)69225-2](https://doi.org/10.1016/s0021-9258(19)69225-2)
- Gutknecht, J., Bisson, M. A., & Tosteson, F. C. (1977). Diffusion of carbon dioxide through lipid bilayer membranes: effects of carbonic anhydrase, bicarbonate, and unstirred layers. *Journal of General Physiology*, 69(6), 779-794. <https://doi.org/10.1085/jgp.69.6.779>
- Hammer, L. W., Ligon, A. L., & Hester, R. L. (2001). Differential Inhibition of Functional Dilation of Small Arterioles by Indomethacin and Glibenclamide. *Hypertension*, 37(2), 599-603. <https://doi.org/10.1161/01.HYP.37.2.599>
- Harada, M., Fuse, A., & Tanaka, Y. (1997). Measurement of nitric oxide in the rat cerebral cortex during hypercapnoea. *NeuroReport*, 8(4). <https://doi.org/10.1097/00001756-199703030-00036>
- Hargreaves, D., Egginton, S., & Hudlická, O. (1990). Changes in capillary perfusion induced by different patterns of activity in rat skeletal muscle. *Microvascular Research*, 40(1), 14-28. [https://doi.org/10.1016/0026-2862\(90\)90003-A](https://doi.org/10.1016/0026-2862(90)90003-A)
- Hastings, A. B., Sendroy, J., & Van Slyke, D. D. (1928). Studies of Gas and Electrolyte Equilibria in Blood. *Journal of Biological Chemistry*, 79(1), 183-192. [https://doi.org/10.1016/s0021-9258\(18\)83945-x](https://doi.org/10.1016/s0021-9258(18)83945-x)
- Hirai, D. M., Tabuchi, A., Craig, J. C., Colburn, T. D., Musch, T. I., & Poole, D. C. (2021). Regulation of capillary hemodynamics by KATP channels in resting skeletal muscle. *Physiol Rep*, 9(8), e14803. <https://doi.org/10.14814/phy2.14803>
- Hoffman, W. E., Albrecht, R. F., & Miletich, D. J. (1984). The role of adenosine in CBF increases during hypoxia in young vs aged rats. *Stroke*, 15(1), 124-129. <https://doi.org/10.1161/01.STR.15.1.124>
- Hogan, R. D., Franklin, T. D., Avery, K. S., & Burke, K. M. (1982). Arteriolar vasoconstriction in rat cremaster muscle induced by local heat stress. *American Journal of Physiology-*

- Heart and Circulatory Physiology*, 242(6), H996-H999.
<https://doi.org/10.1152/ajpheart.1982.242.6.H996>
- Holdsworth, C. T., Copp, S. W., Ferguson, S. K., Sims, G. E., Poole, D. C., & Musch, T. I. (2015). Acute inhibition of ATP-sensitive K⁺ channels impairs skeletal muscle vascular control in rats during treadmill exercise. *Am J Physiol Heart Circ Physiol*, 308(11), H1434-1442. <https://doi.org/10.1152/ajpheart.00772.2014>
- Holdsworth, C. T., Ferguson, S. K., Poole, D. C., & Musch, T. I. (2016a). Modulation of rat skeletal muscle microvascular O₂ pressure via KATP channel inhibition following the onset of contractions. *Respir Physiol Neurobiol*, 222, 48-54.
<https://doi.org/10.1016/j.resp.2015.11.012>
- Holdsworth, C. T., Ferguson, S. K., Poole, D. C., & Musch, T. I. (2016b). Modulation of rat skeletal muscle microvascular O₂ pressure via KATP channel inhibition following the onset of contractions. *Respiratory Physiology & Neurobiology*, 222, 48-54.
<https://doi.org/10.1016/j.resp.2015.11.012>
- Honig, C. R., Odoroff, C. L., & Frierson, J. L. (1982). Active and passive capillary control in red muscle at rest and in exercise. *American Journal of Physiology-Heart and Circulatory Physiology*, 243(2), H196-H206. <https://doi.org/10.1152/ajpheart.1982.243.2.H196>
- Horiuchi, T., Dietrich, H. H., Hongo, K., Goto, T., & Dacey, R. G. (2002). Role of Endothelial Nitric Oxide and Smooth Muscle Potassium Channels in Cerebral Arteriolar Dilation in Response to Acidosis. *Stroke*, 33(3), 844-849. <https://doi.org/10.1161/hs0302.104112>
- Hungerford, J. E., Sessa, W. C., & Segal, S. S. (2000). Vasomotor control in arterioles of the mouse cremaster muscle. *The FASEB Journal*, 14(1), 197-207.
<https://doi.org/10.1096/fasebj.14.1.197>
- Iadecola, C. (1992). Does nitric oxide mediate the increases in cerebral blood flow elicited by hypercapnia? *Proceedings of the National Academy of Sciences of the United States of America*, 89(9), 3913-3916. <https://doi.org/10.1073/pnas.89.9.3913>
- Iadecola, C., & Zhang, F. (1994). Nitric oxide-dependent and -independent components of cerebrovasodilation elicited by hypercapnia. *Am J Physiol*, 266(2 Pt 2), R546-552.
<https://doi.org/10.1152/ajpregu.1994.266.2.R546>
- Iadecola, C., Zhang, F., & Xu, X. (1994). SIN-1 reverses attenuation of hypercapnic cerebrovasodilation by nitric oxide synthase inhibitors. *American Journal of Physiology-Regulatory, Integrative and Comparative Physiology*, 267(1), R228-R235.
<https://doi.org/10.1152/ajpregu.1994.267.1.R228>
- Ibayashi, S., Ngai, A. C., Meno, J. R., & Winn, H. R. (1988). The Effects of Dipyridamole and Theophylline on Rat Pial Vessels during Hypocarbica. *Journal of Cerebral Blood Flow & Metabolism*, 8(6), 829-833. <https://doi.org/10.1038/jcbfm.1988.139>
- Irikura, K., Maynard, K. I., Lee, W. S., & A., M. M. (1994). L-NNA decreases cortical hyperemia and brain cGMP levels following CO₂ inhalation in Sprague-Dawley rats. *American Journal of Physiology-Heart and Circulatory Physiology*, 267(2), H837-H843.
<https://doi.org/10.1152/ajpheart.1994.267.2.H837> , note = PMID: 8067440
- Jackson, W. F. (1993). Arteriolar tone is determined by activity of ATP-sensitive potassium channels. *Am J Physiol*, 265(5 Pt 2), H1797-1803.
<https://doi.org/10.1152/ajpheart.1993.265.5.H1797>
- Jackson, W. F. (2000a). Hypoxia does not activate ATP-sensitive K⁺ channels in arteriolar muscle cells. *Microcirculation (New York, N.Y. : 1994)*, 7(2), 137-145.
<https://doi.org/10.1038/sj.mn.7300102>

- Jackson, W. F. (2000b). Ion Channels and Vascular Tone. *Hypertension*, 35(1), 173-178. <https://doi.org/10.1161/01.HYP.35.1.173>
- Jackson, W. F. (2005). Potassium channels in the peripheral microcirculation. *Microcirculation*, 12(1), 113-127. <https://doi.org/10.1080/10739680590896072>
- Jackson, W. F. (2016). Arteriolar oxygen reactivity: where is the sensor and what is the mechanism of action? *J Physiol*, 594(18), 5055-5077. <https://doi.org/10.1113/JP270192>
- Jagger, J. E., Bateman, R. M., Ellsworth, M. L., & Ellis, C. G. (2001). Role of erythrocyte in regulating local O₂ delivery mediated by hemoglobin oxygenation. *American Journal of Physiology-Heart and Circulatory Physiology*, 280(6), H2833-H2839. <https://doi.org/10.1152/ajpheart.2001.280.6.H2833>
- Janigro, D., West, G. A., Gordon, E. L., & Winn, H. R. (1993). ATP-sensitive K⁺ channels in rat aorta and brain microvascular endothelial cells. *American Journal of Physiology-Cell Physiology*, 265(3), C812-C821. <https://doi.org/10.1152/ajpcell.1993.265.3.C812>
- Japee, S. A., Ellis, C. G., & Pittman, R. N. (2004). Flow visualization tools for image analysis of capillary networks. *Microcirculation*, 11(1), 39-54. <https://doi.org/10.1080/10739680490266171>
- Jensen, F. B. (2004). Red blood cell pH, the Bohr effect, and other oxygenation-linked phenomena in blood O₂ and CO₂ transport. *Acta Physiologica Scandinavica*, 182(3), 215-227. <https://doi.org/10.1111/j.1365-201X.2004.01361.x>
- Jouett, N. P., Watenpaugh, D. E., Dunlap, M. E., & Smith, M. L. (2015). Interactive effects of hypoxia, hypercapnia and lung volume on sympathetic nerve activity in humans. *Exp Physiol*, 100(9), 1018-1029. <https://doi.org/10.1113/EP085092>
- Joyner, M. J., & Casey, D. P. (2015). Regulation of Increased Blood Flow (Hyperemia) to Muscles During Exercise: A Hierarchy of Competing Physiological Needs. *Physiological Reviews*, 95(2), 549-601. <https://doi.org/10.1152/physrev.00035.2013>
- Keller, A. S., Diederich, L., Panknin, C., DeLalio, L. J., Drake, J. C., Sherman, R., Jackson, E. K., Yan, Z., Kelm, M., Cortese-Krott, M. M., & Isakson, B. E. (2017). Possible roles for ATP release from RBCs exclude the cAMP-mediated Panx1 pathway. *Am J Physiol Cell Physiol*, 313(6), C593-C603. <https://doi.org/10.1152/ajpcell.00178.2017>
- Kilmartin, J. V., Breen, J. J., Roberts, G. C. K., & Ho, C. (1973). Direct Measurement of the pK Values of an Alkaline Bohr Group in Human Hemoglobin. *Proceedings of the National Academy of Sciences*, 70(4), 1246-1249. <https://doi.org/10.1073/pnas.70.4.1246>
- Kirby, B. S., Sparks, M. A., Lazarowski, E. R., Lopez Domowicz, D. A., Zhu, H., & McMahon, T. J. (2021). Pannexin 1 channels control the hemodynamic response to hypoxia by regulating O₂-sensitive extracellular ATP in blood. *Am J Physiol Heart Circ Physiol*, 320(3), H1055-H1065. <https://doi.org/10.1152/ajpheart.00651.2020>
- Koller, A., & Kaley, G. (1991). Endothelial regulation of wall shear stress and blood flow in skeletal muscle microcirculation. *Am J Physiol*, 260(3 Pt 2), H862-868. <https://doi.org/10.1152/ajpheart.1991.260.3.H862>
- Kontos, H. A., Raper, A. J., & Patterson, J. L. (1977). Analysis of vasoactivity of local pH, PCO₂ and bicarbonate on pial vessels. *Stroke*, 8(3), 358-360. <https://doi.org/10.1161/01.STR.8.3.358>
- Kontos, H. A., Richardson, D. W., & Patterson, J. L. (1968). Roles of hypercapnia and acidosis in the vasodilator response to hypercapnic acidosis. *American Journal of Physiology-Legacy Content*, 215(6), 1406-1408. <https://doi.org/10.1152/ajplegacy.1968.215.6.1406>

- Kontos, H. A., Wei, E. P., Raper, A. J., & Patterson, J. L. (1977). Local mechanism of CO₂ action of cat pial arterioles. *Stroke*, 8(2), 226-229. <https://doi.org/10.1161/01.STR.8.2.226>
- Korthuis, R. J. (2011). In *Skeletal Muscle Circulation*. <https://www.ncbi.nlm.nih.gov/pubmed/21850766>
- Krolo, I., & Hudetz, A. G. (2000). Hypoxemia alters erythrocyte perfusion pattern in the cerebral capillary network. *Microvasc Res*, 59(1), 72-79. <https://doi.org/10.1006/mvre.1999.2185>
- Kurjiaka, D. T., & Segal, S. S. (1995). Conducted vasodilation elevates flow in arteriole networks of hamster striated muscle. *American Journal of Physiology-Heart and Circulatory Physiology*, 269(5), H1723-H1728. <https://doi.org/10.1152/ajpheart.1995.269.5.H1723>
- Lamb, I. R., & Murrant, C. L. (2015). Potassium inhibits nitric oxide and adenosine arteriolar vasodilatation via KIR and Na⁺/K⁺ATPase: implications for redundancy in active hyperaemia. *The Journal of Physiology*, 593(23), 5111-5126. <https://doi.org/10.1113/JP270613>
- Lamb, I. R., Novielli, N. M., & Murrant, C. L. (2018). Capillary response to skeletal muscle contraction: evidence that redundancy between vasodilators is physiologically relevant during active hyperaemia. *J Physiol*, 596(8), 1357-1372. <https://doi.org/10.1113/JP275467>
- Langheinrich, U., & Daut, J. (1997). Hyperpolarization of isolated capillaries from guinea-pig heart induced by K⁺ channel openers and glucose deprivation. *The Journal of Physiology*, 502(2), 397-408. <https://doi.org/10.1111/j.1469-7793.1997.397bk.x>
- Laughlin, M. H., & Armstrong, R. B. (1982). Muscular blood flow distribution patterns as a function of running speed in rats. *Am J Physiol*, 243(2), H296-306. <https://doi.org/10.1152/ajpheart.1982.243.2.H296>
- Levitzky, M. G. (2017). Transport of Oxygen and Carbon Dioxide in the Blood. In *Pulmonary Physiology*, 9e. McGraw-Hill Education. <https://accessmedicine.mhmedical.com/content.aspx?bookid=2288§ionid=178857270>
- Liang, G., Stephenson, A. H., Lonigro, A. J., & Sprague, R. S. (2005). Erythrocytes of humans with cystic fibrosis fail to stimulate nitric oxide synthesis in isolated rabbit lungs. *American Journal of Physiology-Heart and Circulatory Physiology*, 288(4), H1580-H1585. <https://doi.org/10.1152/ajpheart.00807.2004>
- Lipowsky, H. H., Kovalcheck, S., & Zweifach, B. W. (1978). The distribution of blood rheological parameters in the microvasculature of cat mesentery. *Circ Res*, 43(5), 738-749. <https://doi.org/10.1161/01.res.43.5.738>
- Lipowsky, H. H., Usami, S., & Chien, S. (1980). In vivo measurements of "apparent viscosity" and microvessel hematocrit in the mesentery of the cat. *Microvasc Res*, 19(3), 297-319. [https://doi.org/10.1016/0026-2862\(80\)90050-3](https://doi.org/10.1016/0026-2862(80)90050-3)
- Looft-Wilson, R. C., Payne, G. W., & Segal, S. S. (2004). Connexin expression and conducted vasodilation along arteriolar endothelium in mouse skeletal muscle. *Journal of Applied Physiology*, 97(3), 1152-1158. <https://doi.org/10.1152/japplphysiol.00133.2004>
- Luneva, O. G., Sidorenko, S. V., Ponomarchuk, O. O., Tverskoy, A. M., Cherkashin, A. A., Rodnenkov, O. V., Alekseeva, N. V., Deev, L. I., Maksimov, G. V., Grygorczyk, R., & Orlov, S. N. (2016). Deoxygenation Affects Composition of Membrane-Bound Proteins in Human Erythrocytes. *Cell Physiol Biochem*, 39(1), 81-88. <https://doi.org/10.1159/000445607>

- Ma, J., Meng, W., Ayata, C., Huang, P. L., Fishman, M. C., & Moskowitz, M. A. (1996). L-NNA-sensitive regional cerebral blood flow augmentation during hypercapnia in type III NOS mutant mice. *American Journal of Physiology-Heart and Circulatory Physiology*, 271(4), H1717-H1719. <https://doi.org/10.1152/ajpheart.1996.271.4.H1717>
- Mairbaur, H., Ruppe, F. A., & Bartsch, P. (2013). Role of hemolysis in red cell adenosine triphosphate release in simulated exercise conditions in vitro. *Med Sci Sports Exerc*, 45(10), 1941-1947. <https://doi.org/10.1249/MSS.0b013e318296193a>
- Marshall, J. M. (1982). The influence of the sympathetic nervous system on individual vessels of the microcirculation of skeletal muscle of the rat. *The Journal of Physiology*, 332, 169-186. <https://doi.org/10.1113/jphysiol.1982.sp014408>
- Marshall, J. M., Thomas, T., & Turner, L. (1993). A link between adenosine, ATP-sensitive K⁺ channels, potassium and muscle vasodilatation in the rat in systemic hypoxia. *The Journal of Physiology*, 472(1), 1-9. <https://doi.org/10.1113/jphysiol.1993.sp019931>
- Matthew, J. B., Hanania, G. I. H., & Gurd, F. R. N. (1979a). Coordination complexes and catalytic properties of proteins and related substances. 104. Electrostatic effects in hemoglobin: hydrogen ion equilibria in human deoxy- and oxyhemoglobin A. *Biochemistry*, 18(10), 1919-1928. <https://doi.org/10.1021/bi00577a011>
- Matthew, J. B., Hanania, G. I. H., & Gurd, F. R. N. (1979b). Coordination complexes and catalytic properties of proteins and related substances. 105. Electrostatic effects in hemoglobin: Bohr effect and ionic strength dependence of individual groups. *Biochemistry*, 18(10), 1928-1936. <https://doi.org/10.1021/bi00577a012>
- McClatchey, P. M., Mignemi, N. A., Xu, Z., Williams, I. M., Reusch, J. E. B., McGuinness, O. P., & Wasserman, D. H. (2018). Automated quantification of microvascular perfusion. *Microcirculation*, 25(6), e12482. <https://doi.org/10.1111/micc.12482>
- McCullough, W. T., Collins, D. M., & Ellsworth, M. L. (1997). Arteriolar responses to extracellular ATP in striated muscle. *American Journal of Physiology-Heart and Circulatory Physiology*, 272(4), H1886-H1891. <https://doi.org/10.1152/ajpheart.1997.272.4.H1886>
- McGahren, E. D., Beach, J. M., & Duling, B. R. (1998). Capillaries demonstrate changes in membrane potential in response to pharmacological stimuli. *American Journal of Physiology-Heart and Circulatory Physiology*, 274(1), H60-H65. <https://doi.org/10.1152/ajpheart.1998.274.1.H60>
- Merkel, T. C., Bondar, V. I., Nagai, K., Freeman, B. D., & Pinnau, I. (2000). Gas sorption, diffusion, and permeation in poly(dimethylsiloxane). *Journal of polymer science. Part B, Polymer physics*, 38(3), 415-434. [https://doi.org/10.1002/\(SICI\)1099-0488\(20000201\)38:3<415::AID-POLB8>3.0.CO;2-Z](https://doi.org/10.1002/(SICI)1099-0488(20000201)38:3<415::AID-POLB8>3.0.CO;2-Z)
- Miekisiak, G., Yoo, K., Sandler, A. L., Kulik, T. B., Chen, J.-F., & Winn, H. R. (2009). The role of adenosine in hypercarbic hyperemia: in vivo and in vitro studies in adenosine 2A receptor knockout and wild-type mice: Laboratory investigation. *Journal of Neurosurgery JNS*, 110(5), 981-988. <https://doi.org/10.3171/2008.8.JNS08460>
- Milkau, M., Kohler, R., & de Wit, C. (2010). Crucial importance of the endothelial K⁺ channel SK3 and connexin40 in arteriolar dilations during skeletal muscle contraction. *FASEB J*, 24(9), 3572-3579. <https://doi.org/10.1096/fj.10-158956>
- Minamiyama, M., & Yamamoto, A. (2010). Direct evidence of the vasodilator action of carbon dioxide on subcutaneous microvasculature in rats by use of intra-vital video-microscopy. *Journal of Biorheology*, 24(1), 42-46. <https://doi.org/10.1007/s12573-010-0023-y>

- Miseta, A., Bogner, P., Berényi, E., Kellermayer, M., Galambos, C., Wheatley, D. N., & Cameron, I. L. (1993). Relationship between cellular ATP, potassium, sodium and magnesium concentrations in mammalian and avian erythrocytes. *Biochimica et Biophysica Acta (BBA) - Molecular Cell Research*, 1175(2), 133-139.
[https://doi.org/10.1016/0167-4889\(93\)90015-H](https://doi.org/10.1016/0167-4889(93)90015-H)
- Missner, A., Kügler, P., Saporov, S. M., Sommer, K., Mathai, J. C., Zeidel, M. L., & Pohl, P. (2008). Carbon dioxide transport through membranes. *The Journal of biological chemistry*, 283(37), 25340-25347. <https://doi.org/10.1074/jbc.M800096200>
- Mitchell, D., Yu, J., & Tyml, K. (1997). Comparable Effects of Arteriolar and Capillary Stimuli on Blood Flow in Rat Skeletal Muscle. *Microvascular Research*, 53(1), 22-32.
<https://doi.org/10.1006/mvre.1996.1988>
- Moini, M., Demars, S. M., & Huang, H. (2002). Analysis of carbonic anhydrase in human red Blood cells using capillary electrophoresis/ electrospray ionization-mass spectrometry. *Anal Chem*, 74(15), 3772-3776. <https://doi.org/10.1021/ac020022z>
- Morff, R. J., Harris, P. D., Wiegman, D. L., & Miller, F. N. (1981). Muscle microcirculation: effects of tissue pH, PCO₂, and PO₂ during systemic hypoxia. *American Journal of Physiology-Heart and Circulatory Physiology*, 240(5), H746-H754.
<https://doi.org/10.1152/ajpheart.1981.240.5.H746>
- Morii, S., Ngai, A. C., Ko, K. R., & Winn, H. R. (1987). Role of adenosine in regulation of cerebral blood flow: effects of theophylline during normoxia and hypoxia. *American Journal of Physiology-Heart and Circulatory Physiology*, 253(1), H165-H175.
<https://doi.org/10.1152/ajpheart.1987.253.1.H165>
- Morii, S., Ngai, A. C., & Winn, H. R. (1986). Reactivity of Rat Pial Arterioles and Venules to Adenosine and Carbon Dioxide: With Detailed Description of the Closed Cranial Window Technique in Rats. *Journal of Cerebral Blood Flow & Metabolism*, 6(1), 34-41.
<https://doi.org/10.1038/jcbfm.1986.5>
- Murrant, C. L., Lamb, I. R., & Novielli, N. M. (2017). Capillary endothelial cells as coordinators of skeletal muscle blood flow during active hyperemia. *Microcirculation*, 24(3).
<https://doi.org/10.1111/micc.12348>
- Murrant, C. L., & Sarelius, I. H. (2002). Multiple dilator pathways in skeletal muscle contraction-induced arteriolar dilations. *Am J Physiol Regul Integr Comp Physiol*, 282(4), R969-978. <https://doi.org/10.1152/ajpregu.00405.2001>
- Murrant, C. L., & Sarelius, I. H. (2015). Local control of blood flow during active hyperaemia: what kinds of integration are important? *J Physiol*, 593(21), 4699-4711.
<https://doi.org/10.1113/JP270205>
- Myrhaage, R., & Hudlická, O. (1976). The microvascular bed and capillary surface area in rat extensor hallucis proprius muscle (EHP). *Microvascular Research*, 11(3), 315-323.
[https://doi.org/10.1016/0026-2862\(76\)90061-3](https://doi.org/10.1016/0026-2862(76)90061-3)
- Nakahata, K., Kinoshita, H., Hirano, Y., Kimoto, Y., Iranami, H., & Hatano, Y. (2003). Mild Hypercapnia Induces Vasodilation via Adenosine Triphosphate-sensitive K⁺Channels in Parenchymal Microvessels of the Rat Cerebral Cortex. *Anesthesiology*, 99(6), 1333-1339.
<https://doi.org/10.1097/00000542-200312000-00014>
- Nelson, M. G., Savage, G. A., Cooke, P. J., & Lappin, T. R. (1981). Determination of the oxygen dissociation curve and P₅₀ of whole blood. An evaluation of the Hem-O-Scan and instrumentation of laboratory systems. *Am J Clin Pathol*, 75(3), 395-399.
<https://doi.org/10.1093/ajcp/75.3.395>

- Ngo, A. T., Jensen, L. J., Riemann, M., Holstein-Rathlou, N. H., & Torp-Pedersen, C. (2010). Oxygen sensing and conducted vasomotor responses in mouse cremaster arterioles in situ. *Pflügers Arch*, 460(1), 41-53. <https://doi.org/10.1007/s00424-010-0837-x>
- Nnorom, C. C., Davis, C., Fedinec, A. L., Howell, K., Jaggar, J. H., Parfenova, H., Pourcyrous, M., & Leffler, C. W. (2014). Contributions of KATP and KCa channels to cerebral arteriolar dilation to hypercapnia in neonatal brain. *Physiol Rep*, 2(8). <https://doi.org/10.14814/phy2.12127>
- Novielli, N. M., & Jackson, D. N. (2014). Contraction-evoked vasodilation and functional hyperaemia are compromised in branching skeletal muscle arterioles of young pre-diabetic mice. *Acta Physiol (Oxf)*, 211(2), 371-384. <https://doi.org/10.1111/apha.12297>
- Nyberg, M., Al-Khazraji, B. K., Mortensen, S. P., Jackson, D. N., Ellis, C. G., & Hellsten, Y. (2013). Effect of extraluminal ATP application on vascular tone and blood flow in skeletal muscle: implications for exercise hyperemia. *Am J Physiol Regul Integr Comp Physiol*, 305(3), R281-290. <https://doi.org/10.1152/ajpregu.00189.2013>
- O'Regan, M. (2005). Adenosine and the regulation of cerebral blood flow. *Neurological Research*, 27(2), 175-181. <https://doi.org/10.1179/016164105X21931>
- Okamoto, H., Hudetz, A. G., Roman, R. J., Bosnjak, Z. J., & Kampine, J. P. (1997). Neuronal NOS-derived NO plays permissive role in cerebral blood flow response to hypercapnia. *American Journal of Physiology-Heart and Circulatory Physiology*, 272(1), H559-H566. <https://doi.org/10.1152/ajpheart.1997.272.1.H559>
- Olearczyk, J. J., Stephenson, A. H., Lonigro, A. J., & Sprague, R. S. (2004). Heterotrimeric G protein Gi is involved in a signal transduction pathway for ATP release from erythrocytes. *American Journal of Physiology-Heart and Circulatory Physiology*, 286(3), H940-H945. <https://doi.org/10.1152/ajpheart.00677.2003>
- Padilla, D. J., McDonough, P., Behnke, B. J., Kano, Y., Hageman, K. S., Musch, T. I., & Poole, D. C. (2006). Effects of Type II diabetes on capillary hemodynamics in skeletal muscle. *Am J Physiol Heart Circ Physiol*, 291(5), H2439-2444. <https://doi.org/10.1152/ajpheart.00290.2006>
- Papaioannou, T. G., & Stefanadis, C. (2005). Vascular wall shear stress: basic principles and methods. *Hellenic J Cardiol*, 46(1), 9-15. <https://www.ncbi.nlm.nih.gov/pubmed/15807389>
- Pelligrino, D. A., Koenig, H. M., & Albrecht, R. F. (1993). Nitric Oxide Synthesis and Regional Cerebral Blood Flow Responses to Hypercapnia and Hypoxia in the Rat. *Journal of Cerebral Blood Flow & Metabolism*, 13(1), 80-87. <https://doi.org/10.1038/jcbfm.1993.10>
- Pelligrino, D. A., Wang, Q., Koenig, H. M., & Albrecht, R. F. (1995). Role of nitric oxide, adenosine, N-methyl-D-aspartate receptors, and neuronal activation in hypoxia-induced pial arteriolar dilation in rats. *Brain Research*, 704(1), 61-70. [https://doi.org/10.1016/0006-8993\(95\)01105-6](https://doi.org/10.1016/0006-8993(95)01105-6)
- Perutz, M. F. (1970). Stereochemistry of cooperative effects in haemoglobin. *Nature*, 228(5273), 726-739. <https://doi.org/10.1038/228726a0>
- Perutz, M. F. (1972). Nature of haem-haem interaction. *Nature*, 237(5357), 495-499. <https://doi.org/10.1038/237495a0>
- Perutz, M. F., Wilkinson, A. J., Paoli, M., & Dodson, G. G. (1998). The stereochemical mechanism of the cooperative effects in hemoglobin revisited. *Annu Rev Biophys Biomol Struct*, 27, 1-34. <https://doi.org/10.1146/annurev.biophys.27.1.1>

- Phillis, J. W., & DeLong, R. E. (1987). An involvement of adenosine in cerebral blood flow regulation during hypercapnia. *General Pharmacology: The Vascular System*, 18(2), 133-139. [https://doi.org/10.1016/0306-3623\(87\)90239-4](https://doi.org/10.1016/0306-3623(87)90239-4)
- Phillis, J. W., Lungu, C. L., Barbu, D. E., & O'Regan, M. H. (2004). Adenosine's role in hypercapnia-evoked cerebral vasodilation in the rat. *Neurosci Lett*, 365(1), 6-9. <https://doi.org/10.1016/j.neulet.2004.03.094>
- Phillis, J. W., & O'Regan, M. H. (2003). Effects of adenosine receptor antagonists on pial arteriolar dilation during carbon dioxide inhalation. *European Journal of Pharmacology*, 476(3), 211-219. [https://doi.org/10.1016/s0014-2999\(03\)02187-3](https://doi.org/10.1016/s0014-2999(03)02187-3)
- Pittman, R. N. (2013). Oxygen transport in the microcirculation and its regulation. *Microcirculation*, 20(2), 117-137. <https://doi.org/10.1111/micc.12017>
- Poole, D. C., Copp, S. W., Ferguson, S. K., & Musch, T. I. (2013). Skeletal muscle capillary function: contemporary observations and novel hypotheses. *Exp Physiol*, 98(12), 1645-1658. <https://doi.org/10.1113/expphysiol.2013.073874>
- Prahl, S. (1999). Optical Absorption of Hemoglobin. <https://omlc.org/spectra/hemoglobin/>
- Pries, A. R., Ley, K., Claassen, M., & Gaehtgens, P. (1989). Red cell distribution at microvascular bifurcations. *Microvascular Research*, 38(1), 81-101. [https://doi.org/10.1016/0026-2862\(89\)90018-6](https://doi.org/10.1016/0026-2862(89)90018-6)
- Pries, A. R., Secomb, T. W., Gaehtgens, P., & Gross, J. F. (1990). Blood flow in microvascular networks. Experiments and simulation. *Circulation Research*, 67(4), 826-834. <https://doi.org/10.1161/01.RES.67.4.826>
- Qiu, F., Wang, J., Spray, D. C., Scemes, E., & Dahl, G. (2011). Two non-vesicular ATP release pathways in the mouse erythrocyte membrane. *FEBS Lett*, 585(21), 3430-3435. <https://doi.org/10.1016/j.febslet.2011.09.033>
- Racine, M. L., & Dinunno, F. A. (2019). Reduced deformability contributes to impaired deoxygenation-induced ATP release from red blood cells of older adult humans. *J Physiol*, 597(17), 4503-4519. <https://doi.org/10.1113/JP278338>
- Raper, A. J., Kontos, H. A., & Patterson, J. L. (1971). Response of Pial Precapillary Vessels to Changes in Arterial Carbon Dioxide Tension. *Circulation Research*, 28(5), 518-523. <https://doi.org/10.1161/01.RES.28.5.518>
- Reid, J. M., Davies, A. G., Ashcroft, F. M., & Paterson, D. J. (1995). Effect of L-NMMA, cromakalim, and glibenclamide on cerebral blood flow in hypercapnia and hypoxia. *American Journal of Physiology-Heart and Circulatory Physiology*, 269(3), H916-H922. <https://doi.org/10.1152/ajpheart.1995.269.3.H916>
- Reid, J. M., Paterson, D. J., Ashcroft, F. M., & Bergel, D. H. (1993). The effect of tolbutamide on cerebral blood flow during hypoxia and hypercapnia in the anaesthetized rat. *Pflügers Archiv*, 425(3), 362-364. <https://doi.org/10.1007/BF00374187>
- Richardson, D. W., Wasserman, A. J., & Patterson, J. L., Jr. (1961). General and regional circulatory responses to change in blood pH and carbon dioxide tension. *The Journal of Clinical Investigation*, 40(1), 31-43. <https://doi.org/10.1172/JCI104234>
- Richardson, K. J., Kuck, L., & Simmonds, M. J. (2020). Beyond oxygen transport: active role of erythrocytes in the regulation of blood flow. *Am J Physiol Heart Circ Physiol*, 319(4), H866-H872. <https://doi.org/10.1152/ajpheart.00441.2020>
- Riemann, M., Rai, A., Ngo, A. T., Dziegiel, M. H., Holstein-Rathlou, N. H., & Torp-Pedersen, C. (2011). Oxygen-dependent vasomotor responses are conducted upstream in the mouse cremaster microcirculation. *J Vasc Res*, 48(1), 79-89. <https://doi.org/10.1159/000318777>

- Rocha, M. P., Campos, M. O., Mattos, J. D., Mansur, D. E., Rocha, H. N. M., Secher, N. H., Nobrega, A. C. L., & Fernandes, I. A. (2020). KATP channels modulate cerebral blood flow and oxygen delivery during isocapnic hypoxia in humans. *J Physiol*, 598(16), 3343-3356. <https://doi.org/10.1113/JP279751>
- Rosenblum, W. I. (2003). ATP-sensitive potassium channels in the cerebral circulation. *Stroke*, 34(6), 1547-1552. <https://doi.org/10.1161/01.STR.0000070425.98202.B5>
- Rosenblum, W. I., Kontos, H. A., & Wei, E. P. (2001). Evidence for a KATP ion channel link in the inhibition of hypercapnic dilation of pial arterioles by 7-nitroindazole and tetrodotoxin. *European Journal of Pharmacology*, 417(3), 203-215. [https://doi.org/10.1016/S0014-2999\(01\)00899-8](https://doi.org/10.1016/S0014-2999(01)00899-8)
- Rosenblum, W. I., Wei, E. P., & Kontos, H. A. (2002). Dilation of rat brain arterioles by hypercapnia in vivo can occur even after blockade of guanylate cyclase by ODQ. *European Journal of Pharmacology*, 448(2), 201-206. [https://doi.org/10.1016/S0014-2999\(02\)01935-0](https://doi.org/10.1016/S0014-2999(02)01935-0)
- Rothe, C. F., Maass-Moreno, R., & Flanagan, A. D. (1990). Effects of hypercapnia and hypoxia on the cardiovascular system: vascular capacitance and aortic chemoreceptors. *American Journal of Physiology-Heart and Circulatory Physiology*, 259(3), H932-H939. <https://doi.org/10.1152/ajpheart.1990.259.3.H932>
- Sabino, J. P. J., Oliveira, M., Giusti, H., Glass, M. L., Salgado, H. C., & Fazan-Jr, R. (2013). Hemodynamic and ventilatory response to different levels of hypoxia and hypercapnia in carotid body-denervated rats. *Clinics*, 68(3), 395-399. [https://doi.org/10.6061/clinics/2013\(03\)OA18](https://doi.org/10.6061/clinics/2013(03)OA18)
- Sadraei, H., & Beech, D. J. (1995). Ionic currents and inhibitory effects of glibenclamide in seminal vesicle smooth muscle cells. *Br J Pharmacol*, 115(8), 1447-1454. <https://doi.org/10.1111/j.1476-5381.1995.tb16636.x>
- Saito, Y., McKay, M., Eraslan, A., & Hester, R. L. (1996). Functional hyperemia in striated muscle is reduced following blockade of ATP-sensitive potassium channels. *American Journal of Physiology-Heart and Circulatory Physiology*, 270(5), H1649-H1654. <https://doi.org/10.1152/ajpheart.1996.270.5.H1649>
- Sandoo, A., van Zanten, J. J., Metsios, G. S., Carroll, D., & Kitas, G. D. (2010). The endothelium and its role in regulating vascular tone. *Open Cardiovasc Med J*, 4, 302-312. <https://doi.org/10.2174/1874192401004010302>
- Sarelius, I., & Pohl, U. (2010). Control of muscle blood flow during exercise: local factors and integrative mechanisms. *Acta Physiol (Oxf)*, 199(4), 349-365. <https://doi.org/10.1111/j.1748-1716.2010.02129.x>
- Sarelius, I. H. (1993). Cell and oxygen flow in arterioles controlling capillary perfusion. *American Journal of Physiology-Heart and Circulatory Physiology*, 265(5), H1682-H1687. <https://doi.org/10.1152/ajpheart.1993.265.5.H1682>
- Schemke, S., & de Wit, C. (2021). KATP channels and NO dilate redundantly intramuscular arterioles during electrical stimulation of the skeletal muscle in mice. *Pflugers Arch*, 473(11), 1795-1806. <https://doi.org/10.1007/s00424-021-02607-1>
- Schmetterer, L., Findl, O., Strenn, K., Graselli, U., Kastner, J., Eichler, H.-G., & Wolzt, M. (1997). Role of NO in the O₂ and CO₂ responsiveness of cerebral and ocular circulation in humans. *American Journal of Physiology-Regulatory, Integrative and Comparative Physiology*, 273(6), R2005-R2012. <https://doi.org/10.1152/ajpregu.1997.273.6.R2005>

- Schnitzler, M., Derst, C., Daut, J., & Preisig-Müller, R. (2000). ATP-sensitive potassium channels in capillaries isolated from guinea-pig heart. *The Journal of Physiology*, 525 Pt 2(Pt 2), 307-317. <https://doi.org/10.1111/j.1469-7793.2000.t01-1-00307.x>
- Schrage, W. G., Dietz, N. M., & Joyner, M. J. (2006). Effects of combined inhibition of ATP-sensitive potassium channels, nitric oxide, and prostaglandins on hyperemia during moderate exercise. *J Appl Physiol* (1985), 100(5), 1506-1512. <https://doi.org/10.1152/japplphysiol.01639.2005>
- Segal, S. S. (2005). Regulation of blood flow in the microcirculation. *Microcirculation*, 12(1), 33-45. <https://doi.org/10.1080/10739680590895028>
- Segal, S. S., Damon, D. N., & Duling, B. R. (1989). Propagation of vasomotor responses coordinates arteriolar resistances. *American Journal of Physiology-Heart and Circulatory Physiology*, 256(3), H832-H837. <https://doi.org/10.1152/ajpheart.1989.256.3.H832>
- Segal, S. S., & Duling, B. R. (1986a). Communication between feed arteries and microvessels in hamster striated muscle: segmental vascular responses are functionally coordinated. *Circulation Research*, 59(3), 283-290. <https://doi.org/10.1161/01.RES.59.3.283>
- Segal, S. S., & Duling, B. R. (1986b). Flow Control Among Microvessels Coordinated by Intercellular Conduction. *Science*, 234(4778), 868-870. <https://doi.org/10.1126/science.3775368>
- Segal, S. S., & Jacobs, T. L. (2001). Role for endothelial cell conduction in ascending vasodilatation and exercise hyperaemia in hamster skeletal muscle. *The Journal of Physiology*, 536(Pt 3), 937-946. <https://doi.org/10.1111/j.1469-7793.2001.00937.x>
- Sender, S., Gros, G., Waheed, A., Hageman, G. S., & Sly, W. S. (1994). Immunohistochemical localization of carbonic anhydrase IV in capillaries of rat and human skeletal muscle. *Journal of Histochemistry & Cytochemistry*, 42(9), 1229-1236. <https://doi.org/10.1177/42.9.8064130>
- Sikora, J., Orlov, S. N., Furuya, K., & Grygorczyk, R. (2014). Hemolysis is a primary ATP-release mechanism in human erythrocytes. *Blood*, 124(13), 2150-2157. <https://doi.org/10.1182/blood-2014-05-572024>
- Simpson, R. E., & Phillis, J. W. (1991). Adenosine deaminase reduces hypoxic and hypercapnic dilatation of rat pial arterioles: evidence for mediation by adenosine. *Brain Research*, 553(2), 305-308. [https://doi.org/10.1016/0006-8993\(91\)90839-N](https://doi.org/10.1016/0006-8993(91)90839-N)
- Skalak, T. C., & Schmid-Schönbein, G. W. (1986). The microvasculature in skeletal muscle. IV. A model of the capillary network. *Microvascular Research*, 32(3), 333-347. [https://doi.org/10.1016/0026-2862\(86\)90069-5](https://doi.org/10.1016/0026-2862(86)90069-5)
- Song, H., & Tyml, K. (1993). Evidence for sensing and integration of biological signals by the capillary network. *American Journal of Physiology-Heart and Circulatory Physiology*, 265(4), H1235-H1242. <https://doi.org/10.1152/ajpheart.1993.265.4.H1235>
- Sove, R. J., Milkovich, S., Nikolov, H. N., Holdsworth, D. W., Ellis, C. G., & Fraser, G. M. (2021). Localized Oxygen Exchange Platform for Intravital Video Microscopy Investigations of Microvascular Oxygen Regulation. *Front Physiol*, 12, 654928. <https://doi.org/10.3389/fphys.2021.654928>
- Sprague, R. S., Bowles, E. A., Olearczyk, J. J., Stephenson, A. H., & Lonigro, A. J. (2002). The role of G protein beta subunits in the release of ATP from human erythrocytes. *Journal of Physiology and Pharmacology*, 53(4), 667-674. <https://pubmed.ncbi.nlm.nih.gov/12512701/>

- Sprague, R. S., Ellsworth, M. L., Stephenson, A. H., Kleinhenz, M. E., & Lonigro, A. J. (1998). Deformation-induced ATP release from red blood cells requires CFTR activity. *American Journal of Physiology-Heart and Circulatory Physiology*, 275(5), H1726-H1732. <https://doi.org/10.1152/ajpheart.1998.275.5.H1726>
- Sprague, R. S., Ellsworth, M. L., Stephenson, A. H., & Lonigro, A. J. (2001). Participation of cAMP in a signal-transduction pathway relating erythrocyte deformation to ATP release. *American Journal of Physiology-Cell Physiology*, 281(4), C1158-C1164. <https://doi.org/10.1152/ajpcell.2001.281.4.C1158>
- Sridharan, M., Adderley, S. P., Bowles, E. A., Egan, T. M., Stephenson, A. H., Ellsworth, M. L., & Sprague, R. S. (2010). Pannexin 1 is the conduit for low oxygen tension-induced ATP release from human erythrocytes. *Am J Physiol Heart Circ Physiol*, 299(4), H1146-1152. <https://doi.org/10.1152/ajpheart.00301.2010>
- Sridharan, M., Sprague, R. S., Adderley, S. P., Bowles, E. A., Ellsworth, M. L., & Stephenson, A. H. (2010). Diamide decreases deformability of rabbit erythrocytes and attenuates low oxygen tension-induced ATP release. *Exp Biol Med (Maywood)*, 235(9), 1142-1148. <https://doi.org/10.1258/ebm.2010.010118>
- Sun, X. G., Hansen, J. E., Stringer, W. W., Ting, H., & Wasserman, K. (2001). Carbon dioxide pressure-concentration relationship in arterial and mixed venous blood during exercise. *J Appl Physiol* (1985), 90(5), 1798-1810. <https://doi.org/10.1152/jappl.2001.90.5.1798>
- Sutera, S. P., & Skalak, R. (1993). The History of Poiseuille's Law. *Annual Review of Fluid Mechanics*, 25(1), 1-20. <https://doi.org/10.1146/annurev.fl.25.010193.000245>
- Swietach, P., Tiffert, T., Mauritz, J. M., Seear, R., Esposito, A., Kaminski, C. F., Lew, V. L., & Vaughan-Jones, R. D. (2010). Hydrogen ion dynamics in human red blood cells. *J Physiol*, 588(Pt 24), 4995-5014. <https://doi.org/10.1113/jphysiol.2010.197392>
- Taguchi, H., Heistad, D. D., Kitazono, T., & Faraci, F. M. (1994). ATP-sensitive K⁺ channels mediate dilatation of cerebral arterioles during hypoxia. *Circulation Research*, 74(5), 1005-1008. <https://doi.org/10.1161/01.RES.74.5.1005>
- Tanishita, K., Tanasawa, I., Yamaguchi, T., & Sugawara, M. (1985). Facilitated diffusion of carbon dioxide in whole blood and hemoglobin solutions. *Pflügers Archiv*, 405(2), 83-90. <https://doi.org/10.1007/BF00584527>
- Tian, R., Vogel, P., Lassen, N. A., Mulvany, M. J., Andreasen, F., & Aalkjær, C. (1995). Role of Extracellular and Intracellular Acidosis for Hypercapnia-Induced Inhibition of Tension of Isolated Rat Cerebral Arteries. *Circulation Research*, 76(2), 269-275. <https://doi.org/10.1161/01.RES.76.2.269>
- Toda, N., Hatano, Y., & Mori, K. (1989). Mechanisms underlying response to hypercapnia and bicarbonate of isolated dog cerebral arteries. *American Journal of Physiology-Heart and Circulatory Physiology*, 257(1), H141-H146. <https://doi.org/10.1152/ajpheart.1989.257.1.H141>
- Twynstra, J., Ruiz, D. A., & Murrant, C. L. (2012). Functional coordination of the spread of vasodilations through skeletal muscle microvasculature: implications for blood flow control. *Acta Physiol (Oxf)*, 206(4), 229-241. <https://doi.org/10.1111/j.1748-1716.2012.02465.x>
- Tyckocki, N. R., Boerman, E. M., & Jackson, W. F. (2017). Smooth Muscle Ion Channels and Regulation of Vascular Tone in Resistance Arteries and Arterioles. *Compr Physiol*, 7(2), 485-581. <https://doi.org/10.1002/cphy.c160011>

- Tymk, K., & Budreau, C. H. (1991). A new preparation of rat extensor digitorum longus muscle for intravital investigation of the microcirculation. *International journal of microcirculation, clinical and experimental*, 10, 335-343.
- Van Beekvelt, M. C. P., Shoemaker, J. K., Tschakovsky, M. E., Hopman, M. T. E., & Hughson, R. L. (2001). Blood flow and muscle oxygen uptake at the onset and end of moderate and heavy dynamic forearm exercise. *American Journal of Physiology-Regulatory, Integrative and Comparative Physiology*, 280(6), R1741-R1747.
<https://doi.org/10.1152/ajpregu.2001.280.6.R1741>
- VanTeeffelen, J. W. G. E., & Segal, S. S. (2003). Interaction between sympathetic nerve activation and muscle fibre contraction in resistance vessels of hamster retractor muscle. *The Journal of Physiology*, 550(Pt 2), 563-574.
<https://doi.org/10.1113/jphysiol.2003.038984>
- Waheed, A., Zhu, X. L., Sly, W. S., Wetzel, P., & Gros, G. (1992). Rat skeletal muscle membrane associated carbonic anhydrase is 39-kDa, glycosylated, GPI-anchored CA IV. *Archives of Biochemistry and Biophysics*, 294(2), 550-556. [https://doi.org/10.1016/0003-9861\(92\)90724-B](https://doi.org/10.1016/0003-9861(92)90724-B)
- Wan, J., Ristenpart, W. D., & Stone, H. A. (2008). Dynamics of shear-induced ATP release from red blood cells. *Proc Natl Acad Sci U S A*, 105(43), 16432-16437.
<https://doi.org/10.1073/pnas.0805779105>
- Wang, L., Olivecrona, G., Gotberg, M., Olsson, M. L., Winzell, M. S., & Erlinge, D. (2005). ADP acting on P2Y₁₃ receptors is a negative feedback pathway for ATP release from human red blood cells. *Circ Res*, 96(2), 189-196.
<https://doi.org/10.1161/01.RES.0000153670.07559.E4>
- Wang, Q., Bryan, R. M., & Pelligrino, D. A. (1998). Calcium-dependent and ATP-sensitive potassium channels and the 'permissive' function of cyclic GMP in hypercapnia-induced pial arteriolar relaxation. *Brain Research*, 793(1), 187-196.
[https://doi.org/10.1016/S0006-8993\(98\)00173-5](https://doi.org/10.1016/S0006-8993(98)00173-5)
- Wang, Q., Paulson, O. B., & Lassen, N. A. (1992). Effect of Nitric Oxide Blockade by NG-Nitro-L-Arginine on Cerebral Blood Flow Response to Changes in Carbon Dioxide Tension. *Journal of Cerebral Blood Flow & Metabolism*, 12(6), 947-953.
<https://doi.org/10.1038/jcbfm.1992.131>
- Wang, Q., Pelligrino, D. A., Koenig, H. M., & Albrecht, R. F. (1994). The Role of Endothelium and Nitric Oxide in Rat Pial Arteriolar Dilatory Responses to CO₂ in vivo. *Journal of Cerebral Blood Flow & Metabolism*, 14(6), 944-951.
<https://doi.org/10.1038/jcbfm.1994.126>
- Wang, X., Wu, J., Li, L., Chen, F., Wang, R., & Jiang, C. (2003). Hypercapnic acidosis activates KATP channels in vascular smooth muscles. *Circ Res*, 92(11), 1225-1232.
<https://doi.org/10.1161/01.RES.0000075601.95738.6D>
- Ward, M. E. (1996). Interaction between hypoxia and hypercapnia in regulating canine diaphragm arteriolar diameter. *Journal of Applied Physiology*, 80(3), 802-809.
<https://doi.org/10.1152/jappl.1996.80.3.802>
- Wei, E. P., & Kontos, H. A. (1999). Blockade of ATP-Sensitive Potassium Channels in Cerebral Arterioles Inhibits Vasoconstriction From Hypocapnic Alkalosis in Cats. *Stroke*, 30(4), 851-854. <https://doi.org/10.1161/01.STR.30.4.851>


- Wei, E. P., Kontos, H. A., & Patterson, J. L. (1980). Dependence of pial arteriolar response to hypercapnia on vessel size. *American Journal of Physiology-Heart and Circulatory Physiology*, 238(5), H697-H702. <https://doi.org/10.1152/ajpheart.1980.238.5.H697>
- Wei, E. P., Thames, M. D., Kontos, H. A., & Patterson, J. L. (1974). Inhibition of the Vasodilator Effect of Hypercapnic Acidosis by Hypercalcemia in Dogs and Rats. *Circulation Research*, 35(6), 890-895. <https://doi.org/10.1161/01.RES.35.6.890>
- Welsh, D. G., & Segal, S. S. (1996). Muscle Length Directs Sympathetic Nerve Activity and Vasomotor Tone in Resistance Vessels of Hamster Retractor. *Circulation Research*, 79(3), 551-559. <https://doi.org/10.1161/01.RES.79.3.551>
- Welsh, D. G., & Segal, S. S. (1998). Endothelial and smooth muscle cell conduction in arterioles controlling blood flow. *American Journal of Physiology-Heart and Circulatory Physiology*, 274(1), H178-H186. <https://doi.org/10.1152/ajpheart.1998.274.1.H178>
- White, R., & Hiley, C. R. (2000). Hyperpolarisation of rat mesenteric endothelial cells by ATP-sensitive K⁺ channel openers. *European Journal of Pharmacology*, 397(2), 279-290. [https://doi.org/10.1016/S0014-2999\(00\)00271-5](https://doi.org/10.1016/S0014-2999(00)00271-5)
- White, R. P., Deane, C., Vallance, P., & Markus, H. S. (1998). Nitric Oxide Synthase Inhibition in Humans Reduces Cerebral Blood Flow but Not the Hyperemic Response to Hypercapnia. *Stroke*, 29(2), 467-472. <https://doi.org/10.1161/01.STR.29.2.467>
- Wieth, J. O., Andersen, O. S., Brahm, J., Bjerrum, P. J., Borders, C. L., Keynes, R. D., & Ellory, J. C. (1982). Chloride-bicarbonate exchange in red blood cells: physiology of transport and chemical modification of binding sites. *Philosophical Transactions of the Royal Society of London. B, Biological Sciences*, 299(1097), 383-399. <https://doi.org/10.1098/rstb.1982.0139>
- Wright, C. I. (1934). The diffusion of carbon dioxide in tissues. *The Journal of general physiology*, 17(5), 657-676. <https://doi.org/10.1085/jgp.17.5.657>
- Xia, J., & Duling, B. R. (1995). Electromechanical coupling and the conducted vasomotor response. *American Journal of Physiology-Heart and Circulatory Physiology*, 269(6), H2022-H2030. <https://doi.org/10.1152/ajpheart.1995.269.6.H2022>
- Xia, J., Little, T. L., & Duling, B. R. (1995). Cellular pathways of the conducted electrical response in arterioles of hamster cheek pouch in vitro. *American Journal of Physiology-Heart and Circulatory Physiology*, 269(6), H2031-H2038. <https://doi.org/10.1152/ajpheart.1995.269.6.H2031>
- Xu, H., Cui, N., Yang, Z., Wu, J., Giwa, L. R., Abdulkadir, L., Sharma, P., & Jiang, C. (2001). Direct activation of cloned K(atp) channels by intracellular acidosis. *J Biol Chem*, 276(16), 12898-12902. <https://doi.org/10.1074/jbc.M009631200>
- You, J. P., Wang, Q., Zhang, W., Jansen-Olesen, I., Paulson, O. B., Lassen, N. A., & Edvinsson, L. (1994). Hypercapnic vasodilatation in isolated rat basilar arteries is exerted via low pH and does not involve nitric oxide synthase stimulation or cyclic GMP production. *Acta Physiologica Scandinavica*, 152(4), 391-397. <https://doi.org/10.1111/j.1748-1716.1994.tb09821.x>
- Zwart, A., Kwant, G., Oeseburg, B., & Zijlstra, W. G. (1982). Oxygen dissociation curves for whole blood, recorded with an instrument that continuously measures pO₂ and sO₂ independently at constant t, pCO₂, and pH. *Clin Chem*, 28(6), 1287-1292. <https://www.ncbi.nlm.nih.gov/pubmed/6804125>

Appendix A



Request to Include Copyright Material

Adobe Reader, minimum version 8, is required to complete this form. Download the latest version at <http://get.adobe.com/reader>. (1) Save the form by clicking on the diskette icon on the upper left side of the screen; (2) Ensure that you are saving the file in PDF format; (3) Specify where you would like to save the file, e.g. Desktop; (4) Review the [How to create and insert a digital signature](#) webpage for step by step instructions; (5) Fill in the required data and save the file; (6) Send the completed form to the copyright holder.

| Student Contact Information | |
|--|--|
| Last name: McCarthy | First name: Meaghan |
| Academic Unit: Division of BioMedical Sciences | Degree: MSc |
| Email Address: mamccarthy@mun.ca | Telephone No.: (506) 461-2649 |
| Copyright Material Request | |
| <p>I, <u>Meaghan McCarthy</u>, request that you permit the inclusion of the described material in the thesis/report/practicum listed below and grant an irrevocable, non-exclusive licence to Memorial University of Newfoundland and to Library and Archives Canada to reproduce, lend or sell the material described below as part of my thesis/report/practicum. The title of the thesis/report/practicum is:</p> <p>Characterization of CO₂-mediated Microvascular Blood Flow Responses in Skeletal Muscle Tissue and Investigation of Underlying Mechanisms Using Direct CO₂ Microenvironment</p> <p>to be submitted in partial fulfilment of the requirements for the degree of <u>MSc</u> at Memorial University of Newfoundland.</p> | |
| Description of the Material to be Included | |
| <p>Adaptation of a figure showing a visual representation of oxy- and deoxy- hemoglobin molar attenuation coefficient curves and associated visible light spectrum from Figure 1.3 of the thesis:</p> <p>Fraser, G. M. (2012). Modeling Oxygen Transport in Three-Dimensional Capillary Networks. Electronic Thesis and Dissertation Repository. 500. https://ir.lib.uwo.ca/etd/500</p> | |
| Permission of Copyright Holder | |
| <p>I, <u>Graham Fraser</u>, <input checked="" type="checkbox"/> do <input type="checkbox"/> do not grant permission for the indicated use of the material described above.</p> <p>(Name - type)</p> | |
| Company/Organization: | <u>Memorial University of</u> |
| Position Title: | <u>Associate Professor</u> |
| Address: | <u>300 Prince Phillip, Room H-5337</u> |
| | <u>St. John's, NL, A1B3V6</u> |
| Signature: | <u>Date: June 22, 2022</u> |
|  | |
| <i>Note: Signature required on each additional attachment</i> | |

Memorial University protects privacy and maintains the confidentiality of personal information. The information requested in this form is collected under the general authority of the Memorial University Act ([RSNL1990CHAPTER-7](#)). It is required for administrative purposes of the School of Graduate Studies. If you have any questions about the collection and use of this information please contact the School of Graduate Studies at 709.864.2445 or sgs@mun.ca.

Updated September 2020

Appendix B



November 13, 2019

Dear: Dr. Graham Fraser, Faculty of Medicine\Division of BioMedical Sciences

Researcher Portal File No.: 20200860

Animal Care File: 19-01-GF

Entitled: (19-01-GF) Microvascular Blood Flow, Regulation, and Insulin Sensitivity in Type 2 Diabetes

Status: Active

Approval Date: November 13, 2019

Annual Report Due: November 13, 2020

Ethics Clearance Expires: November 13, 2022

Your Animal Use Protocol (AUP) renewal application to engage in procedures involving animals has been approved for a three-year term. This AUP replaces the previous protocol [[16-01-GF]] as the active ethics clearance associated with this project. Please note the new AUP number when referring to this protocol.

This ethics clearance includes the following Team Members: Dr. Graham Fraser (Principal Investigator)

An Event [Annual Report] will be required following each year of protocol activity.

Should you encounter an unexpected incident that negatively affects animal welfare or the research project relating to animal use, please submit an Event [Incident Report].

Any alterations to the protocol requires prior submission and approval of an Event [Amendment].

Sincerely,

Anulika Mbakwe

ANULIKA MBAKWE | ACC COORDINATOR

Department of Animal Care Services

Memorial University of Newfoundland

Health Sciences Centre | Room H1848

P: 709-777-6621

E-Mail: ambakwe@mun.ca